Master's thesis

NTNU
Norwegian University of Science and Technology
Faculty of Information Technology and Electrical Engineering
Department of Electric Power Engineering

William Flesland Blytt

Investigation of the Application of Optimal Power Flow in the Assessment of Power System Reliability

Master's thesis in Energy and Environmental Engineering
Supervisor: Vijay Venu Vadlamudi
Co-supervisor: Matias Vistnes
June 2023

NTNU
Norwegian University of
Science and Technology

William Flesland Blytt

Investigation of the Application of Optimal Power Flow in the Assessment of Power System Reliability

Master's thesis in Energy and Environmental Engineering
Supervisor: Vijay Venu Vadlamudi
Co-supervisor: Matias Vistnes
June 2023

Norwegian University of Science and Technology
Faculty of Information Technology and Electrical Engineering
Department of Electric Power Engineering

NTNU
Norwegian University of
Science and Technology

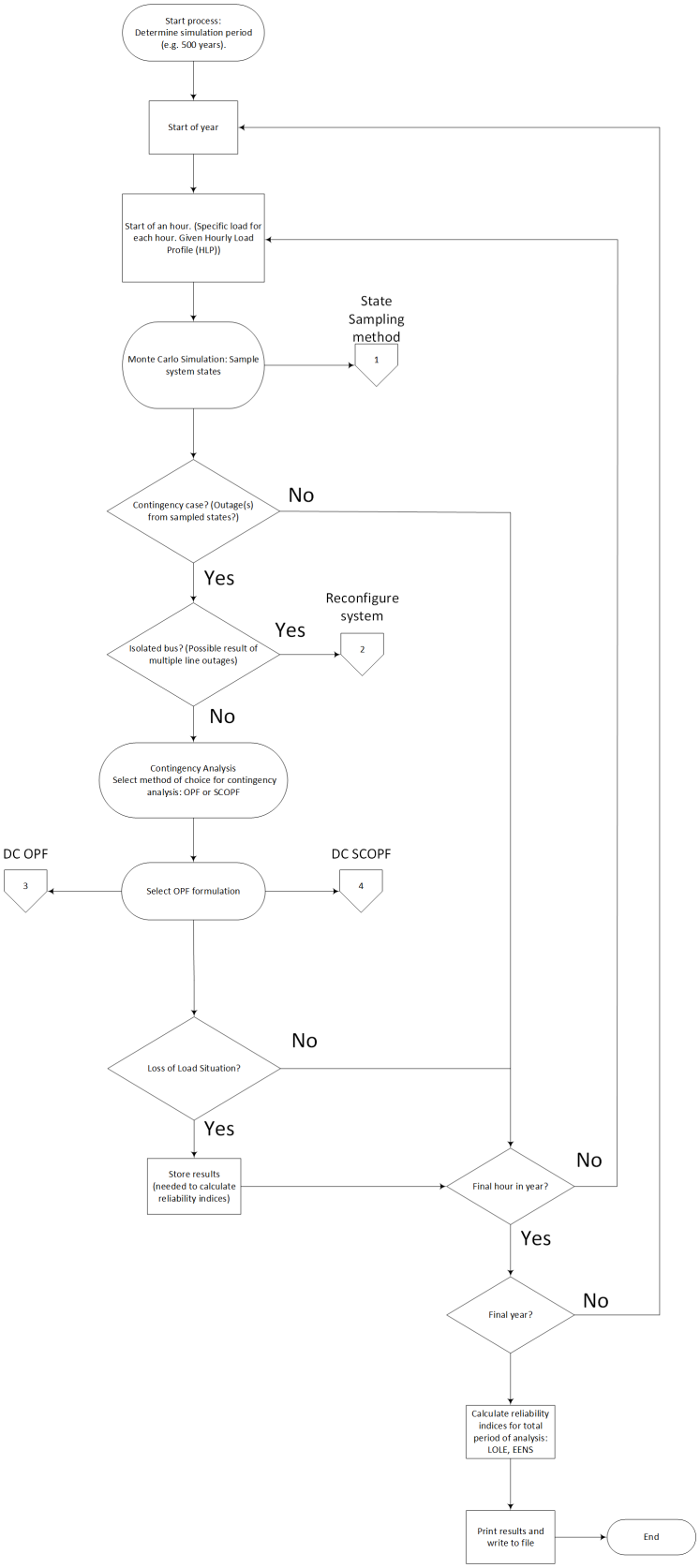
Start process: Determine simulation period (e.g. 500 years).
Start of year
Start of an hour. (Specific load for each hour. Given Hourly Load Profile (HLP))
Monte Carlo Simulation: Sample system states
State Sampling method
1
Contingency case? (Outage(s) from sampled states?)
No
Yes
Isolated bus? (Possible result of multiple line outages)
Yes
Reconfigure system
2
No
Contingency Analysis
Select method of choice for contingency analysis: OPF or SCOPF
DC OPF
3
Select OPF formulation
DC SCOPF
4
Loss of Load Situation?
No
Yes
Store results (needed to calculate reliability indices)
Final hour in year?
No
Yes
Final year?
No
Calculate reliability indices for total period of analysis: LOLE, EENS
Print results and write to file
End

Abstract

With the modernisation of the electric grid, it is crucial to have smart solutions for effective and secure system planning and operation. Traditional power system optimisation methods are being reevaluated and are becoming relevant for new applications. One such method is the Security Constrained Optimal Power Flow (SCOPF), which is an extension of the Optimal Power Flow (OPF) problem. In this thesis, the objective of SCOPF is to minimise cost of load curtailments, while satisfying all system constraints not only in normal operation conditions, but also in anticipated contingencies such as line outages and generator outages.

The objective of this Master's thesis is to make use of a non-sequential Monte Carlo Simulation and integrate it with a DC optimal power flow (DCOPF) approach using the Python programming language and the Pyomo framework. The primary focus is on assessing the reliability (adequacy aspect) of composite power systems. A novel DC preventive security constrained optimal power flow (DC-PSCOPF) approach has been developed for assessing the reliability of composite power systems. The main contribution of this thesis is the implementation of DC-PSCOPF in the OPF analysis of the algorithmic approach in calculating the reliability indices.

This thesis intends to pioneer the application of SCOPF in the assessment of power system reliability, representing a research area that has not been extensively explored before. The integration of SCOPF techniques, in this case DC-PSCOPF, in the composite system adequacy assessment, further develops the framework for evaluating the reliability of power systems available at the Department of Electric Energy (formerly, Department of Electric Power Engineering), NTNU. By considering both pre- and post-contingency constraints, this fresh perspective aims to offer helpful insights into the adequacy assessment of composite power systems. One of the goals of this thesis work is to create a reproducible method, which could be used as a stepping-stone for future research on the topic. Reliability indices utilising DCOPF and DC-PSCOPF are presented. A comprehensive deployment of the methodological approach used is presented, including the necessary adaptations and underlying assumptions. The details provided offer a clear understanding of the approach utilised, ensuring transparency in the method.

Two main scripts are developed for the implementation of DCOPF and DC-PSCOPF in the Pyomo framework in Python. These scripts are used in conjunction with the previously developed in-house scripts at the Department of Electric Energy, for evaluating and quantifying power system reliability indices. The first script focuses on the standard composite system adequacy assessment, utilising the DCOPF approach applied to the Roy Billinton Test System (RBTS) and the IEEE-Reliability Test System (IEEE RTS). The second script builds upon the first script by incorporating DC-PSCOPF, and it is also applied to the RBTS and IEEE RTS systems. In order to give some sense of verification of the developed code, a comparison of the obtained reliability indices is conducted using similar methodological approaches.

Sammendrag

Med modernisering av kraftnettet er det avgjørende å ha smarte løsninger for effektiv og sikker systemplanlegging og drift. Tradisjonelle optimeringsmetoder av kraftsystemer blir reevaluert, siden de nå er relevante for nye bruksområder. En slik metode er "Security Constrained Optimal Power Flow" (SCOPF), som er en utvidelse av optimal lastflyt (OPF). I denne avhandlingen, er målet med SCOPF er minimere kostnader gjennom å finne den mest kostnadseffektive fordelingen av kraftproduksjon for et gitt system, samtidig som alle systembegrensninger oppfylles, ikke bare under normale driftsforhold, men også under eventuelle utfall av linjer eller generatorer.

Målet med denne avhandlingen er å benytte en ikke-sekvensiell Monte Carlo-simuleringsmetode og integrere den med en DC optimal lastflyt (DCOPF) ved bruk av programmeringsspråket Python, og rammeverket Pyomo. Hovedfokuset er å vurdere påliteligheten til kraftsystemer. En ny tilnærming for DC "Preventive Security Constrained Optimal Power Flow" (DC-PSCOPF) som er en utvidelse OPF, er utviklet for å vurdere påliteligheten til kraftsystemer. Hovedbidraget i denne oppgaven er implementering av DC-PSCOPF i OPF-analysen av den algoritmiske tilnærmingen ved beregning av pålitelighetsindekser.

Denne avhandlingen er et pionerarbeid innen anvendelsen av SCOPF i pålitelighetsstudier på kraftsystemer, og representerer et forskningsområde som ikke tidligere har blitt grundig utforsket. Integreringen av SCOPF-teknikker, i dette tilfellet DC-PSCOPF, i pålitelighetsanalysen for kraftsystemer videreutvikler rammeverket og dataverktøyene for pålitelighetsanalyse ved Institutt for Elektrisk Energi (tidligere Institutt for Elkraftteknikk), NTNU. Ved å ta hensyn til både normale driftsforhold og eventuelle utfall, har denne nyskapende tilnærmingen som mål å gi verdifulle innsikter i pålitelighetsanalysen av kraftsystemer. Et av målene med avhandlingen er å skape en reproduserbar metode som kan brukes som et springbrett for fremtidig forskning innen emnet. Pålitelighetsindikatorer basert på DCOPF og DC-PSCOPF blir presentert. Det gis en omfattende beskrivelse av den metodiske tilnærmingen brukt, inkludert nødvendige tilpasninger og underliggende antakelser. De detaljerte opplysningene gir en klar forståelse av den anvendte tilnærmingen og sikrer tydelighet i metoden.

Det er utviklet to dataverktøy for implementeringen av DCOPF og DC-PSCOPF i Pyomo-rammeverket i Python. Disse dataverktøyene brukes i kombinasjon med tidligere utviklede dataverktøy tilgjengelig ved Institutt for Elektrisk Energi på NTNU, for å evaluere og kvantifisere pålitelighetsindikatorer for kraftsystemer ved hjelp av de nevnte optimeringsmetodene. Det første skriptet fokuserer på den grunnleggende metoden for pålitelighetsanalyse ved DCOPF, og blir anvendt på *Roy Billinton Test System (RBTS)* og *IEEE-Reliability Test System (IEEE RTS)*. Det andre skriptet bygger videre på det første skriptet ved å inkludere DC-PSCOPF, og blir også anvendt på systemene *RBTS* og *IEEE RTS*. For å gi en viss verifikasjon av koden, gjennomføres det en sammenligning av de oppnådde pålitelighetsindikatorene ved lignende metodiske tilnærminger.

Acknowledgement

I would like to express my gratitude to my supervisor, Associate Professor Vijay Venu Vadlamudi, at the Department of Electric Energy (formerly, Department of Electric Power Engineering), NTNU, for providing invaluable guidance and inspiration throughout the Master's thesis work. It is with great appreciation that I acknowledge his unwavering support.

I am grateful for the discussions and inputs generously shared by Vijay. His availability and willingness to engage in conversations on whatever I had on my mind have been important in not only shaping my understanding of power system reliability, but also in nurturing personal growth and self-reflection. Through these discussions, I have gained insights not only as a researcher but also as an individual, discovering new dimensions of my capabilities and refining my approach in handling challenges.

Vijay's eccentricity, characterised by his memorable analogies, has left a lasting impression on me, one that I am confident will endure in my memory for years to come. I will cherish this memory as a treasured part of my academic journey.

I would also like to express my gratitude to my co-supervisor, Matias Vistnes. His willingness to assist me during technical struggles has been important, providing guidance that helped overcome challenging obstacles. I am grateful for him expecting the best from me, making me challenge myself and my capabilities. I thank him for sharing his knowledge in the field of power system reliability and optimal power flow with me.

I wish both Vijay and Matias all the best in their future endeavours. Their guidance and support have been greatly appreciated, and I am confident they will continue to have positive impacts on the lives of others.

William Flesland Blytt

Trondheim, June 2023

Contents

List of Figures

List of Tables

Abbreviations

AC	Alternating Current
ACOPF	Alternating Current Optimal Power Flow
COPT	Capability Outage Probability Table
CoV	Coefficient of Variation
CSCOPF	Corrective Security Constrained Optimal Power Flow
CYPL	Constant Yearly Peak Load
DC	Direct Current
DC-PSCOPF	Direct Current Preventive Security Constrained Optimal Power Flow
DCOPF	Direct Current Optimal Power Flow
DPL	Daily Peak Load
EDLC	Expected Duration of Load Curtailments
EENS	Expected Energy Not Supplied
ELC	Expected Load Curtailment
FOR	Forced Outage Rate
HLI	Hierarchical Level I
HLII	Hierarchical Level II
HLIII	Hierarchical Level III
HPL	Hourly Peak Load
IEAR	Interrupted Energy Assessment Rate
IEEE	Institute of Electrical and Electronics Engineers

IEEE RTS	IEEE-Reliability Test System
LDC	Load Duration Curve
LOL	Loss of Load
LOLE	Loss of Load Expectation
LOLP	Loss of Load Probability
MCS	Monte Carlo Simulation
NTNU	Norwegian University of Science and Technology
OPF	Optimal Power Flow
PLC	Probablity of Load Curtailments
PSCOPF	Preventive Security Constrained Optimal Power Flow
PSR	Power System Reliability
RBTS	Roy Billinton Test System
SCOPF	Security Constrained Optimal Power Flow
SD	Standard Deviation
TTF	Time To Fail
TTR	Time To Repair
WPL	Weekly Peak Load
YPL	Yearly Peak Load

1 Introduction

1.1 Background and Motivation

Over the years, electricity has been a crucial source of energy delivered to industrial, commercial and residential consumers. Its use is expanding quickly in response to the demand for automation in advanced technologies, and necessary environment friendly energy. The operation and planning of the power system, particularly the transmission system, are to guarantee the economical and secure real-time matching of power generation and demand. Future power systems will need to have the potential to expand into complicated topologies while maintaining cost-effectiveness, security, and reliability in the distribution of electricity. This makes power delivery planning critically important to the large and complex power system.

The challenges of achieving cost efficiency in the power system has been extensively discussed by researchers. In [1], it is shown that billions of dollars could be saved every year in the U.S., as a result of a 5% increase in dispatch efficiency. More efficient methods for solving optimal power flow problems in transmission system planning can be used to achieve this improvement. With adequate control of the power system, the potential savings could be massive. The need for an effective method of solving system operating problems is imposed by both the economic well-being as well as environmental sustainability.

Another important aspect of energy supply and consumption in the modern power system is the need for security and reliability for system operation. The power system may be divided into two parts, the transmission network and the distribution network. A parallel can be drawn to the design of traffic systems. The transmission system is designed to carry huge amounts of energy with minimal loss similar to highways, while the distribution system is responsible for distributing the electricity to end consumers, similar to local roads. For some operating conditions, "traffic jams" may occur in the power system. This can be the power transmitted over a transmission line violating the capabilities of the line, and the congestion may result in cascading failures which may result in blackouts over an expanded scale of the system. Operation of the modern power system often face

stressed conditions. As per Statnett's Annual report [2], the Energy-not-served (ENS) for the last three years is presented, relating to the system operating under stressed conditions. The outages were mainly short, being results from strong storms during the winter, but no significant blackouts due to errors on Statnett's facilities. Table 1.1 shows the operational key figures from the last three years. Delivery reliability and security of supply in the transmission network was satisfactory in 2022. The volume of ENS has been low, the number operational disruptions at Statnett's facilities were at the level of previous years, and the frequency quality was better than the last three the years. It is crucial for the power system, especially the transmission system, to maintain voltage and frequency within the required levels to prevent equipment damage, outages, and blackouts, and ensure uninterrupted power supply.

In the event of a contingency, the power system needs to reconfigure its topology and restore operation according to the different criteria [3], by means of restoring loads and prevent events such as cascading failures. Such critical failures may result in damage of equipment, financial losses, or even deaths. For system security, safety, and economic benefits it is essential to solve the challenges of power system operation taking into account possible contingencies. As a result, in order to ensure overall efficiency, reliability, and security, the operation and planning of a system must not only take into account the normal cases but also need to be designed to withstand uncertainties and disturbances in potentially hazardous circumstances. Such an approach is known as the N-1 criterion.

Table 1.1: *Operational key figures on security of supply from [2].*

Security of supply	Unit	2022	2021	2020
Frequency deviation*	Minutes	9376	10670	9693
Energy not served (ENS)	MWh	83	701	1381
Delivery reliability (1 - ENS/ES)	%	99.9999	99.9986	99.9939

*Frequency deviation measures stability in the power balance. In the Nordic countries, the requirement is that the frequency must be within a band of 50.00 +/- 0.10 Hz.

However, planning that takes into account all risks and circumstances is challenging since

there are additional constraints from different scenarios that need to be identified and considered [4]. There are still unsolved challenges with network topology, uncertainties from renewable energy resources, non-linear performance of network components and computational complexities, to name a few. It is thus necessary to conduct more research on problems related to efficiency and reliability in the planning and operation of the power system.

System operators need to run a load flow model with immense amounts of data to assess the impact and power flows in the power system. Due to the non-convex nature of the load flow equations, it proves troublesome to find global optimal solutions, and no efficient approach is guaranteed in such a problem. In addition, the power system are typically large in size. This leads to difficulties in constructing and solving full-scale mathematical models.

In recent years, a variety of optimisation algorithms have been proposed and assessed in research papers for solving transmission system planning and operation problems. This includes utilising linear approximations [5], convex relaxations [6], interior point method with barrier function [7], distributed methods [8], dual decomposition methods [8][9] and heuristic methods [10]. There has also been developed software and tools offering system operators to make decisions in planning and operation. Some of these tools include Ipopt [11] and LOQO [12]. Although being solutions, they need consideration in the following aspects [13]:

1. Simplified assumptions: To minimise solving time and memory usage, it is preferable to keep the computational burden light. However, many methods rely on assumptions that cannot be realistically achieved in actual operations. For instance, neglecting voltage or reactive power fluctuations may simplify nonlinear constraints, but this approach may result in infeasible solutions and compromise voltage safety.

2. Time and resource issues: While certain approaches can solve non-linear and large-scale problems, they may only be suitable for research purposes. In actual operations, they may encounter difficulties in meeting the required time constraints.

Considering the challenges and difficulties in current power system planning and opera-

tion, this thesis aims to solve power system optimisation problems while ensuring secure power delivery and preventing network violations under contingency situations, following the deterministic N-1 criteria. The main focus is on solving the DCOPF (DC Optimal Power Flow) and DC-SCOPF (DC - Security Constrained Optimal Power Flow) problems in the algorithmic approach of calculating reliability indices, see Figure 1.1.

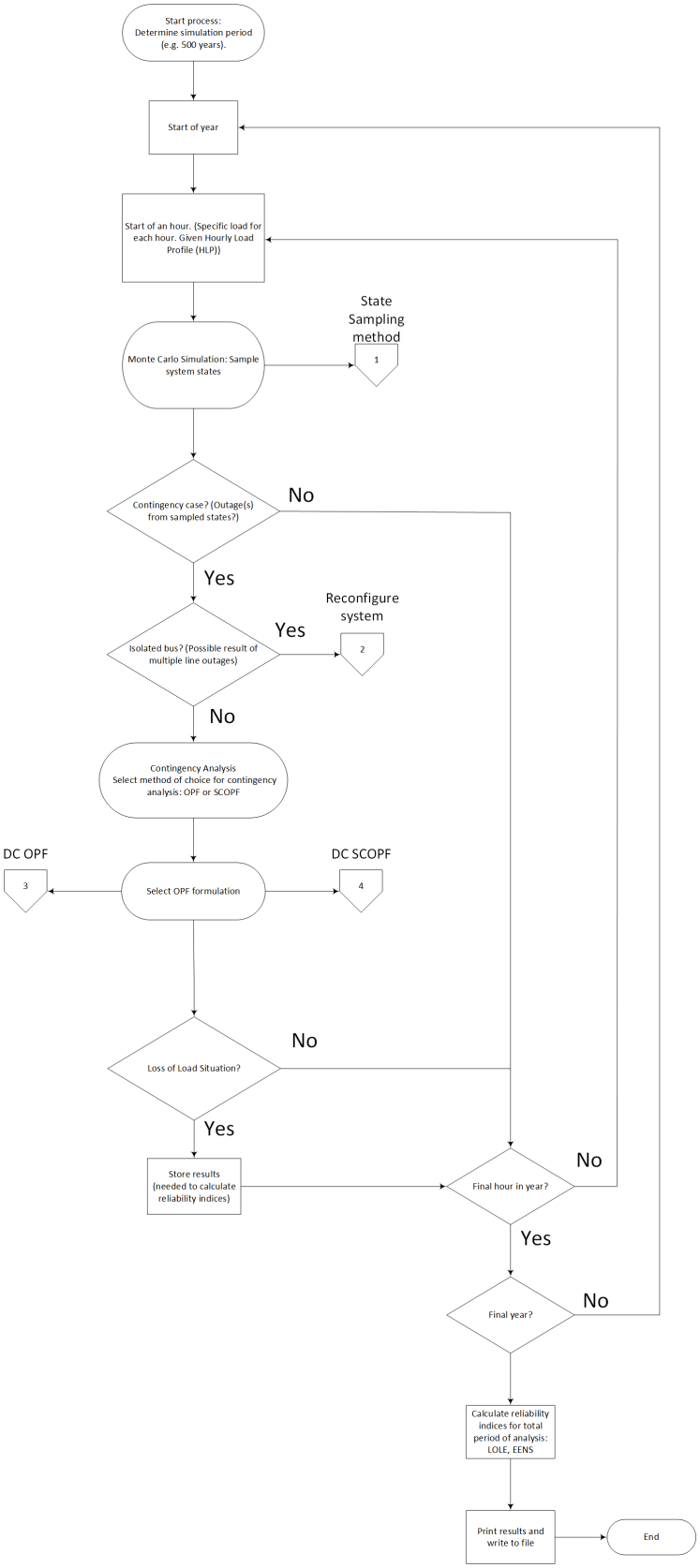

Figure 1.1: *Algorithmic approach in calculating reliability indices.*

1.2 Scope

The scope of work is focused on developing an algorithmic approach for calculating composite power system reliability indices. To achieve this, the OPF analysis is extended to include SCOPF in the contingency solver. By incorporating this technique, the aim is to improve the accuracy and reliability of power system operation and planning.

The intention of this thesis was to conduct a comprehensive analysis of SCOPF in the context of both AC and DC approaches in the contingency solver. Originally, it was planned to incorporate the Corrective SCOPF (CSCOPF) in the analysis, but constraining circumstances necessitated a modification of the approach. As a consequence, the scope of the thesis was adjusted to focus solely on the Preventive SCOPF (PSCOPF) instead. Additionally, due to constraints in resources and time, the analysis was limited to the DC based approach, with the AC based approach excluded from the study. However, the thesis aims to provide valuable insights into the application of DC based PSCOPF, hereby referred to as DC-PSCOPF, in the assessment of power system reliability.

Contributions

The work on this thesis, conducted during Spring 2023, has the following problem statement: *Develop in-house software tools (Python-based) as a part of a comprehensive framework for assessing power system adequacy studies for composite systems, using Monte Carlo simulation methods.*

The adequacy of the composite systems has been quantified using the following reliability indices: Loss of Load Expectation (LOLE) and Expected Energy Not Served (EENS).

1. The main research contribution lies in incorporating SCOPF to the OPF-based in-house code used for power system reliability assessment. This allows for a more comprehensive evaluation of reliability indices and provides a more accurate representation of real-world power system operations. The approach represents an improvement over the previous OPF-based algorithmic approach used for calculating reliability indices, making it a small yet significant contribution to the field of power system reliability assessment.

1.3 Structure of Thesis

At the outset, it must be pointed out that none of the work from the specialisation project report is included in this Master's thesis; during the specialisation project phase, much time was devoted to gaining a better understanding of OPF (theory, scripts, illustrative studies) and conducting a comprehensive literature review on OPF. It was only at the start of the Master's thesis work that it was decided that applicability of OPF and SCOPF in power system reliability studies should be looked into. The thesis is organised into 6 chapters as follows:

Chapter 1 - *Introduction*: This chapter provides background, scope and structure of the thesis.

Chapter 2 - *Conceptual background*: Theoretical fundamentals are presented in this chapter as a prelude to this thesis work. This includes fundamental Power System Reliability (PSR), Monte Carlo Simulations (MCS), Optimal Power Flow (OPF), Security Constrained Optimal Power Flow (SCOPF), and contingency analysis.

The core of the thesis work is presented in Chapters 3 through 6.

Chapter 3 - *Methodology*: This chapter focuses on the methodological approach in the calculation of reliability indices. It presents the implementation of an HLII adequacy assessment, in a step-by-step manner, following the approach illustrated in Figure 1.1. The chapter includes illustrative examples that demonstrate the conceptual background, as deemed necessary.

Chapter 4 - *Code Development and Programming*: This chapter presents the code development of the thesis work. This includes a presentation of the modelling approach.

Chapter 5 - *Case Studies*: In this chapter, the developed standard HLII reliability assessment software is implemented, tested and compared using the RBTS and the IEEE RTS.

Chapter 6 - *Conclusions and Further Work*: A summary of the findings of this thesis work are presented in this chapter, followed by a suggestion of ideas for future work.

2 Conceptual Background

This chapter serves as a foundational introduction to the theoretical fundamentals essential for this thesis work. It covers key concepts such as Power System Reliability (PSR), Optimal Power Flow (OPF), Security Constrained Optimal Power Flow (SCOPF), contingency analysis, and Monte Carlo Simulations (MCS). These concepts form the basis for the subsequent chapters, providing the necessary background knowledge for understanding the methodologies and analyses presented in this thesis.

2.1 Introduction to Power System Reliability (PSR)

The theoretical basis of this Master's thesis' methodology is rooted in the Power System Reliability (PSR) framework. The term "reliability" refers to a system's capacity to perform its intended function within specified conditions for a specific duration of time [14]. However, the PSR framework is intricate, and its evaluation can be generally split into two areas: adequacy and security [15]. Each of these domains takes into account different aspects of the reliability analysis.

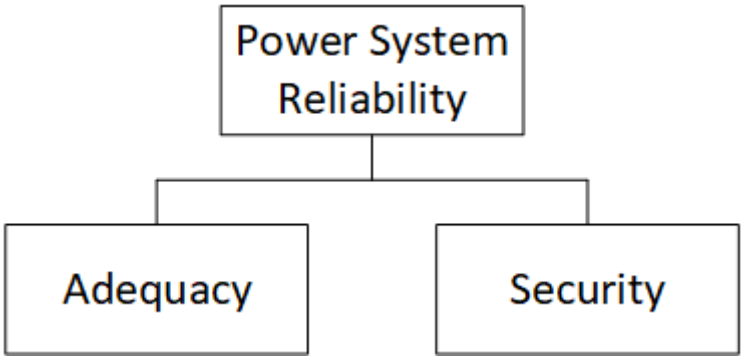

Figure 2.1: *Power System Reliability.*

The two sub-domains of the PSR framework differ mainly in their focus on either the static or dynamic conditions of a system. Adequacy studies primarily evaluate the static conditions of a power system, such as whether the system's generation capacity is adequate to meet its load requirement. Other factors may also be considered, such as whether the transmission and distribution infrastructure can adequately transport energy from

generating facilities to end consumers. In contrast, security assessment primarily deals with the dynamic aspects of a system.

The security assessment focuses on the dynamic events that occur within a system when exposed to disturbances, such as line faults or the loss of generating units. The critical concern during such disturbances is whether the system can remain within its stability limits, when transient effects are induced during such disturbances. Additionally, these effects can occur when the system transitions between different states. However, adequacy studies typically overlook these effects and instead concentrate on whether the system meets its steady-state requirements for each state [15]. In this thesis, only the adequacy aspect of PSR will be considered.

2.1.1 Hierarchical Levels

Typically, PSR studies are categorized into hierarchical levels (HL) based on the functional zones of the power system they encompass [15].

The first level, HLI, evaluates the adequacy of generation capacity, while HLII, the second level, considers both the generation and transmission facilities. A complete adequacy assessment of the system, HLIII studies, examines not only the previously mentioned functional zones but also includes the distribution facilities. The inclusion of the distribution facilities poses a significant challenge for conducting HLIII studies, as it typically results in large-scale models. Nevertheless, this challenge can often be overcome by conducting isolated studies focused solely on the distribution functional zone, which reduces the scale of the problem [15]. A representation of the HLs is shown in Figure 2.2. The focus of this thesis will revolve around the adequacy studies related to HLII, but some background on HLI is supplied.

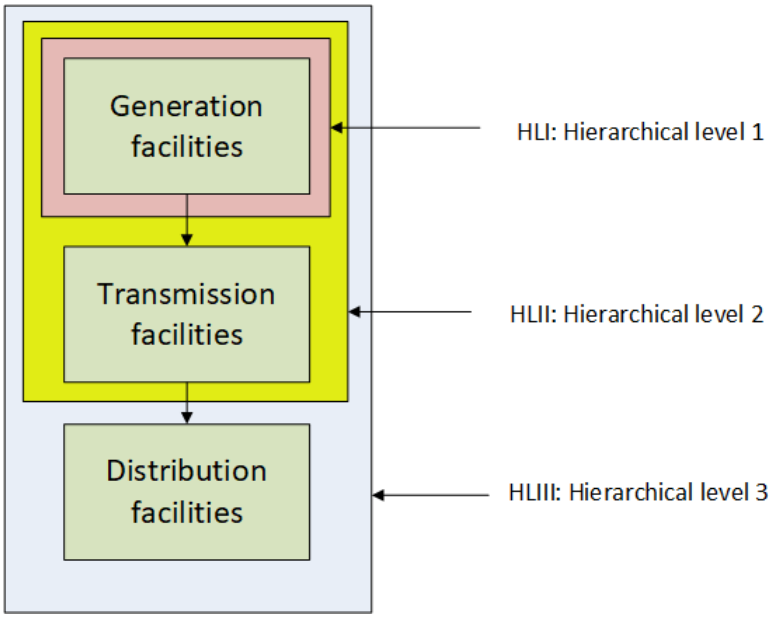

Figure 2.2: *Hierarchical levels.*

HLI studies focus on assessing the ability of a power system's generation facilities to meet a power system's load demand. These studies do not concern the energy transport capabilities of the power system. To create a HLI model, the generating units and loads of the system are combined into equivalent models, as seen in Figure 2.3. The fundamental modeling technique in HLI studies involves merging the generation and load models to create a probabilistic risk model. To determine reliability indices, the total generation capacity is compared to the total load requirement [15].

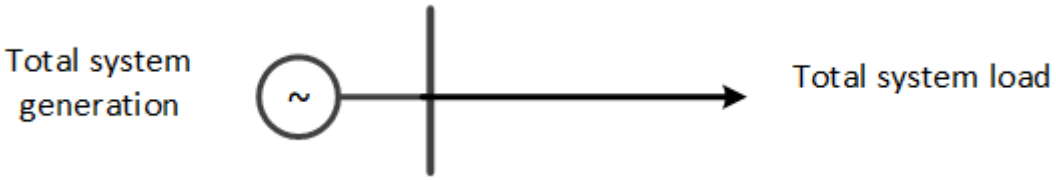

Figure 2.3: *HLI.*

HLII studies incorporate the transmission system's network topology in their adequacy assessment, which involves analyzing the system with additional parameters. While the focus of HLII studies is related to the adequacy of the system, they typically take into account steady-state security constraints such as voltage limits on buses in the system during the evaluation process [16]. Including a model of the network topology in HLII

makes it possible to obtain reliability indices both for the system, and the buses themselves. However, performing assessments at this level can be more complex due to the need for load flow analysis, which can significantly increase computation time. To improve the evaluation process speed, various techniques have been developed, including intelligent system methodologies that classify system state vectors through algebraic comparisons against pre-solved vectors, rather than solving each system state using OPF methods [17]. One method suggested is the use of Self-Organizing Maps [18].

Regarding the load flow analysis being a part of the HLII studies, there will in this thesis be two OPF approaches examined: one DCOPF formulation, and one DC-PSCOPF formulation. Both will be presented in detail in Chapter 3. The DC power flow approach simplifies the OPF problem by disregarding reactive power and voltage limit considerations. Consequently, a linear OPF problem is obtained instead of the nonlinear OPF problem associated with the AC-based approach. As a result, the optimisation process is less complex, and computation time is reduced compared to the AC-based OPF approach. The OPF approach is extended to consider the more complex Security-Constrained-Optimal Power Flow (SCOPF).

Reliability methods that are based on probability can be broadly classified as either analytical or simulation based. Analytical methods represent the system using a mathematical model and calculate reliability indices using a set of equations. Several analytical methods are available: the state space method, minimal cut set method, and contingency enumeration method are among the more common methods used [19]. The state space method evaluates all potential system states during the assessment. However, for larger systems, this can result in an excessive number of states to analyze, which necessitates the use of network reduction techniques to simplify the process and reduce computational effort. The minimal cut set method concentrates on determining reliability indices only at selected load points, rather than the entire system. Therefore, only contingencies that have the potential to impact the load points are considered, leading to a reduction in computation time. Finally, the contingency enumeration method assesses only a predetermined number of contingencies, with the depth of contingencies chosen based on the desired level of accuracy.

On the other hand, there are the simulation methods. They often are based on MCS

methodology, and they replicate a sequence of experiments on a mathematical model of the system [20]. Through such simulations, the stochastic nature of the system may be captured. In addition to providing mean values, MCS methods can also produce distributions for the indices if a sequential method is selected instead of a non-sequential method [21]. Sequential methods are preferred when operation of the system is dependent on its history [20]. The work of this thesis has its emphasis in the simulation methods.

2.2 Load Model

Load variations within a specified time frame, typically a year, can be effectively captured through the implementation of a load model. The time period can be divided into increments based on the desired level of model accuracy. The simplest form of such a model is the constant yearly peak load (CYPL), which corresponds to the highest load demand observed within a year. However, the CYPL model suffers from limited accuracy as it only represents a few days out of the entire year. To achieve improved accuracy, alternative models such as the weekly peak load (WPL), daily peak load (DPL), and hourly peak load (HPL) are used. It should be noted that the use of the DPL and HPL models results in increased computational time, but they offer a more precise representation of the behavior of the load variations throughout the year [22].

Figure 2.4 illustrates chronological representations of CYPL, WPL, DPL and HPL for the first week of the year for the load model presented in [23]. Each time increment within this period is associated with a distinct load level. Furthermore, it is important to highlight that WPL is determined by selecting the peak load value from DPL for each week. The same relationship holds true for HPL. Consequently, both CYPL and WPL tend to exhibit more pessimistic load levels compared to DPL and HPL.

An alternative approach to representing the load model is through a load duration curve (LDC), which arranges the load values in descending order [24]. Figure 2.5 depicts the LDC for each of the distinct load models. Observing the LDC, it becomes apparent the the CYPL model remains constant at 185 MW, while the load demand range for HPL extends from 160 MW down to 72 MW. Once again, it is evident that the CYPL model exhibits a significantly more pessimistic representation compared to the use of the HPL

model.

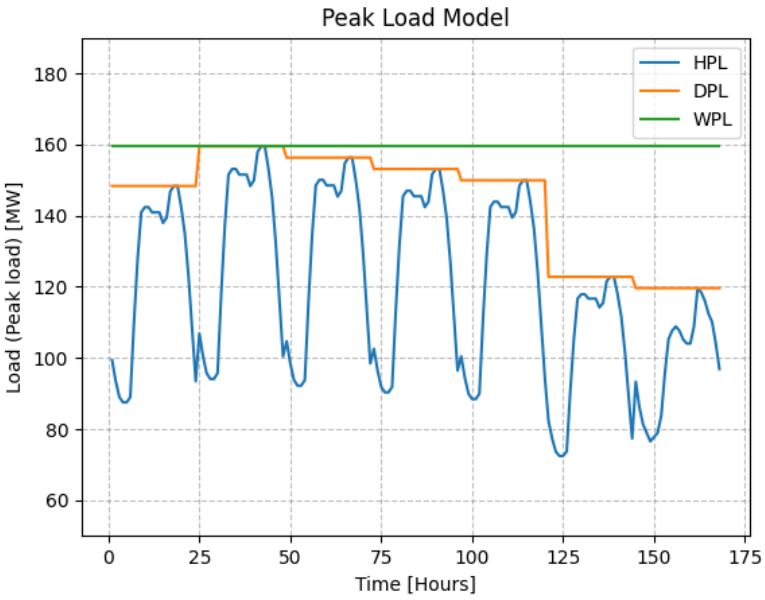

Figure 2.4: *Chronological load representation from the first week of the year in the load data from [23].*

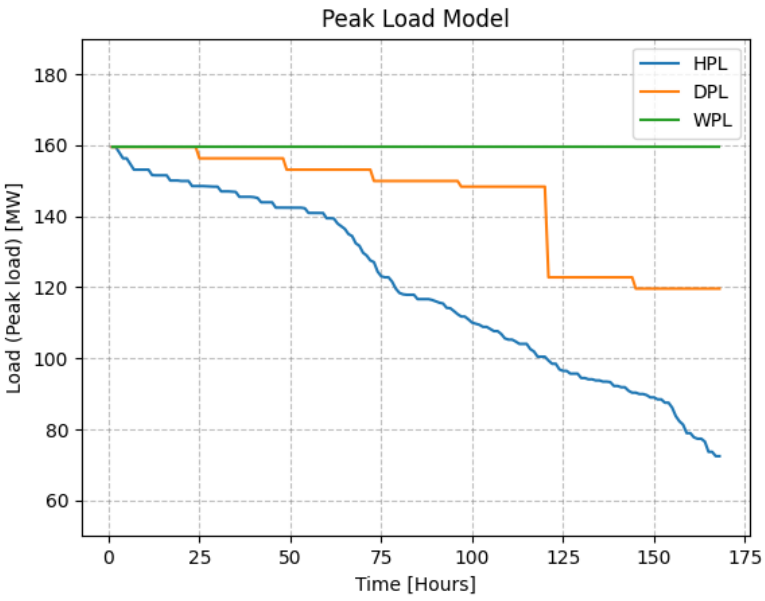

Figure 2.5: *Descending load representation from the first week of the year in the load data from [23].*

2.3 State Models

In the field of reliability assessment, there are two distinct state models that can utilised: a two-state model and a multi-state model. The two-state model operates on the premise that each component can exist in one of two states, namely fully available or fully unavailable [24]. The availability of a component is determined by its forced outage rate (FOR), which represents the probability of the component being entirely unavailable. If FOR is equal to 0.01, it signifies a 1% probability of the component being in an outage state, while there is a 99% probability of it being available [24]. Figure (2.6) illustrates this concept.

In contrast, a multi-state model involves more than two states, known as derated states, which are characterized by partial availability. Figure (2.7) provides an illustration of this concept. In the scenario in the figure, the system can exist in three distinct states: fully available, fully unavailable or derated with half of its capacity being available [23]. This thesis will solely cover the two-state model.

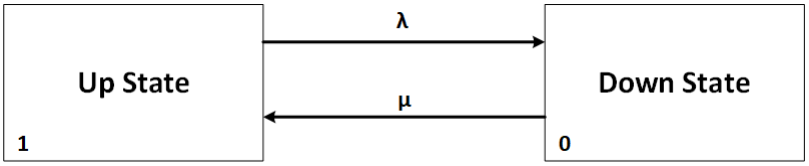

Figure 2.6: *Two-state model. Figure adapted from [25].*

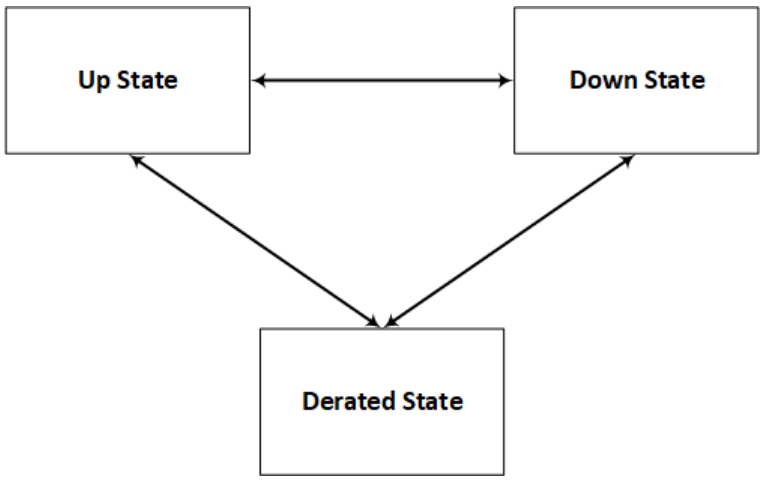

Figure 2.7: *Example of multi-state model. Figure adapted from [25].*

2.4 Probabilistic Indices in HLII Assessment

In the literature, several variations for HLII indices are provided [26], [27], [28]. It is worth noting that the descriptions, abbreviations, and notations utilised for the indices may vary. This disparity arises from the fact that the indices are designed to convey diverse information, subject to the specific objective of the assessment at hand.

According to [25], the indices used in HLI assessments may be extended to the HLII assessments. In the HLII assessment, transmission lines are included in addition to the generation capacity and load which are parts of the HLI assessment. This means that for example Loss-of-Load (LOL) events do not only depend on the generators and loads, but also the capacities of the transmission lines. LOL-indices are dependent on the load model, and must be interpreted differently for each load model [24].

The probabilistic indices of HLII can be categorized into two groups: individual load point and system indices [26]. The individual load point indices are determined by assessing each load bus individually, while the system indices assess the overall adequacy of the system. This thesis encompasses the application of indices from both categories. Considering the extensive range of HLII indices available, this thesis focuses on the most comprehensive ones, as documented from [25][26].

2.4.1 Loss of Load Probability (LOLP)

The LOLP is a probability index that displays the probability of a LOL situation for a given time period. LOL situations occur if the load demand exceed available capacity, which can happen for different reasons, such as a generation unit out of service or an unexpected increase in demand [22]. In an analytical approach, the LOLP is calculated by comparing the load model to the generation model, known as the capacity outage probability table (COPT). Equation (2.1) shows the LOLP-value in time increment t [22].

$$LOLP_t = P(L_t > C - X) = P(X > C - L_t) \tag{2.1}$$

X is the capacity outage, C is the installed capacity of the system, and L_t is the load at

a specific time increment t. $P(L_t > C - X)$ is the probability of demand exceeding the available capacity, while $P(X > C - L_t)$ is the probability of having an outage capacity that is larger than the installed capacity, minus the load at that particular time increment [22]. This is shown to illustrate that $LOLP_t$ can be expressed in two different ways.

2.4.2 Loss of Load Expectation (LOLE)

The LOLE is a well recognised reliability index used by power system planners and operators. It displays the expected number of days (or hours, depending on load model used), on which a load loss will occur. The calculation of LOLE consist of the summation of all $LOLP_t$ values over a time period [24].

Typically LOLE-values are zero when excess generating capacity is present, as well ass off-peak load periods. Similarly, non-zero values are present during peak periods or during periods that generating capacity are undergoing maintenance, and therefore not able to provide capacity. The LOLE does not indicate the severity and neither does it indicate the frequency nor the duration of the loss of load [15]. Equation (2.2) and Equation (2.3) illustrates how to calculate LOLE in terms of days/year (DPL-model) and hours/year (HPL-model), respectively.

$$LOLE = \sum_{t=1}^{365} P(X > C - L)\Delta T, \quad \left[\frac{days}{year}\right] \tag{2.2}$$

$$LOLE = \sum_{t=1}^{8760} P(X > C - L)\Delta T, \quad \left[\frac{hours}{year}\right] \tag{2.3}$$

$P(X > C - L)$ is the probability that peak load is not met. ΔT is the time period for which a given peak load exists. C is the total installed generation capacity in the system not on outage. L is the system load for a given time [22].

LOLE analysis is used to determine the level of installed generation that is necessary to achieve a certain level of resource adequacy. According to [29] European reliability regulation is not uniform. LOLE-standards for some countries are presented in Table 2.1.

Table 2.1: *Reliability standard for LOLE in Europe [29].*

	LOLE [hour/year]
Belgium	3
France	3
Great Britain	3
Ireland	8
The Netherlands	4

2.4.3 Probability of Load Curtailments (PLC)

The Probability of Load Curtailments (PLC) represents the probability of load curtailment, including all states denoted as S where such curtailment, or load shedding, occurs [25]. The expression for PLC, as illustrated in Equation (2.4), involves the summation of curtailment values x_i for each system state i in which curtailment is present [22].

$$PLC = \sum_{i \in S} P(x_i) \tag{2.4}$$

2.4.4 Expected Load Curtailments (ELC)

The Expected Load Curtailments (ELC) quantifies the anticipated capacity shortage, as defined by Equation (2.5). In this equation, C_i represents the curtailment of state i, and F_i denotes the frequency of state i [22].

$$ELC = \sum_{i \in S} C_i F_i \tag{2.5}$$

The determination of F_i can be elaborated using Equation (2.6), which involves the set $\mathcal{N}$ comprising all feasible departure rates corresponding to state i, p_i denoting the the probability of the state, and δ_k representing the departure rate [25].

$$F_i = p_i \sum_{k \in \mathcal{N}} \delta_k \tag{2.6}$$

2.4.5 Expected Duration of Load Curtailments (EDLC)

The Expected Duration of Load Curtailments (EDLC) represents the anticipated duration, measured in hours or days, during which load curtailments are expected to occur within a year [25]. The calculation of EDLC depends on the model employed, as demonstrated by Equation (2.7), for the HPL model, and Equation (2.8) for the DPL model [22].

$$EDLC_{HPL} = PLC \cdot 8760 \tag{2.7}$$

$$EDLC_{DPL} = PLC \cdot 365 \tag{2.8}$$

2.4.6 Expected Energy Not Served (EENS)

EENS is an important index in HLII assessment [25]. Equation (2.9) illustrates the EENS for HLII assessments. x_j is the curtailment in MW, and $p(X = x_j)$ is the probability that the curtailment is x_j. For a more thorough description of the EENS from HLI assessments, the reader is referred to [25]. The thesis [22] also provides a concise overview.

$$EENS = \sum_{t=1}^{8760} \sum_{x_j = C - L_{tot}}^{C} \left[x_j - (C - L_{tot})\right] \cdot p\left(X = x_j\right) \tag{2.9}$$

2.5 Monte Carlo Simulation Methods

Broadly speaking, the assessment of Power System Reliability (PSR) adequacy can be classified into two approaches: deterministic and probabilistic methods, as is shown in Figure 2.8. Deterministic methods primarily focus on estimating the required generation and network capacities within the system. However, they overlook the inherent randomness of the system, such as uncertain load variations and random failures [30]. In contrast, probabilistic reliability assessment specifically addresses the stochastic characteristics of the power system, taking into account its probabilistic nature.

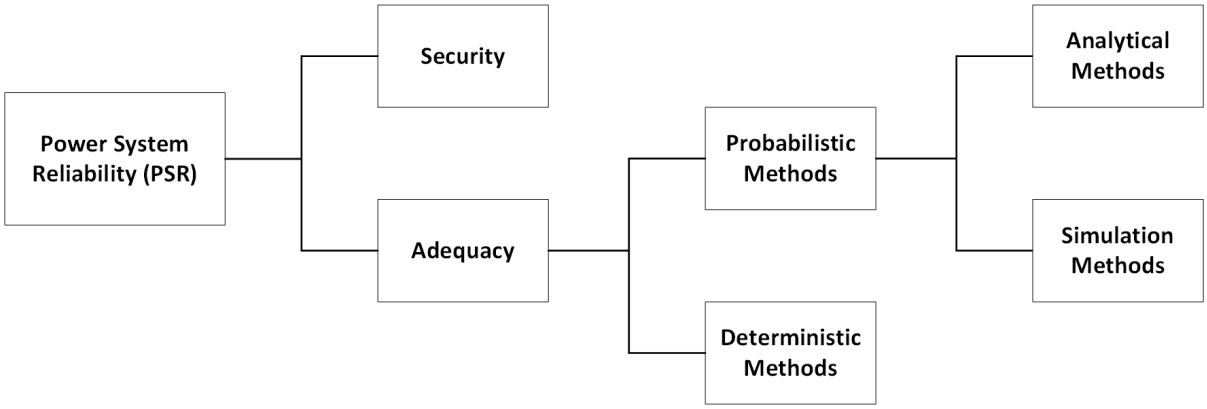

Figure 2.8: *PSR methods, adapted from [15] and [22].*

As seen from Figure 2.8, probabilistic methods may be divided into analytical methods and simulation methods. Analytical techniques apply mathematical formulations to assess the adequacy of the system, whereas simulation techniques replicate the stochastic behavior of the system [22]. One commonly utilized simulation technique for evaluating PSR is Monte Carlo Simulation (MCS), which will be discussed in detail in subsequent sections of this chapter.

This thesis excludes the examination and discussion of analytical methods. Instead, the emphasis will be placed on simulation methods, particularly MCS, which is presented in this section.

Within PSR, MCS serves as a technique for sampling system states by using random numbers derived from probability distributions. This methodology enables the simulation of the stochastic characteristics inherent in a system [25].

In practical use, MCS involves the generation of random numbers to determine the system state of components at a given time increment. MCS offers several advantages over analytical methods. Firstly, MCS is not contingent upon system size and demonstrates superior performance when assessing larger systems. Additionally, an advantage lies in the capability of MCS to simulate probability distributions associated with failure and repair events, which is generally challenging to address using analytical methods [25].

MCS methods can be classified into two categories: sequential and non-sequential simulation methods. Non-sequential MCS methods involve sampling a set of independent

system states by generating random variates. In contrast, sequential MCS methods generate a sequence of system states where the current state depends on the previous state. The forthcoming sections of this chapter will delve into the State Sampling method, State Duration method, and the State Transition method, all based on the approach in [25], providing detailed explanations of these methods. Before the methods are explained, a basis of the mathematical understanding of random number generation and probability distributions are presented. At the end of the chapter, the convergence criteria of MCS is shown.

2.5.1 Random Number Generation in MCS

Random number generation uses what is called a random variate, which is a random variable that follows a certain distribution [25]. The uniform distribution is frequently encountered. It is characterized by a range $[0, 1]$, wherein intervals of equal length possess an equal probability of occurrence. The exponential distribution, shown in Equation (2.10), is also commonly used in MCS [25].

$$f(X) = \lambda \cdot e^{-\lambda X} \tag{2.10}$$

Here, X is the random variate, and λ is called the shape parameter. Following the methodology of [25], the inverse transform of the exponential distribution is defined, in order to be able to obtain random variates with the exponential distribution. The cumulative distribution of Equation (2.10) is defined, given in Equation (2.11).

$$F(X) = 1 - e^{-\lambda X} \tag{2.11}$$

To obtain the inverse transform, Equation (2.11) is set equal to U as defined above, a number that is uniformly distributed between $[0, 1]$. As shown in Equation (2.12), the equation is solved for X. It is utilised that the distribution of U and $1 - U$ are identical, with U having the range of $[0, 1]$ [25].

$$X = F^{-1}(U) = -\frac{1}{\lambda} \ln 1 - U = -\frac{1}{\lambda} \ln(U) \tag{2.12}$$

In methods where time to failure and time to repair follow the exponential distribution,

as in the State Duration and State Transition method, the method described is used to obtain the random variates [25].

2.5.2 State Sampling Method

First, the State Sampling method is considered. It is a non-sequential approach for the sampling of system states meaning it is not dependent on previous states, it is chronologically independent [25]. In this approach, each component of the system is subject to sampling. These components are characterized by a uniform distribution spanning the interval $[0, 1]$. For every component, a random number U is generated, and then compared with the FOR value of the component. If U exceeds or equals the FOR value, the component is considered available; otherwise, if U is smaller, the component is deemed unavailable. The aggregate of available capacities provides insight into the overall system state. Conducting the sampling process over a significant number of years, allows for the derivation of indices. Nevertheless, the method's main drawback resides in its inability to capture information regarding frequency and duration [25].

2.5.3 State Duration Method

The State Duration technique instead examines the state duration distribution functions rather than concentrating on the likelihood that a particular component will be in a given condition at any given moment. The distributions for a component with two states are operational and repair [25]. These are assumed distributed exponentially in this example, but they might have any distribution.

Through the inverse transform method from [25] used on the cumulative probability function of an exponential distribution, the time each component stays in one state is given by Equation (2.13) and Equation (2.14) [25].

$$T_{TTF,i} = -\frac{1}{\lambda_i} \ln U_i \tag{2.13}$$

$$T_{TTR,i} = -\frac{1}{\mu_i} \ln U_i \tag{2.14}$$

$T_{TTF,i}$ is the time to failure, $T_{TTR,i}$ is the time to repair, λ_i is the failure rate and μ_i is

the repair rate. U_i is a uniformly distributed variable in the range $[0, 1]$ [25].

To exercise the State Duration approach, the following steps are necessary, depicted from [25]:

- An initial state for each i-th component must be determined. A typical assumption is to set each component to up-state.
- For each i-th component, determine the time it is present in its initial state and record it. Then, determine the time it takes for the component to change state again. This process is repeated until the chronological component state is found for the required observing time.
- The individual component chronological state is combined to obtain the total system chronological state.
- From the chronological state the system state vector, S, can be found for a given point in time, and used to calculate reliability indices.

Figure 2.9 illustrates the chronological component state transition process, and Figure 2.10 the chronological system state transition process.

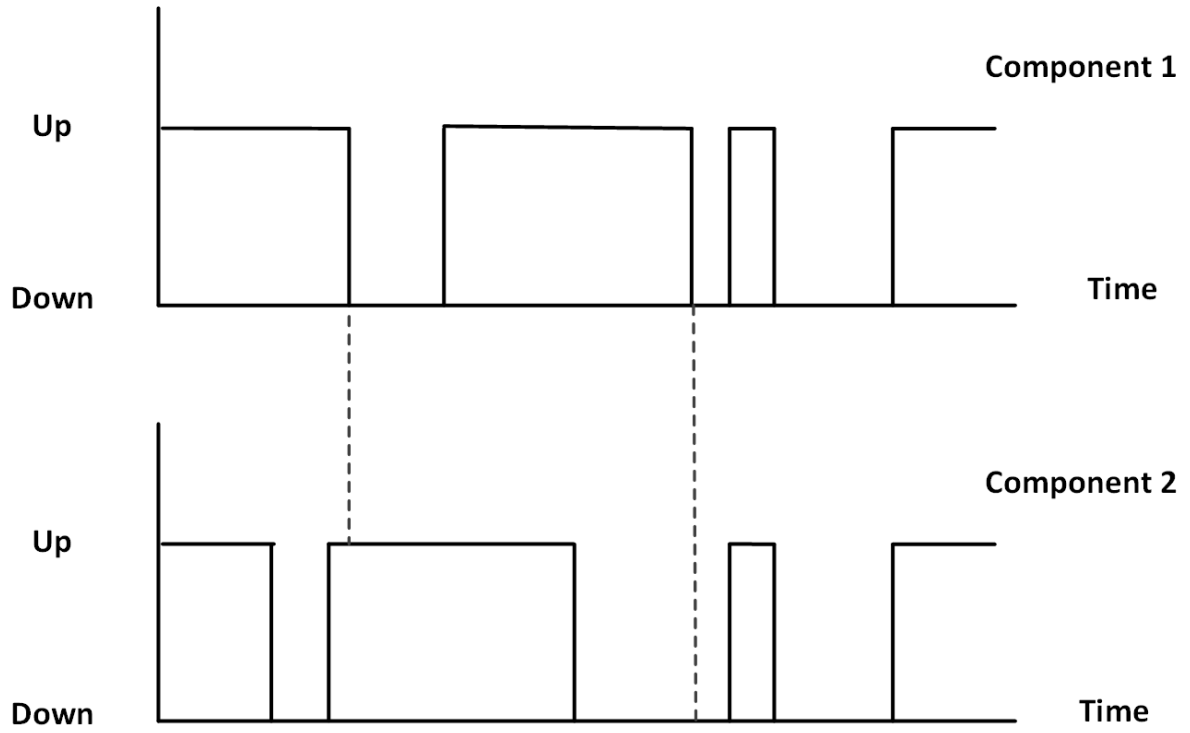

Figure 2.9: *Component state transition process. Figure adapted from [25].*

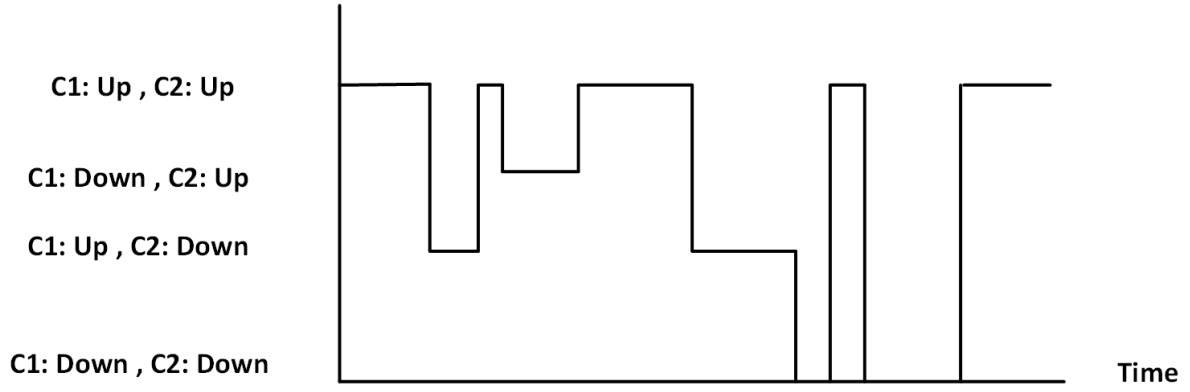

Figure 2.10: *System state transition process. Figure adapted from [25].*

2.5.4 State Transition Method

The State Transition approach emphasizes on how the whole system transitions from one state to another, instead of each individual component as in the State Duration approach [25].

Again, all system components are assumed to follow the exponential distribution. A

state S consisting of m components, each with a transition rate λ_i is assumed. In this case, λ denotes both failure rate and repair rate. The transition rate for the whole system, λ, with a given system state is given by the sum of all the individual components transition rate. As all the components are exponentially distributed, so is the system [25]. Equation (2.15) shows that the total transition rate out of the given system state is found as the sum of the transition rates out of it [31].

$$\lambda = \sum_{i=1}^{m} \lambda_i \tag{2.15}$$

When a component transitions, the system transfers from one state to the next. In other words, transition of the system state depends randomly on the state duration of the component which departs earliest from its current state. Therefore, the duration T of the system state is a random variable expressed in Equation (2.16) [25].

$$T = \min T_i \tag{2.16}$$

The time between transitions may be sampled from Equation (2.17), which follows from T being exponentially distributed.

$$T = -\frac{1}{\sum_{i=1}^{m} \lambda_i} \ln U \tag{2.17}$$

Exploiting that T_i and T follow an exponential distribution, the probability for the transition from the present state due to a change in the state at component j is given by Equation (2.18) [25].

$$P_j = P(T_j = t_0 / T = t_0) = \frac{\lambda_j}{\sum_{i=1}^{m} \lambda_i} \tag{2.18}$$

$$\sum_{j=1}^{m} P_j = 1 \tag{2.19}$$

P_j is the probability that the next component to change is component j. t_0 is the time at which the change occurs. λ_j is the transition rate for component j. $\sum_{i=1}^{m} \lambda_i$ is the transition rate for the system. $P(T_j = t_0/T = t_0)$ is the probability that the transition in component j coincides with the transition of the whole system, which is equal to P_j. A more in-depth derivation of this result can be seen in [25].

To illustrate the result from Equation (2.18), Figure 2.11 is provided. A random variable U in the interval $[0, 1]$ is generated, and Equation 2.18 gives intervals for each component. When U in present in the interval for component j, this implies that the system state will transition due to a transition in component j. In Figure 2.11, when U falls in the interval for P_j, leading to state P_j being the next state for the system [25].

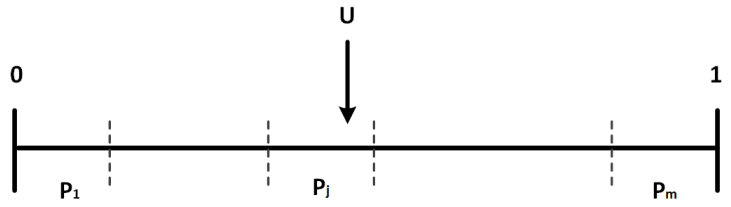

Figure 2.11: *Selection of next state in State Transition approach. Figure adapted from [25].*

Similarly to the State Duration approach, λ_i for the component that transitions must be updated before the subsequent calculation is done.

A summarized step-by-step approach can be formulated, as described in [25]:

1. An initial state S_0 is determined. Typically, all units are set to up-state.
2. Time is recorded from initial to the next system state by generating a random variable U_1 and using Equation (2.17).
3. The next system state is determined by generating random uniformly distributed variable U_2 in the range $[0, 1]$, and Equation (2.18) is applied.
4. λ_j is updated for the component that transitioned.
5. Repeat from step two until required observing time is found.
6. System states are determined, and reliability indices calculated.

Being a sequential approach, frequency indices may be calculated, which is a benefit [25]. Another positive feature is that it is less computationally extensive compared to State Duration approach as it needs fewer random variables and information to be stored.

A drawback is the necessity for T and T_j to be exponentially distributed, making it a requirement for the approach. This is, however, common in PSR analysis [25].

2.5.5 Concept of Monte Carlo Simulation

The behavior of a group of n identical systems operating in real time will vary to some extent. This includes the number of failures, time duration between failures, and the restoration times. This variation arises from the random nature from the processes involved. In turn, this means any particular system may exhibit any of these behavior patterns. The purpose of the simulation process is to predict these real-life behavior patterns in a simulated environment, in order to estimate the expected or mean value of reliability parameters. [24]

To illustrate the concepts of understanding system behavior, a simple example is considered: the toss of a coin. Using the relative frequency interpretation of probability, Equation (2.20), the probability of getting heads or tails in a throw can be estimated [24].

$$P(tails) = \lim_{N \to \infty} \left(\frac{T}{N} \right) \tag{2.20}$$

where T is the number of tails, and N is the number of tosses. Figure 2.12, 2.13, 2.14 shows the results from throwing a coin 30, 250, and 10 000 times, respectively. The graphs are plotted in Python. The selection of random values is done through the `numpy` library, using the method `random.choice()`.

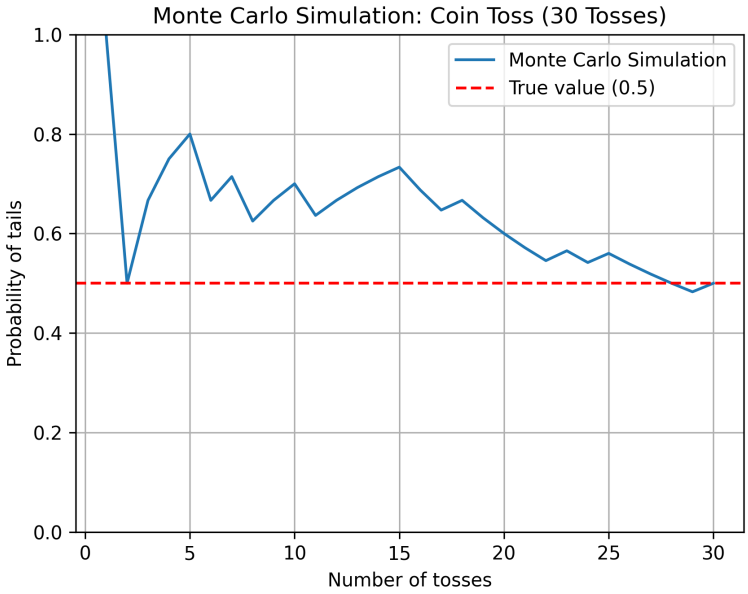

Figure 2.12: *Probability of tossing tails over 30 tosses. Figure inspired from [24].*

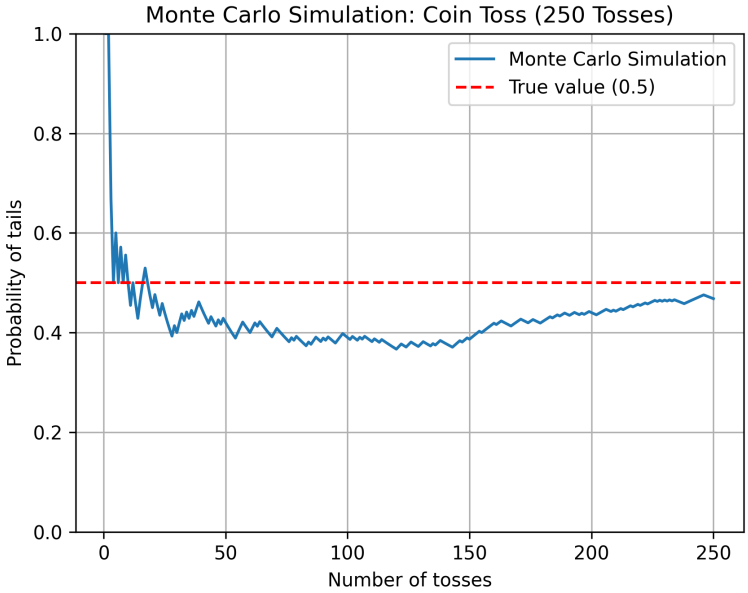

Figure 2.13: *Probability of tossing tails over 250 tosses. Figure inspired from [24].*

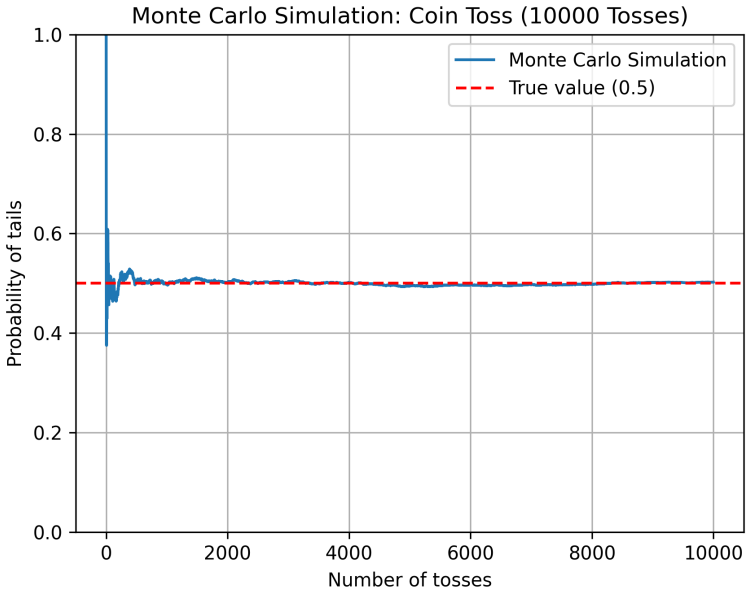

Figure 2.14: *Probability of tossing tails over 10000 tosses. Figure inspired from [24].*

Some key takeaways can be indicated from the results of the coin tossing example, which are essential to keep in mind when working with MCS [24].

- From a limited number of coin tosses, there is significant inaccuracy in the estimation of probability, necessitating a larger number of tosses for a more reliable assessment.
- The probability value fluctuates, but tends to converge towards the true value as the sample size increases.
- Despite not being shown, for a repeated sample, the sequence of outcomes could differ, resulting in a completely distinct pattern of probabilities.
- The true value may occur during the random process. This is not generally known.

2.5.6 Reliability Indices Using Monte Carlo Simulations

As depicted in Section 2.5.5, it is impossible to come to a firm conclusion since MCS is stochastic rather than analytical. Instead, the MCS is run for several simulated years, and the indices for each year are stored. Using this, the mean and variance of the results

may be calculated using Equation (2.21) and Equation (2.22) [24]. In the two equations, N represents the number of simulations, and x_i the value of parameter.

$$E\left[x\right] = \mu_x = \frac{1}{N}\sum_{i=1}^{N} x_i \tag{2.21}$$

$$Var\left[x\right] = \sigma^2 = \frac{1}{N-1}\sum_{i=1}^{N}(x_i - \mu_x)^2 \tag{2.22}$$

It should be noted that these values only provide an estimate of the true values, as shown in Equation (2.20). Only when the value of N tends towards infinity, the mean and variance of the MCS approach their true expected value μ_x and true variance σ_x for the system. Because of this, the mean of the yearly indices is used to calculate the MCS indices. This results in an augmentation of the equations for LOLE and EENS, shown in Equation (2.23) and Equation (2.24). This comes from the combination of Equation (2.21) with Equation (2.3) and Equation (2.9) [22].

$$LOLE_{MCS} = \frac{\sum_{i=1}^{N}\left[\sum_{j=1}^{M} x_j \cdot \Delta t\right]}{N} \tag{2.23}$$

$$EENS_{MCS} = \frac{\sum_{i=1}^{N}\left[\sum_{j=1}^{M} x_j \cdot C_j \cdot \Delta t\right]}{N} \tag{2.24}$$

N is the number of years sampled. M is the number of time steps per year, depending on the time scale used per year (e.g. DPL or HPL). x_j is a binary variable that takes the value 0 or 1 and represents if a LOL situation has occured at the time step j. Δt is the time increment per step. C_j is the severity of the outage in MW [22].

Obtaining the true indices with absolute accuracy is impossible because it is not possible to execute an infinite number of simulations. The potential error of the indices can, however, be calculated. According to the central limit theorem, the population produced by the estimated mean values from the MCS has a normal distribution. This distribution is given as $\mathcal{N}\left[E\left[\bar{x}\right], Var\left[\bar{x}\right]\right]$. For the normal distribution $E\left[\bar{x}\right] = \bar{x}$, and $Var\left[\bar{x}\right] = \frac{\sigma^2}{N}$. As N increases, the obtained average will be increasingly more likely to be located close to the true mean. Because of this, the variance of the distribution is used to determine the accuracy of a MCS [31], given by Equation (2.25).

$$Var\left[\bar{x}\right] = \frac{1}{N(N-1)}\sum_{i=1}^{N}(x_i - \bar{x})^2 \tag{2.25}$$

2.5.7 Monte Carlo Simulation Convergence Criteria

The convergence of MCS is a fluctuating process, because it relies on generating random number, as illustrated in Section 2.5.5. Therefore, the addition of a few more samples does not necessarily lead to improved accuracy [25]. However, as the number of samples increases, the range errors become smaller. This phenomena where the sample mean approaches the true mean when the number of samples tends towards infinity, is shown in Section 2.5.5. Consequently, a larger number of samples decreases the variance and brings the value closer to the true mean. Thus, the variance can be utilised as a criterion for determining the convergence of the MCS approach [22].

The precision of reliability assessment using MCS can be effectively evaluated by using the CoV, which is illustrated in Equation (2.26). The CoV serves as a convergence criterion in this context [22].

$$\beta = \frac{s(X)}{\sqrt{N} \cdot E(X)} \tag{2.26}$$

$s(X)$ represents the standard deviation (SD) of a sample, N denotes the number of samples, and $E(X)$ corresponds to the population mean [31]. Examining the expression, it is revealed that minimising the CoV necessitates either reducing the variance or increasing the number of samples.

It is important to acknowledge that the indices used in PSR adequacy assessments have variations in convergence speed. For example, the EENS demonstrates the slowest convergence speed. Therefore, when determining the amount of samples for a simulation, it is desired to utilise the EENS index when calculating the CoV [25]. By adopting this approach, a more accurate evaluation of the reliability indices can be achieved.

As previously mentioned, the convergence criteria of the MCS play an important role in deciding the required number of samples for achieving an accurate evaluation of the reliability of a system. The chosen CoV representss a trade-off between evaluation accuracy and computational time in the MCS. In accordance with [25], it is emphasized that specifying a reasonable stopping criterion specific to a particular system is essential to strike a balance between accuracy and computing time. This consideration may need an examination of the system that is being investigated. Hence, the selection of CoV should

also be tailored to the characteristics of the system analyzed [22].

In order to determine an accurate evaluation of reliability indices, various approaches exist for utilising the CoV to secure a sufficient number of samples in the simulation [25]. As mentioned, one method involves terminating the simulations once the CoV attains a predefined tolerance value: a tolerance criterion. In practice, the CoV is acquired for each sampled state, and upon reaching the specified tolerance criterion, the simulations conclude and the indices are calculated. Another method is to set a predetermined number of samples, and then calculate the CoV. If convergence is not achieved, the number of samples should be increased. This results in some instances where more samples are simulated than strictly necessary, which further leads to an unnecessarily high computational time [22].

2.6 Power Flow Analysis

In this thesis, the definition of power flow analysis is the calculation of the voltage magnitudes and angles in a power system. The input is the load and generation data, and the system topology in the form of a single line diagram including the line impedances. A brief presentation of the theory is laid out in this section, as it serves as a basis for the modelling described in Section 3.2.1.

2.6.1 Representation of the Power System (HLII)

The power system in this case is modelled as a network of buses interconnected by branches. The buses are referenced by a node index $i \in \mathcal{N}$. Branches are referenced as arcs between two nodes $(i, j) \in \mathcal{L}$. The system size is described by the number of buses $N = |\mathcal{N}|$, and number of lines $L = |\mathcal{L}|$. Each bus in the system has an associated complex voltage, $|V_i|\angle\delta_i$. Branches are described by their admittance, y_{ij}. A useful way to represent the connectivity, is through the bus-admittance matrix. This way admittances are included [32].

2.6.2 Network Model and the Bus Admittance Matrix

In order to establish the formulation and simulation procedure for the HLII assessment, it is necessary to provide a concise overview of the network model. This step is crucial to gain a thorough understanding of the power system theory required for defining the OPF problems and system constraints discussed later in this chapter.

Various approaches exist for representing a network model, and in this thesis, the bus injection model is utilised. This model primarily emphasizes nodal variables, which encompass quantities such as voltages, currents and power injections at each bus [32]. The utilisation of this model offers the advantage of expressing power flow equations in a concise manner. However, it is important to note that this model does not directly address the power flow on individual branches. Therefore the branch flow model is also used in some cases [32].

Moreover, the interconnection between two buses can be depicted by the π-model, as can be seen in Figure 2.15. This model includes a series impedance denoted as z_{ij} and a shunt susceptance, $C/2$. The shunt susceptance is equally distributed between the two buses. The power flow across a transmission line can be determined by employing the parameters of the π-model [32].

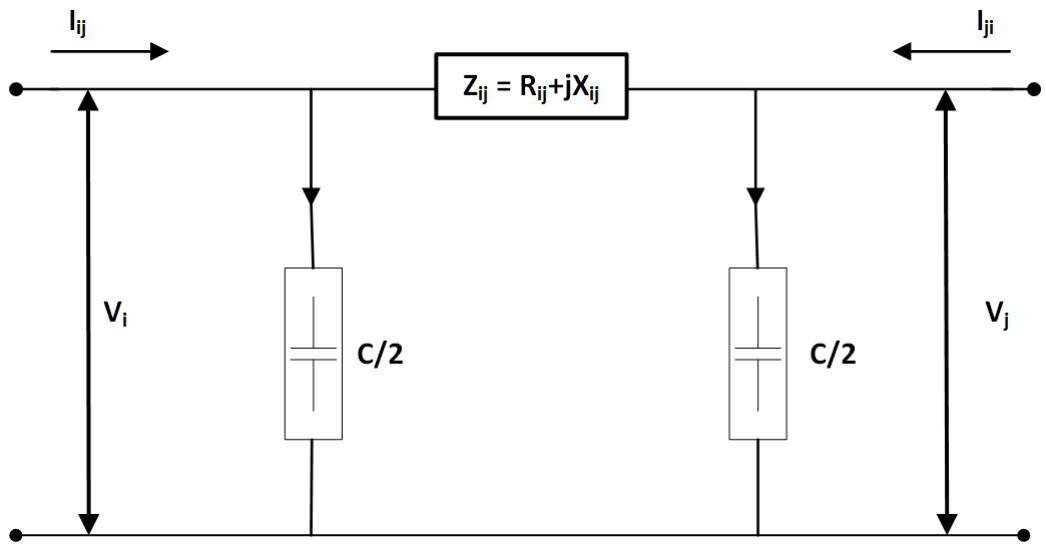

Figure 2.15: *Nominal π-line model for a medium length transmission line. Figure adapted from [33].*

From the π-line model the admittance matrix may be derived. The diagonal in the matrix is obtained by adding the admittance of the lines connected to the bus under consideration, along with the shunt admittance connected to the bus [32]. The off-diagonal elements represents the negative value of the admittance of the transmission line connecting the two considered buses. This relationship is shown in Equation (2.27). The admittance matrix can be decomposed into a conductance and a susceptance matrix, as depicted in Equation (2.30) [32]. This is a useful tool when applying DC approximations for the load flow analysis, which will be shown.

The bus-admittance matrix may be seen in Equation (2.27).

$$\mathbf{Y_{bus}} = \begin{bmatrix} Y_{11} & Y_{12} & \dots & Y_{1n} \\ Y_{21} & Y_{22} & \dots & Y_{2n} \\ \vdots & \vdots & \ddots & \vdots \\ Y_{n1} & Y_{n2} & \dots & Y_{nn} \end{bmatrix} \tag{2.27}$$

The diagonal elements Y_{ii}, the self admittance are calculated as:

$$Y_{ii} = y_{i0} + \sum_{j=1, j\neq i}^{n} y_{ij}, \tag{2.28}$$

and off-diagonal elements as,

$$Y_{ij} = -y_{ij}, \tag{2.29}$$

where y_{ij} is the admittance of the line between bus i and bus k, and y_{i0} is the shunt admittance on bus i. The Y_{bus}-matrix consists of complex numbers, which can be expressed in rectangular coordinates as

$$Y_{ij} = G_{ij} + jB_{ij} \tag{2.30}$$

For more details on the construction of the $\mathbf{Y_{bus}}$ the reader is referred to [32].

2.6.3 Bus Classification

Each bus in the power system is characterized by four variables: active power injection P_i, reactive power injection Q_i, voltage magnitude $|V|$ and voltage angle δ_i (typically

expressed in radians). For a solvable system, two of the variables are specified, and two must be calculated. The two being specified determine the classification of the bus, and the classifications are as follows [32]:

- Load bus (PQ): At the load bus, only loads are associated. Here, the active and reactive power demand, P_i and Q_i, are known, hence the name PQ-bus. That leaves the task at hand to determine the voltage magnitude and angle, $|V_i|$ and δ_i.
- Generator bus (PV): The PV bus is connected to a generator, where active power P_i and voltage magnitude $|V_i|$ are known. The unknown voltage angle δ_i and reactive power Q_i must be calculated.
- Slack Bus: The slack bus is introduced serving as both a physical and mathematical reference. Here, $|V_i|$ and δ_i are specified, while P_i and Q_i need to be calculated.

A brief summary is presented in Table 2.2 illustrating the relations of the variables of buses in a power system.

Table 2.2: *Power system bus types [32].*

Type	Slack	PQ	PV
Number of buses in the system	1	M	$N-M-1$
Known quantities	δ, V	P, Q	P, V
Unknown quantities	P, Q	δ, V	δ, Q

2.6.4 Power Flow Equations

Two models are normally used to represent a network: the bus injection model and the branch flow model. The branch flow model is in some cases utilised because of its application to convex relaxation [34]. The bus injection model is a more compact model [32], and is the model used in this thesis.

Applying Kirchhoff's current law (KCL) and utilising the $\mathbf{Y_{bus}}$, the nodal equations for

a given network may be written as Equation (2.31) [32].

$$\mathbf{I} = \mathbf{Y_{bus}}\mathbf{V} \tag{2.31}$$

where $\mathbf{I}$ is a vector of the current injected at each bus, and $\mathbf{V}$ is a vector of the bus voltages. Thus, for bus i, the nodal equation is written in Equation (2.32).

$$I_i = \sum_{j=1}^{n} Y_{ij}V_j, \tag{2.32}$$

where n is the total number of buses. Further, the complex power injected at bus i is shown in Equation (2.33).

$$S_i = P_i + jQ_i = V_i I_i^* \tag{2.33}$$

Expressing the voltages in polar coordinates as $|V|\angle\delta$ and the admittance in rectangular coordinates as Equation (2.30), inserting Equation (2.32) into Equation (2.33), and separating into a real and imaginary part yields the PF equations, given in Equation (2.34) and Equation (2.35) [32].

$$P_i(V,\delta) = |V_i|\sum_{j=1}^{n}|V_j|\left[G_{ij}\cos\left(\delta_i - \delta_j\right) + B_{ij}\sin\left(\delta_i - \delta_j\right)\right] \tag{2.34}$$

$$Q_i(V,\delta) = |V_i|\sum_{j=1}^{n}|V_j|\left[G_{ij}\sin\left(\delta_i - \delta_j\right) - B_{ij}\cos\left(\delta_i - \delta_j\right)\right] \tag{2.35}$$

These equations are simultaneously solved for all buses in a system in a PF solution, with exception of the reference bus. This yields $2(n-1)$ nonlinear equations, with the four variables $P_i, Q_i, |V_i|$ and $\angle\delta_i$. These are solved numerically in an iterative approach [35].

As the AC approach is not emphasized in this thesis, the numerical approaches will not be presented. For a more comprehensive understanding and derivation of the power flow equations, reference can be made to literature on power flow analysis, such as [36] which provide an overview and computational methods.

2.6.5 DC Power Flow

The AC Power Flow is computationally heavy. Different measures have been exercised to simplify the problem. A result of these measures have resulted in the DC power flow.

The DC power flow is a linearisation of the AC power flow equations. The AC power flow equations are nonlinear, and therefore require numerical methods. With the DC power flow, the need for numerical methods is eliminated [32]. The DC power flow contains the following simplifications from the AC power flow equations [32]:

- Branch resistances are zero. This implies lossless transmission, and $G_{ij} = 0$.
- Small angle difference between buses, which implies $\sin(\delta_i - \delta_j) \approx \delta_i - \delta_j$ and $\cos(\delta_i - \delta_j) \approx 1$.
- All voltage magnitudes are set to 1.0 p.u.
- The reactive power flow is neglected.

Applying the aforementioned assumptions to Equation (2.34) (and Equation (2.35)), the DC power flow Equation (2.36) is obtained [32].

$$P_i(\delta) \approx \sum_{j=1}^{n} B_{ij} \left(\delta_i - \delta_j\right). \tag{2.36}$$

The DC power flow can give reasonable estimates for the power flow in a power system. However, no information is supplied for the voltage magnitudes and reactive power flow in the system. Also, a significant drawback is the errors produced when the method is applied for stressed systems, which is often the situation when a power flow solution is necessary [37].

2.7 Optimal Power Flow (OPF)

Optimal Power Flow (OPF) is the key to solving operation and planning problems for power systems with respect to economic efficiency and reliability requirements. The goal of optimal power flow is to determine the optimal dispatches, as well as control settings for network elements. These network elements include generators, transformer tap changers, voltages, and other continuous and discrete variables [32]. The optimal settings are found with respect to one or more objectives, such as minimizing production cost or minimizing

losses, while satisfying all constraints imposed on the problem. Typically these constraints are physical and safety limitations [32].

One approach for solving the OPF problem is to linearise the formulation of the problem to create the DCOPF problem, using assumptions. The approach linearises the non-linear power flow equations, which eliminates the non-convex constraints and thus simplifies the computation [32]. However, the approach does not include voltage and reactive power. Therefore, compared to the ACOPF, the DCOPF lacks in accurate planning and operation decisions [32].

The main difficulty facing ACOPF is handling the non-convexity included in the model while taking into account all the properties of power flow. Similar to other non-convex problems, ACOPF has concerns with regards to convergence, sub-optimal solutions, and computational time, discussed in [38]. In [39], a decomposition approach is discussed. More recent studies have shifted to convex relaxations on solving the non-convex ACOPF. For example, SOCP (Second order cone programming) [40] has been formulated for finding global optimal solutions. Heuristic methods such as genetic algorithms [41], and neural networks [42] are also found used as solutions for non-convex problems.

The OPF problem is commonly expressed as a minimisation problem. The objective is minimise an objective function denoted as $f(\mathbf{x}, \mathbf{u})$, imposed by a set of equality constraints represented by $\mathbf{g}(\mathbf{x}, \mathbf{u})$ and inequality constraints denoted as $\mathbf{h}(\mathbf{x}, \mathbf{u})$. The problem may be formulated as shown in Equation (2.37) [43].

$$\left.\begin{array}{ll} \text{minimize} & f(\mathbf{x_0}, \mathbf{u}) \\ \text{s.t} & \mathbf{g}(\mathbf{x_0}, \mathbf{u}) = 0 \\ & \mathbf{h}(\mathbf{x_0}, \mathbf{u}) \leq 0 \end{array}\right\} \tag{2.37}$$

where $\mathbf{x}$ and $\mathbf{u}$ are vectors of state variables and control variables, respectively [43].

2.7.1 Objective Function

The objective of the OPF problem is to determine the most optimal operational configuration for the power system. Achieving this requires making decisions regarding the

specific aspects to be optimised, which is contingent upon the intended goals of the OPF. Several illustrative objectives are outlined below:

- **Minimisation of cost of generation**: One of the more common objectives is to minimise the cost of power production. The objective in this case is set to minimise the total cost of generation of active power [44], and a formulation may be seen in Equation (2.38).

$$\min \quad \sum_{i=1}^{N_{gen}} C_i(P_{G_i}) \tag{2.38}$$

  where $C_i(P_{G_i})$ is a cost function of generator i [44].

- **Maintaining constant voltage profile**: It can be of importance for a system operator to maintain a constant voltage profile to avoid voltage instability problems. OPF can be used to identify the actions necessary to achieve this goal. the objective may be formulated as Equation (2.39).

$$\min \quad \sum_{i=1}^{n} \left(V_i - V_{setpoint,i}\right)^2 \tag{2.39}$$

  [44].

- **Minimise load curtailment cost**: By minimising the load curtailment cost, one aims to avoid Loss-of-Load situations. From a perspective of reliability this is an important consideration which will be emphasised in this thesis.

$$\min \quad \sum_{i=1}^{n} F(C_i) \tag{2.40}$$

  where $F(C_i)$ is a function describing the curtailment costs, and C_i is the curtailment at each bus.

2.7.2 Variables

The classic power flow analysis aims to find the unknown voltage magnitudes and angles. The OPF, rather aims to find the optimal system state within a feasible region. This means that variables which are kept fixed in power flow calculations, may be able to vary in an OPF calculation. The variables in an OPF calculation may be classified as the following [32]:

- **Control variables**: These variables may, as the name implies, be controlled to achieve the desired operating state of the system. This means they are independent variables of the optimisation problem, and are connected to the known values of the PF equations, typically being the active and reactive power output of generators.
- **State variables**: Variables that describe the system state, but are not controllable. These are influenced by the control variables and are dependent variables of the optimisation problem. Typically, these are the voltage angles (except for the slack bus), and voltage magnitudes at PQ buses.
- **Parameter values**: These are fixed values. These are known values in the PF calculation, that cannot change in the OPF calculation either. This is for example the voltage angle at the slack bus, which is kept fixed at zero as a reference for the system. The active and reactive power at PQ buses also fall within this category.

2.7.3 Constraints

The constraints of an optimisation problem define the feasible region. The constraints are divided into two: inequality and equality constraints [32].

2.7.3.1 Equality constraints

A common equality constraint for all OPF problems is the satisfaction of the power flow Equations (2.34) and (2.35). The satisfaction of the constraint is necessary for all buses for any operating point of the system to be a true operating point [44]. The constraints are presented in Equation (2.41) and Equation (2.42).

$$P_i(V,\theta) = P_i^G - P_i^L, \quad \forall i \in \mathcal{N} \tag{2.41}$$

$$Q_i(V,\theta) = Q_i^G - Q_i^L, \quad \forall i \in \mathcal{N} \tag{2.42}$$

2.7.3.2 Inequality constraints

The inequality constraints represent the operational limits of the power system. As for the objective function, these may vary depending on the defined problem. Some typical

constraints are presented below:

- **Active power constraints:** Active power constraints dictate that each generator must operate within its designated limits, which usually consts of minimum and maximum production thresholds. A general formulation of shown in Equation (2.43) [44].

$$P_{Gi,min} \leq P_{Gi} \leq P_{Gi,max}, \quad \forall i \in \mathcal{G} \tag{2.43}$$

- **Reactive power constraints:** Similar to active power limits, the reactive power must be considered as well. The limits are typically determined by reactive power capabilities of connected generators or other controllable reactive power devices. A general formulation is shown in Equation (2.44) [44].

$$Q_{Gi,min} \leq Q_{Gi} \leq Q_{Gi,max}, \quad \forall i \in \mathcal{G} \tag{2.44}$$

- **Voltage magnitude constraints:** There is a limit for the voltage at buses, which must not exceed a certain limit around the nominal value. This limit may vary, but typically falls within the range of $5 - 10\%$ around nominal value. A general formulation is shown in Equation (2.45) [44].

$$V_{i,min} \leq V_i \leq V_{i,max}, \quad \forall i \in \mathcal{N} \tag{2.45}$$

- **Voltage angle constraints:** Setting limits on voltage angles is crucial for non-linear solvers used in ACOPF. The use of complex numbers can result in multiple instances of the same power flow solution. For instance, $1.01\angle 0.349 = 1.01\angle 6.616 = 1.01\angle -5.937$. To ensure a unique solution and avoid cases where the solver oscillates between two equivalent solutions shifted by 2π rad, bus voltage angles are restricted to the range of 0 to 2π. A formulation is shown in Equation (2.46) [44].

$$\delta_{i,min} = -\pi \leq \delta_i \leq \pi = \delta_{max}, \quad \forall i \in \mathcal{N} \tag{2.46}$$

- **Line flow constraints:** Power transfer constraints in a power system limit the flow of power between buses. The choice of variables for constraining line flows depends on the limiting factor. Short transmission lines are often constrained by

thermal limits, which closely relate to current. Transformers are typically constrained by apparent power limits. For longer transmission lines, the steady-state stability limit becomes the limiting factor, and line flow can be constrained using active power [44].

2.7.4 DC Optimal Power Flow (DCOPF)

The description provided in the previous section depicts the OPF problem called ACOPF. Essentially, this comes from the fact that the full AC power flow equations are considered in the constraints. An alternative exists, which utilises the DC power flow formulation described in Section 2.6.5. This approach is called DCOPF. One of the main benefits of DCOPF compared to ACOPF is that the constraints become linear, and the optimisation problem is convex [44]. This makes it possible to solve the problem using optimisation methods as LP or QP, which are relatively simple compared to the non-convex problem that is featured in ACOPF.

DCOPF carries with it the same limitations as the DC power flow, that it is an approximation. It follows that the accuracy of the results then depends on the validity of the assumptions. The focus of this thesis is on the DCOPF problem, while the ACOPF algorithm is not extensively covered.

2.8 Security Constrained Optimal Power Flow (SCOPF)

Security Constrained Optimal Power Flow (SCOPF) is an extended version of ACOPF. One formulation, is that the objective is to determine a minimum cost generation schedule in hand with power demand at each node in the network, while maintaining a functioning transmission network whether the operations are in either pre-contingency or a post-contingency state [45]. Extending the normal operational conditions is not sufficient to maintain network operation. It is necessary for system operators to also include contingency scenarios in the model, to meet N-1, 2N or N-1-1 criteria. Thus, system reliability, security, economical benefits and efficiency are guaranteed [38].

SCOPF problems are divided in two types: preventive and corrective. The preventive

approach optimises subject to the base case. The preventive SCOPF (PSCOPF) can be implemented by adding security constraints to the original OPF problem. These constraints further establish boundaries on the power flow on transmission lines, and bus voltages for the post-disturbance configuration caused by specific contingencies. In essence, the SCOPF enforces preventive control measures within the system, and thus enhances the level of system security [46].

However, the aforementioned definition of PSCOPF is conservative, since it fails to consider the corrective capabilities of the system after an outage has occurred. The corrective SCOPF (CSCOPF) considers corrective actions including generation rescheduling, overload rotation, switching, etc., which can play an important role in elimination of constrained violations [46].

For security reasons, preventive approach is preferred in industrial practice [47]. PSCOPF can be expensive, as no remedial actions can be exercised to eliminate violations. Thus, extra costs under normal operation condition are a necessity to prevent contingencies. For CSCOPF, this allows for generation units to reschedule, and lines to be switched, with the underlying assumption that the violation is corrected before damage of equipment or cascading failures occur. Reaching a solution of the corrective model is demanding, because of model size and the increased number of constraints and decision variables. The SCOPF formulation is an extension of the OPF formulation, and may be formulated as seen in Equation (2.47) [43].

$$\left.\begin{aligned} &\text{minimize} && f(\mathbf{x_0}, \mathbf{u}) && \\ &\text{s.t} && \mathbf{g}(\mathbf{x_0}, \mathbf{u}) = 0 && \\ & && \mathbf{h}(\mathbf{x_0}, \mathbf{u}) \leq 0 && \\ & && \mathbf{g}(\mathbf{x_c}, \mathbf{u}) = 0 && \forall c \in \mathcal{C} \\ & && \mathbf{h}(\mathbf{x_c}, \mathbf{u}) \leq 0 && \forall c \in \mathcal{C} \end{aligned}\right\} \tag{2.47}$$

where $\mathcal{C} = \{1, \ldots, N_c\}$ is the set of considered contingencies.

2.8.1 Post-Contingency Corrective Rescheduling

The solution to the SCOPF problem, as defined in Equation (2.47), entails the implementation of preventive control measures. These measures are necessary to ensure the system remains in a feasible state during contingencies, without the need for corrective actions. By adjusting the power output of a generator within a certain range before an overload reaches a critical point, it is possible to achieve an equivalent level of security while minimising operating costs. This observation is emphasized in [46], which introduces a solution strategy for the SCOPF problem involving post-contingency rescheduling. The range of rescheduling actions is represented by coupling constraints of the form $|\mathbf{u_0} - \mathbf{u_c}| \leq \mathbf{\Delta c}$. The problem formulation for SCOPF may then be formulated as Equation (2.48).

$$\left.\begin{aligned}
&\text{minimize} && f(\mathbf{x_0}, \mathbf{u}) \\
&\text{s.t} && \mathbf{g}(\mathbf{x_0}, \mathbf{u}) = 0 \\
& && \mathbf{h}(\mathbf{x_0}, \mathbf{u}) \leq 0 \\
& && \mathbf{g}(\mathbf{x_c}, \mathbf{u_c}) = 0 \quad \forall c \in \mathcal{C} \\
& && \mathbf{h}(\mathbf{x_c}, \mathbf{u_c}) \leq 0 \quad \forall c \in \mathcal{C} \\
& && |\mathbf{u_0} - \mathbf{u_c}| \leq \mathbf{\Delta c} \quad \forall c \in \mathcal{C}
\end{aligned}\right\} \tag{2.48}$$

where $\mathbf{u_0}$ are the control variables during the base case. $\mathbf{u_c}$ are the control variables during contingency c. $\mathbf{\Delta c}$ are the allowed changes in control variables from the base case to contingency case. In other words, stating that $\mathbf{\Delta} = 0$ would be the same as requiring preventive security. From this point forward in this thesis, the preventive SCOPF will be referred to as PSCOPF, and the SCOPF with post-contingency corrective rescheduling will be referred to as CSCOPF. In [46], it is suggested employing Benders Decomposition to solve the CSCOPF problem, which will be further discussed as well.

2.8.2 Benders Decomposition

Benders Decomposition, which was initially proposed in [48], has been widely used for addressing various SCOPF problems. Even though this approach is not adopted in the thesis, what follows in this subsection is a compact account of the fundamentals of Benders

decomposition, based on the knowledge gained from literature. This approach involves decomposing the problem into a master problem and multiple subproblems, which interact iteratively. Benders decomposition is attractive because it keeps both the master problem and subproblems manageable. It allows for computation to be distributed across multiple processors [45]. However, the Benders Decomposition algorithm may not converge reliably unless the feasible region is convex, which is not always the case in the AC SCOPF. Therefore, caution should be used when utilising Benders Decomposition [43].

Following the methodology of [46] and utilising the notation used in Equation (2.48), Benders decomposition may be described as a two stage process:

- First, solve the master problem (base case) depicted by Equation (2.37), to achieve an operating point $(\mathbf{x_0}, \mathbf{u_0})$.
- Second, from the base case operating point $(\mathbf{x_0}, \mathbf{u_0})$, find new operating points $(\mathbf{x_c}, \mathbf{u_c})$ that satisfies $\mathbf{g}(\mathbf{x_c}, \mathbf{u_c}) = 0$ and $\mathbf{h}(\mathbf{x_c}, \mathbf{u_c}) \leq 0$, as well as $|\mathbf{u_0} - \mathbf{u_c}| \leq \mathbf{\Delta c}$ for all contingencies $c \in \mathcal{C}$.

The primary goal is to minimise operational costs while simultaneously ensuring the feasibility of the subproblems. To accomplish this, the base case operation and the N_c post-contingency operating states are examined separately. If the post-contingency state proves feasible, no alterations to the base case are necessary. Conversely, if the post-contingency subproblem results in infeasible conditions, constraints related to the base case operation must be introduced to ensure the feasibility of the subproblem. [43]

One formulation of the subproblem may be as shown in Equation (2.49) [43].

$$\left.\begin{array}{lll} \text{minimize} \quad w(\mathbf{x_0}, \mathbf{u_0}) = & \mathbf{d^r} \cdot \mathbf{r} + \mathbf{d^s} \cdot \mathbf{s} \\ \text{s.t} & \mathbf{g}(\mathbf{x}, \mathbf{u}) + \mathbf{r} = 0, \\ & \mathbf{h}(\mathbf{x}, \mathbf{u}) + \mathbf{s} \leq 0, \\ & |\mathbf{u_0} - \mathbf{u}| - \mathbf{s} \leq \mathbf{\Delta c}, \end{array}\right\} \tag{2.49}$$

where, $\mathbf{d^r}$ and $\mathbf{d^s}$ are positive cost vectors. $\mathbf{r}$ and $\mathbf{s}$ are positive vectors of penalty variables for operating and coupling constraints, respectively. The objective value, represented as

w, is expressed as a function of the base case operating point. From Equation (2.49) the following statement is made:

$$w = 0 \Leftrightarrow \text{The subproblem is feasible}$$
$$w \geq 0 \Leftrightarrow \text{The subproblem is not feasible}$$

Thus, requiring that $w_c(\mathbf{x_0}, \mathbf{u_0}) \leq 0 \quad \forall c \in \mathcal{C}$, is identical to requiring the feasibility of the post-contingency subproblems [46]. In a compact form, the CSCOPF may be written as Equation (2.50).

$$\left.\begin{array}{lll} \text{minimize} & f(\mathbf{x_0}, \mathbf{u_0}) & \\ \text{s.t} & \mathbf{g}(\mathbf{x_0}, \mathbf{u_0}) = 0 & \\ & \mathbf{h}(\mathbf{x_0}, \mathbf{u_0}) \leq 0 & \\ & w_c(\mathbf{x_c}, \mathbf{u_c}) \leq 0 \quad \forall c \in \mathcal{C} & \end{array}\right\} \tag{2.50}$$

Benders Decomposition is used to approximate $w_c(\mathbf{x_0}, \mathbf{u_0})$ [43]. The approximation is refined by solving the base case and the set of N_c contingencies. Each subproblem has an associated collection of Lagrange multipliers that provide insight into the impact of the marginal changes in the in the base case operational point $(\mathbf{x_0}, \mathbf{u_0})$ on the infeasibility of the subproblem. These dual values, along with the objective value w, are used to construct a linear constraint derived from a specific infeasible subproblem. This constraint, referred to as a Benders Cut, solely contains the base case variables $(\mathbf{x_0}, \mathbf{u_0})$. Benders Cuts are iteratively appended to the base case problem [46]. It should be noted that it is also possible to solve the subproblems in parallel [43], which can be beneficial to reduce computational efforts. Figure 2.16 illustrates the procedure described.

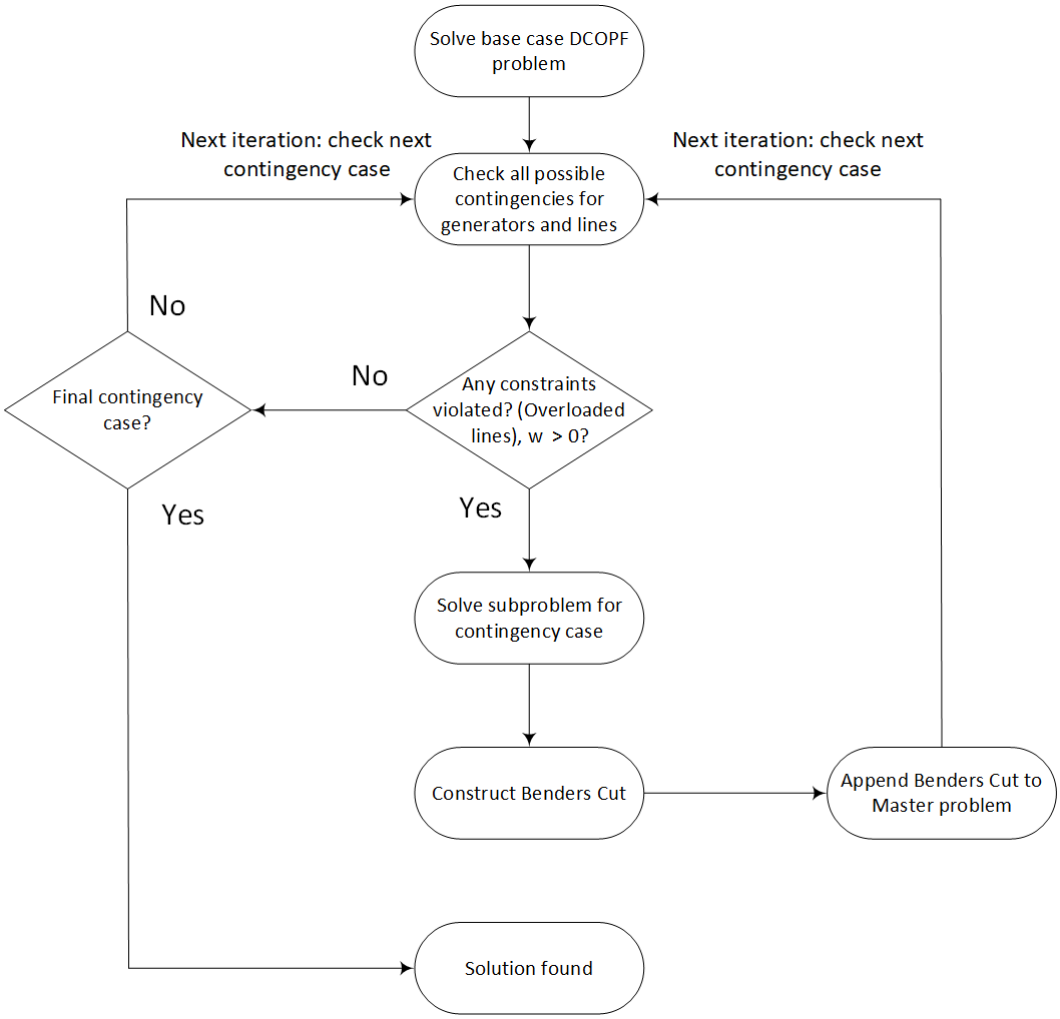

Figure 2.16: *Flow chart of SCOPF algorithm. Adapted from [43].*

2.9 Contingency Analysis and Distribution Factors

As emphasized, ensuring the reliable and secure operation of the electrical grid is of utmost importance. Maintaining a reliable power supply even under unforeseen circumstances and disruptions is a complex task. This is where contingency analysis emerges as a tool of importance, providing information about the potential risks and vulnerabilities that can emerge due to the outage of a component in the power system.

Contingency analysis involves the evaluation of the performance of a system, after the occurrence of a specific contingency. This can be line outages, generator outages or other power system equipment failure. By simulating failure scenarios, it is possible to gain insight to the ability to withstand disturbances and deliver power to consumers without

interruptions.

This thesis focuses on the use of line outage distribution factors (LODFs), which may be utilised to perform contingency analysis in power systems. The work of [49] is applied, and an understanding of the method is presented in this section.

2.9.1 Power Transfer Distribution Factors (PTDFs)

Continuing from Equation (2.36), Equation (2.28) and Equation (2.29), along with the assumptions stated for the DC power flow, the susceptance elements are defined according to Equation (2.51) [31].

$$B_{ij} = -\frac{1}{X_{ij}}, \quad B_{ii} = -\sum_{i=1, j\neq i}^{k} B_{ij} \tag{2.51}$$

Further, the formulation of Equation (2.36) is reformulated to its matrix representation shown in Equation (2.52). Here the net power injections, $P_i \quad \forall i \in \mathcal{N}$, are expressed as a column vector through the susceptance matrix, $\mathbf{B}$, and voltage angles, $\delta_i \quad \forall i \in \mathcal{N}$. The set $\mathcal{N}$ is the set of buses for the considered system [31].

$$\mathbf{B}\boldsymbol{\delta} = \mathbf{P} \tag{2.52}$$

The susceptance matrix represents singularity, as each row could be formulated through a linear combination of the other rows [31]. The slack bus expresses its utility in order to overcome the problem. The new matrix $\mathbf{B_{sub}}$ is introduced, shown in Equation (2.53). It is identical to $\mathbf{B}$, but with the rows and columns associated with the slack bus removed. The choice of slack bus can be decided, and is here selected as bus 1 of the system [31].

$$\mathbf{B_{sub}} = \begin{bmatrix} B_{22} & B_{23} & \dots & B_{2n} \\ B_{32} & B_{33} & \dots & B_{3n} \\ \vdots & \vdots & \ddots & \vdots \\ B_{n2} & \dots & \dots & B_{nn} \end{bmatrix} \tag{2.53}$$

The slack bus compensates for either the surplus or deficit of power generation in the system. The slack bus is included into the system again with the row and column corresponding to it being filled with values of zero. This matrix is called $\mathbf{Z}$, and shown in

Equation (2.54) [31].

$$\mathbf{Z} = \begin{bmatrix} 0 & 0 \\ 0 & \mathbf{B_{sub}}^{-1} \end{bmatrix} \tag{2.54}$$

This gives the opportunity to calculate the voltage angles through Equation (2.55).

$$\boldsymbol{\delta} = \mathbf{Z} \cdot \mathbf{P} \tag{2.55}$$

With knowledge of the voltage angles, it is possible to calculate the power flow between bus i and bus j through Equation (2.56).

$$P_{ij} = \frac{\delta_i - \delta_j}{X_{ij}} \tag{2.56}$$

With the notations used in Equation (2.55), one could express the voltage angles as a row of the $\mathbf{Z}$ matrix times the net active power injection vector. This way, the power flow through a line located between bus i and bus j is found as depicted in Equation (2.57).

$$P_{ij} = \frac{z_{i1} - z_{j1}}{X_{ij}} \cdot P_1 + \frac{z_{i2} - z_{j2}}{X_{ij}} \cdot P_2 + ... + \frac{z_{in} - z_{jn}}{X_{ij}} \cdot P_n \tag{2.57}$$

This leads to the introduction of the power transfer distribution factors (PTDFs) in the formulation, which gives opportunity to formulate the set of line flows in a simplified format. The PTDFs are denoted as in Equation (2.58),

$$a_{ij,n} = \frac{z_{in} - z_{jn}}{X_{ij}}, \tag{2.58}$$

yielding Equation (2.59),

$$P_{ij} = a_{ij,1} \cdot P_1 + a_{ij,2} \cdot P_2 + \ldots + a_{ij,n} \cdot P_n \tag{2.59}$$

Now, this expression can be generalised for all lines in the system. This is denoted as the sensitivity matrix, $\mathbf{A}$, which can be said to be the collection of PTDFs. Multiplying $\mathbf{A}$ with the net power injection vector, $\mathbf{P}$ yields Equation (2.60) which described all line flows, $\mathbf{T}$, for the system [31].

$$\mathbf{T} = \mathbf{A} \cdot \mathbf{P} \tag{2.60}$$

2.9.2 Line Outage Distribution Factors (LODFs)

The LODFs represents the incremental real power flows on monitored transmission lines caused by line outages with a pre-contingency real power flow of 1 p.u. [49].

$$\mathbf{PL}^{\mathbf{c}}_{\mathcal{A}} = \mathbf{PL}^{\mathbf{0}}_{\mathcal{A}} + \mathbf{LODF}_{\mathcal{A},\mathcal{O}}\mathbf{PL}^{\mathbf{0}}_{\mathcal{O}} \tag{2.61}$$

where,

- Superscripts 0 and c represent base case and contingency case, respectively.
- Subscript $\mathcal{A}$ and $\mathcal{O}$ represent the set of u monitored transmission lines, and set of v transmission lines on outage, respectively.
- $\mathbf{PL}^{\mathbf{c}}_{\mathcal{A}}$ and $\mathbf{PL}^{\mathbf{0}}_{\mathcal{A}}$ are $u \times 1$ vectors of post- and pre-contingency power flows on monitored lines.
- $\mathbf{PL}^{\mathbf{0}}_{\mathcal{O}}$ is a $v \times 1$ vector of pre-contingency power flows for lines on outage.
- $\mathbf{LODF}_{\mathcal{A},\mathcal{O}}$ is a $u \times v$ matrix.

The approach used to calculate $\mathbf{LODF}_{\mathcal{A},\mathcal{O}}$ utilises the PTDFs of the pre-contingency network. Based on the definition of PTDFs, the following equations are present.

$$\left.\begin{aligned} \mathbf{PTDF}^{\mathbf{c}}_{\mathcal{A},\mathcal{O}} &= \mathbf{X}^{-\mathbf{1}}_{\mathcal{A}}\mathbf{\Phi}^{\mathbf{T}}\left[\mathbf{B}\right]^{c^{-1}}\mathbf{\Psi} \\ \mathbf{PTDF}^{\mathbf{0}}_{\mathcal{A},\mathcal{O}} &= \mathbf{X}^{-\mathbf{1}}_{\mathcal{A}}\mathbf{\Phi}^{\mathbf{T}}\left[\mathbf{B}\right]^{0^{-1}}\mathbf{\Psi} \\ \mathbf{PTDF}^{\mathbf{0}}_{\mathcal{O},\mathcal{O}} &= \mathbf{X}^{-\mathbf{1}}_{\mathcal{O}}\mathbf{\Psi}^{\mathbf{T}}\left[\mathbf{B}\right]^{0^{-1}}\mathbf{\Psi} \end{aligned}\right\} \tag{2.62}$$

where,

- $\mathbf{X}_{\mathcal{A}}$ and $\mathbf{X}_{\mathcal{O}}$ are diagonal matrices with elements representing the reactances of the monitored and outaged lines, respectively.
- $\mathbf{\Phi}$ and $\mathbf{\Psi}$ is a bus-to-monitored line incident matrix and a bus-to-outaged line incident matrix, respectively.

- $[\mathbf{B}]^c$ and $[\mathbf{B}]^0$ are susceptance matrices for contingency and base case conditions, respectively. The case of $\mathbf{PTDF}^{\mathbf{c}}_{\mathcal{A},\mathcal{O}}$ is not used in this thesis, but it is shown as an alternative in calculating the post-contingency PTDFs, which is the same as the LODF described in this section. For proof on the calculation of $[\mathbf{B}]^c$, the reader is referred to [49].

The incidence matrices are behaving as follows: If lines $i-j$ and $m-n$ are monitored, and lines $a-b$ and $p-q$ are on outage, then the following incidence matrices exist,

$$\mathbf{\Phi^T} = \begin{bmatrix} 0 & \dots & 1^{\swarrow i} & \dots & -1^{\swarrow m} & \dots & \dots & 0 \\ 0 & \dots & \dots & 1^{\swarrow j} & \dots & -1^{\swarrow n} & \dots & 0 \end{bmatrix} \tag{2.63}$$

$$\mathbf{\Psi^T} = \begin{bmatrix} 0 & \dots & 1^{\swarrow a} & \dots & -1^{\swarrow p} & \dots & \dots & 0 \\ 0 & \dots & \dots & 1^{\swarrow b} & \dots & -1^{\swarrow q} & \dots & 0 \end{bmatrix} \tag{2.64}$$

with,

$$\mathbf{X_M} = \begin{bmatrix} x_{ij} & & \\ & & x_{mn} \end{bmatrix}, \quad \mathbf{X_O} = \begin{bmatrix} x_{ab} & & \\ & & x_{pq} \end{bmatrix}. \tag{2.65}$$

Then the matrices defined in (2.63) through (2.65) are inserted into Equation (2.62). With this, the next step is matrix operations. This is of helpful use, as it illustrates clearly the sizes of the different matrices, supporting the understanding of what is actually calculated.

With these matrices defined, the $\mathbf{PTDF}^{\mathbf{c}}_{\mathcal{A},\mathcal{O}}$, and thus the $\mathbf{LODF}_{\mathcal{A},\mathcal{O}}$ may be calculated as in Equation (2.66) [49].

$$\mathbf{LODF}^{\mathbf{c}}_{\mathcal{A},\mathcal{O}} = \mathbf{PTDF}^{\mathbf{c}}_{\mathcal{A},\mathcal{O}} = \mathbf{PTDF}^{\mathbf{0}}_{\mathcal{A},\mathcal{O}} \left(\mathbf{E} - \mathbf{PTDF}^{\mathbf{0}}_{\mathcal{O},\mathcal{O}} \right)^{-1} \tag{2.66}$$

$\mathbf{E}$ is an identity matrix of size $v \times v$. In the methodological approach, an example is provided to illustrate the use of the approach in order to calculate the post-contingency lines flows of a power system network.

2.10 Preventive Security Constrained DC Optimal Power Flow (DC-PSCOPF) using PTDFs and LODFs

Following is a presentation of the theory involved with the formulation of DC-PSCOPF, which is applied in this thesis. This involves the combination of the fundamental idea behind SCOPF from Section 2.8, combined with the contingency analysis and distribution factors addressed in Section 2.9. In Section 3.2.2, a more thorough description is given of how the DC-PSCOPF is formulated through the LODFs in particular for this thesis.

Compared to the CSCOPF, the PSCOPF offers some advantages and some disadvantages. The computational complexity is lower, since it aims to prevent violations in the first place rather than correcting them after they occur through methods as described in Section 2.8.1. However, this is a less accurate approach, that leads to higher operating costs [46]. The consequences of this feature with regards to implementation in Python is discussed in the Chapter of Code Development (Chapter 4), Section 4.1.4.

The DCOPF problem can be extended to incorporate the impact of a transmission line outage. By integrating such a security constraint, the DCOPF problem gains the feature to address both pre- and post-contingency constraints [50]. In power systems, it should be noted that not all contingencies lead to a state of post-overload [50]. To reduce the computational complexity of the SCOPF problem, it is assumed that the most severe potential cases will be included in the analysis. This approach aims to limit the number of contingencies that need to be considered in the security assessment [50]. The selection of the potential contingencies included in the DC-PSCOPF problem, will be further elaborated upon in Section 5.5.

Using the sensitivity matrix, $\mathbf{A}$, from Equation (2.60) and the LODFs from Equation (2.66), the post-contingency power flow constraint for a given transmission line can be obtained by Equation (2.67) [50].

$$-\mathbf{T_{lim}}+ \leq [\mathbf{A} + \mathbf{LODF} \cdot \mathbf{A}] \cdot (\mathbf{P} - \mathbf{P_{load}}) \leq \mathbf{T_{lim}} \tag{2.67}$$

It is important to highlight that the pre- and post-contingency power flows are dependent on the net power injection, meaning the decision variable is solely the active power

injected, $\mathbf{P}$. In this thesis, the active power curtailment, $\mathbf{C_P}$, will be included as a decision variable. This augmentation of the mathematical formulation of the optimisation problem will be addressed in the methodological approach, in Section 3.2.2. For this modelling approach is it not necessary obtaining the post-contingency bus voltages for the modelling of the line flows.

Ultimately, in this DC-PSCOPF formulation, the pre- and post-contingency constraints may be mathematically formulated as Equation (2.68) and Equation (2.69), respectively [50].

$$-\mathbf{T_{lim,pre}} + \mathbf{A} \cdot \mathbf{P_{load}} \leq \mathbf{A} \cdot \mathbf{P} \leq \mathbf{T_{lim,pre}} + \mathbf{A} \cdot \mathbf{P_{load}} \tag{2.68}$$

$$\begin{aligned} -\mathbf{T_{lim,post}} + [\mathbf{A} + \mathbf{LODF} \cdot \mathbf{A}] \cdot \mathbf{P_{load}} &\leq [\mathbf{A} + \mathbf{LODF} \cdot \mathbf{A}] \cdot \mathbf{P} \\ &\leq \mathbf{T_{lim,post}} + [\mathbf{A} + \mathbf{LODF} \cdot \mathbf{A}] \cdot \mathbf{P_{load}} \end{aligned} \tag{2.69}$$

The optimisation problem illustrated in the modelling approach in Section 3.2.2 includes these constraints under the assumption that the active power generation and load curtailments, which are the decision variables of the problem, remain unchanged in both pre- and post-contingency conditions. Consequently, the inclusion of ramp-up and ramp-down constraints is deemed unnecessary [50]. In other words, corrective actions are not present. The complete DC-based PSCOPF formulation applied in this thesis can be seen in Section 3.2.2.

3 Methodological Approach

This chapter looks into the methodological approach used in the calculation of reliability indices, with the focus on the implementation of the HLII adequacy assessment. The assessment requires modelling for the system's load and generation, as well as a model representing the network topology. Throughout the chapter, the work of [22] and [31] are used as fundamentals, as they have implemented similar approaches. Their efforts are used as a stepping-stone towards integrating DC-PSCOPF in the HLII adequacy assessment.

A step-by-step walkthrough of the HLII assessment applied in this thesis, following the approach of Figure 3.1. This systematic methodology offers a framework for evaluating select reliability indices of a power system. By understanding and applying this approach, one can gain knowledge into the adequacy of the system under consideration.

Throughout the chapter, illustrative examples are provided to enhance the conceptual understanding of the methodology. These examples demonstrate how calculations are performed, enabling an understanding of the principles behind the HLII adequacy assessment.

The utilised MCS method of [22] and [31], the State Sampling method, will be applied. The sampled states are assessed as OPF problems, where the key work of this thesis has been in the extension of OPF to SCOPF, in particular DC-PSCOPF.

Again, it needs to be emphasized that the methodology presented is based on the inspiring and foundational work of [22] and [31]. An understanding of the methods formulated by [22] and [31], is presented from the perspective of the author of this thesis. The aim is to provide the necessary building blocks, in order to formulate the algorithmic approach in Python code in an object-oriented manner.

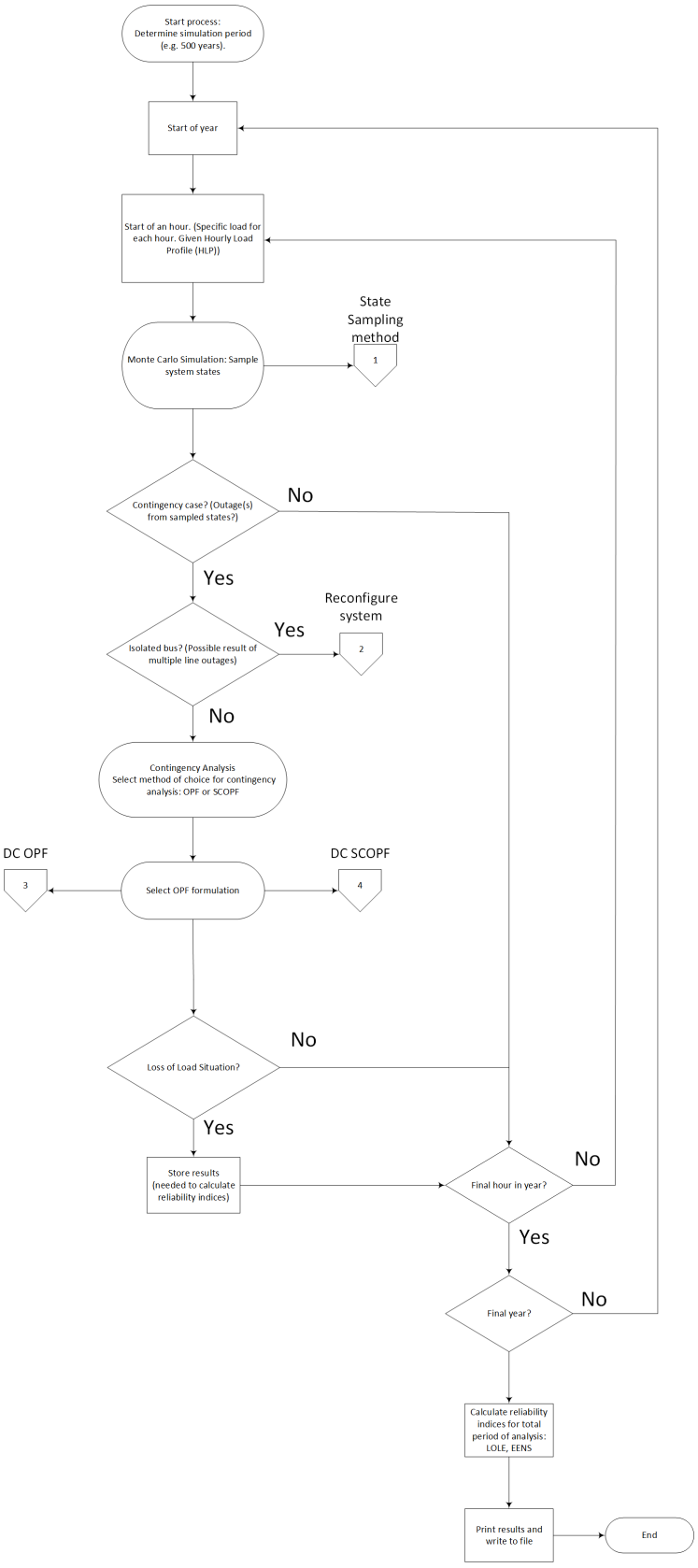

Figure 3.1: *Algorithmic approach in calculating reliability indices.*

3.1 Elements in HLII Adequacy Assessment

The following section presents the elements in the HLII assessment conducted in this thesis. Descriptive steps of each part of the algorithmic approach in the calculation of reliability indices are presented, in order to provide transparency and opportunity to reproduce the approach discussed.

As explained in Section 2.1.1, the network topology is included in the HLII adequacy assessment, which makes it necessary to perform a load flow analysis of the system. In this step of the analysis, a choice can be made regarding the desired level of accuracy. For instance, one could use the AC-based approach, trading computational resources for accuracy. Another approach is to simplify the problem, and use the decoupled load flow, or even DC-based load flow. For any of the approaches utilised for the HLII adequacy assessment, it is needed network data, load data, as well as generation data which is subject to the MCS sampling. Input data is required to be of a specific format, which is fed to the OPF solver. As mentioned, this thesis puts emphasis on the DC-based load flow analysis, which means the AC load flow input data will not be considered. The reader is referred to [22][31] for a detailed description of the AC load flow contingency solver.

3.1.1 Input Data

Table 3.1 illustrates the line data which is subject to the MCS state sampling and DC load flow analysis.

Table 3.1: *Line input data for the MCS state sampling DC contingency solver.*

Line	From bus	To bus	FOR	Reactance [p.u.]	Current Rating [p.u.]
1	1	2	FOR_1	X_{12}	T_{lim_1}
2	2	3	FOR_2	X_{23}	T_{lim_2}
n	i	j	FOR_3	X_{ij}	T_{lim_n}

Table 3.2 shows the generator input data.

Table 3.2: *Generator input data, DC contingency solver.*

Generator	Capacity [MW]	Bus number	FOR
1	$P_{cap,1}$	1	FOR_1
2	$P_{cap,2}$	2	FOR_2
n	$P_{cap,n}$	N	FOR_3

Table 3.3 is also included, illustrating specific data for each bus in the system. The allocation of load and cost of curtailment are specified for each bus.

Table 3.3: *Bus input data, DC contingency solver.*

Bus	Share of Load	Cost of curtailment [$/kWh]
1	$\%_{load,1}$	C_1
2	$\%_{load,2}$	C_2
N	$\%_{load,N}$	C_N

3.1.2 MCS State Sampling Method - System Sampling

Instead of employing a conventional approach of iterating through each hour of each year, the State Sampling method adopts a simultaneous sampling approach to assess the availability of generators and lines. This method involves generating random numbers U, which follow a uniform distribution in the range of $[0, 1]$, to ascertain whether the system states can be classified as available or unavailable. The approach is the same as from the work of [22], adapted to fit for the developed software. The following description of the procedure is the interpretation of the work of [22], in the eyes of the author. The procedure is as follows; The process begins by sampling the states of all generators and lines, and storing them in a matrix of size $n_{components} \times n_{states}$, which can be seen in

Equation (3.1). The subscripts in the equation denote the component number and the corresponding state number.

$$M_{samples} = \begin{bmatrix} U_{1,1} & U_{1,2} & \dots & U_{1,n_{states}} \\ U_{2,1} & U_{2,2} & \dots & U_{2,n_{states}} \\ \vdots & \vdots & \ddots & \vdots \\ U_{n_{componemt},1} & U_{n_{componemt},2} & \dots & U_{n_{componemt},n_{states}} \end{bmatrix} \tag{3.1}$$

Subsequently, an additional matrix of identical dimensions is created, containing the FOR values associated with each component, as can be seen in Equation (3.2). The subscript number represents the component number. It is worth noting that the FOR values remain constant across all generated states. By comparing the corresponding elements of the state matrix and the FOR matrix, a decision is made regarding the availability of the components within each state, denoted as either available (0) or unavailable (1), shown in Equation (3.3) [22].

$$M_{FOR} = \begin{bmatrix} FOR_1 & FOR_1 & \dots & FOR_1 \\ FOR_2 & FOR_2 & \dots & FOR_2 \\ \vdots & \vdots & \ddots & \vdots \\ FOR_{n_{component}} & FOR_{n_{component}} & \dots & FOR_{n_{component}} \end{bmatrix} \tag{3.2}$$

$$M_{States} = \begin{bmatrix} S_{1,1} & S_{1,2} & \dots & S_{1,n_{states}} \\ S_{2,1} & S_{2,2} & \dots & S_{2,n_{states}} \\ \vdots & \vdots & \ddots & \vdots \\ S_{n_{component},1} & S_{n_{component},2} & \dots & S_{n_{component},n_{states}} \end{bmatrix} \tag{3.3}$$

In order to provide a more thorough illustration of the State Sampling approach, consider an example involving the investigation of three system states. The system under consideration comprises three buses, with Bus 1 and Bus 2 featuring one generator each, and three lines interconnecting the buses. This configuration can be seen in Figure 3.2. The FOR values assigned to each component, as indicated in Figure 3.2, are used to construct the M_{FOR} matrix, as presented in Equation (3.4). Random numbers are generated to

generate the three system states, and the corresponding samples, $M_{samples}$ are also seen in Equation (3.4). Element-wise, the M_{FOR} is then compared with the $M_{samples}$ matrix to assess the availability status of each component. The resulting matrix, M_{states}, illustrates the availability of the components for the three system states.

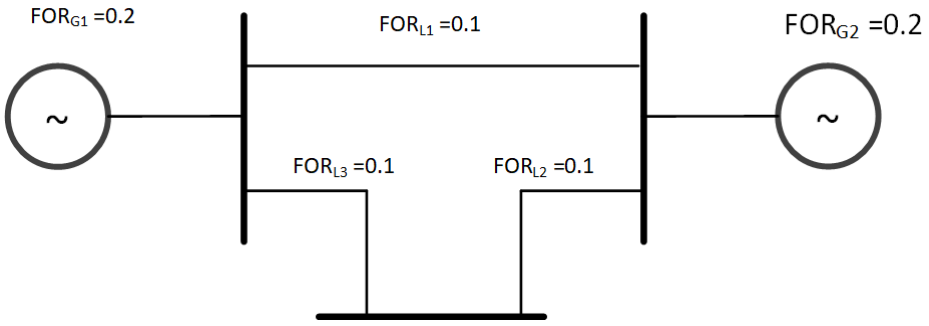

Figure 3.2: *System with two generators, three buses and three lines.*

Following the reasoning above, the size of the matrices are

$$M_{samples} = \begin{bmatrix} 0.05 & 0.5 & 0.9 \\ 0.6 & 0.05 & 0.8 \\ 0.2 & 0.8 & 0.3 \\ 0.7 & 0.9 & 0.4 \\ 0.05 & 0.3 & 0.6 \end{bmatrix}$$

$$M_{FOR} = \begin{bmatrix} 0.2 & 0.2 & 0.2 \\ 0.2 & 0.2 & 0.2 \\ 0.1 & 0.1 & 0.1 \\ 0.1 & 0.1 & 0.1 \\ 0.1 & 0.1 & 0.1 \end{bmatrix} \tag{3.4}$$

$$M_{states} = \begin{bmatrix} 1 & 0 & 0 \\ 0 & 1 & 0 \\ 0 & 0 & 0 \\ 0 & 0 & 0 \\ 1 & 0 & 0 \end{bmatrix}$$

The evaluation of a large number of system states becomes necessary when simulating over many years, leading to a significant challenge in achieving convergence. Consequently, the

utilisation of filtering techniques becomes crucial to reduce the number of states analysed in the contingency solver. Chapter 4 of this thesis will provide a detailed explanation of the screening and filtering techniques employed during the HLII assessment, again following the excellent work done in [22].

Following are three examples to provide some clarity on how to use MCS and calculate reliability indices. The first example showcases how the State Sampling method (Section 2.5.2) may be used. The second example illustrates similarly for the State Transition method (Section 2.5.4). The third and final example illustrates a calculation of reliability indices LOLE and EENS.

3.1.3 State Sampling Example

An example is provided for clarity of the method. Consider a system consisting of four generating units, each with a capacity of 20 MW and a FOR of 0.02 is considered. The aim of this example is to sample one state using the State Sampling approach. The system consists of four units, so a vector of four uniformly distributed variables in the range $[0, 1]$ is generated. This is illustrated in Equation (3.5).

$$R = \begin{Bmatrix} 0.6581 & 0.2783 & 0.9419 & 0.0032 \end{Bmatrix} \tag{3.5}$$

The system matrix, S, is found by comparing the elements of R against the FOR value of the generating units. The system matrix is given in Equation (3.6), where 1 indicates up-state.

$$S = \begin{Bmatrix} 1 & 1 & 1 & 0 \end{Bmatrix} \tag{3.6}$$

Equation (3.6) yields an available capacity of 60 MW, and 20 MW on outage.

3.1.4 State Transition Example

The State Transition method is also applicable for MCS methods. An example is provided to describe the method. The aim of the example is to obtain the two next system states

and the duration to those states using State Transition. Assume a system consisting of four generators with a capacity of 20 MW, expected failure rate of 1, and a repair rate of 100. The initial system state is set to all units functioning, meaning $S_0 = \begin{Bmatrix} 1 & 1 & 1 & 1 \end{Bmatrix}$. For state S_0, the λ values are given in the second column in Table 3.5. For this specific system state, the next system state intervals, used to determine which component transitions, are given by Equation (3.7). (Calculated from Equation (2.18))

$$R = \begin{Bmatrix} 0.25 & 0.5 & 0.75 & 1 \end{Bmatrix} \tag{3.7}$$

Table 3.4: *Randomly generated variables for the State Transition method.*

	State 0	State 1
U_1	0.2341	0.9321
U_2	0.1389	0.8012

Randomly generated variables U_i are given in Table 3.4.

Using that $\sum_{i=1}^{m} \lambda_i = \lambda_{sys} = 4$ and $U_1 = 0.2341$ in Equation (2.17), the time until next transition is $T_0 = 0.3630$ years. From $U_2 = 0.1389$ and Equation (3.7), Generator 1 is found to transition.

Table 3.5: λ *values for the State Transition example.*

Component	λ for S_0 [Incidents/year]	λ for S_1 [Incidents/year]
Generator 1	1	100
Generator 2	1	1
Generator 3	1	1
Generator 4	1	1
System	4	103

This means $S_1 = \begin{Bmatrix} 0 & 1 & 1 & 1 \end{Bmatrix}$. The λ values for S_1 are found in the third column of Table 3.5. This gives the intervals shown in Equation (3.8) for the next State Transition

iteration, again using Equation (2.18).

$$R = \begin{Bmatrix} 0.9709 & 0.9806 & 0.9903 & 1 \end{Bmatrix} \tag{3.8}$$

Now, the time to the next transition is found by using, $\sum_{i=1}^{m} \lambda_i = \lambda_{sys} = 103$ and $U_1 = 0.9321$, yielding $T_1 = 0.000683$ years. From $U_2 = 0.8012$ and Equation (3.8), again Generator 1 is found to transition. (Since $U_2 < R\,[0]$ from Equation (3.8)). The system states are now $S_2 = \begin{Bmatrix} 1 & 1 & 1 & 1 \end{Bmatrix}$.

The results for this example can be found in Table 3.6.

Table 3.6: *State Transition example: Resulting states and duration*

	$i = 0$	$i = 1$	$i = 2$
S_n	$\begin{Bmatrix} 1 & 1 & 1 & 1 \end{Bmatrix}$	$\begin{Bmatrix} 0 & 1 & 1 & 1 \end{Bmatrix}$	$\begin{Bmatrix} 1 & 1 & 1 & 1 \end{Bmatrix}$
T_n [years]	0.3630	0.000683	

3.1.5 Reliability Index Calculation - An Example of LOLE and EENS

An example is presented on how a reliability index may be calculated. Consider a system of four generators, where each of the generators has a capacity of 40 MW. It is assumed a constant yearly peak load of 150 MW. Based on the simulated states, shown in Table 3.7, the LOLE and EENS indices are obtained. In this example, the states are simulated once per year. The MCS approach used in this example is the State Sampling approach. A FOR of 0.1 is set for each generator. The hours for a year is set to 8736 hours/year.

Table 3.7: *MCS data for calculation of reliability index.*

Simulation year number	Random generated variables	System State Vector	LOL [year]	ENS [MWh]
1	$\{0.823 \quad 0.6968 \quad 0.6466 \quad 0.1597\}$	$\{1 \quad 1 \quad 1 \quad 1\}$	0	0
2	$\{0.2445 \quad 0.2421 \quad 0.1525 \quad 0.2803\}$	$\{1 \quad 1 \quad 1 \quad 1\}$	0	0
3	$\{0.8268 \quad 0.0764 \quad 0.6789 \quad 0.7746\}$	$\{1 \quad 0 \quad 1 \quad 1\}$	1	262 080
4	$\{0.0357 \quad 0.3714 \quad 0.9336 \quad 0.5028\}$	$\{0 \quad 1 \quad 1 \quad 1\}$	1	262 080
5	$\{0.7849 \quad 0.6116 \quad 0.081 \quad 0.1565\}$	$\{1 \quad 1 \quad 0 \quad 1\}$	1	262 080

The average for LOLE and EENS are found in Equation (3.9) and Equation (3.10), respectively.

$$LOLE = \frac{0 \cdot 2 + 1 \cdot 3}{5} = 0.6 \left[\text{years/year}\right] \tag{3.9}$$

$$EENS = \frac{0 \cdot 2 + 262080 \cdot 3}{5} = 157248 \left[\text{MWh/year}\right] \tag{3.10}$$

The standard deviation (SD) is also found by taking the square root of the variance from Equation (2.25). The SD for the LOLE and EENS reliability indices are shown in Equation (3.11) and Equation (3.12).

$$SD_{LOLE} = 0.245 \left[\text{years/year}\right] \tag{3.11}$$

$$SD_{EENS} = 64196 \left[\text{MWh/year}\right] \tag{3.12}$$

3.1.6 Convergence Criteria

In the context of this thesis, the simulation approach involves calculating the coefficient of variation (CoV) after completing the simulations. The purpose of this calculation is to assess the convergence of the reliability indices. The CoV can in many cases be used as a stopping criterion for MCS methods [22]. In this thesis, because of the use of the simultaneous sampling in order to achieve lower computational time as done in [22], this is not the case.

As explained in Section 2.5.7, selecting an appropriate CoV involves finding a balance between accuracy and computational time. In [25][51] the CoV used in case studies varies between 1% and 10%. The selection depends on the demanded accuracy of the results. In this thesis, this is used as a benchmark, similarly to [22]. This means that successful convergence is achieved for CoV in the lower end of the interval of 1% to 10%.

3.1.7 Isolated Buses

In the process of evaluating the sampled states of a power system network, it is necessary to examine the potential on the isolation of buses or specific parts of the system. Isolation refers to situations where one or more lines are on outage, leading to a lack of connection

between a bus or a group of buses and the remainder of the system. It is an important aspect to consider due to the disconnection of loads at the isolated buses. Mathematically, the complications that arise from the isolation of buses, have their origin in the singularity of the Jacobian matrix [52].

Literature has been investigated for methods that handle detection and management of isolated buses. Among others is the approach of [52], where bus isolation is detected for multiple line outages. Methods like linked list approaches, numerical methods, and graph-theoretic schemes are mentioned in [52] as the main categories of the tools available to detect island formations. Several of these propose interesting implementations, which could have been adapted into this thesis. However, to limit the scope of work, the approach proposed by [31] is followed. The reader is referred to [31] for an in-depth explanation of the bus isolation algorithm applied. The approach is here presented briefly.

3.1.7.1 Bus Isolation Detection Algorithm

1. Step 1: If any of the power system components, i.e. generators and lines, subject to the MCS state sampling are on outage, they are removed from the system under consideration.

2. Step 2: The conductance and susceptance matrices are then constructed with respect to the MCS state sampling, and are utilised to check if any buses are isolated from the system.

3. Step 3: Each bus is checked for line connections to a bus with a lower number, if is is not, the bus is marked as isolated. This has a control step where a check is conducted to see if any bus is marked incorrectly: If that is the case, it is corrected to be marked as not isolated.

4. Step 4: Confirmed isolated buses are then removed from the conductance and susceptance matrices.

The described approach is only applied for contingency cases where one or more line outages are present, since an outage of a generator would not result in the isolation of a bus.

3.2 OPF in HLII Adequacy Assessment

OPF is used in this HLII adequacy assessment to find a feasible operating point subject to the system states that are the output from the MCS state sampling. This section uses the theory presented in Section 2.7, in order to formulate a specific description for the OPF problem which is solved for each system state. First, the model of the system is presented, in hand with the theory presented on power flow and OPF studies. The implemented DCOPF method is tested in the algorithmic approach, and compared to results of [22], which can be seen in Chapter 5. Note again that the following OPF formulation, and in general this section, is based on the deduction and work of [31].

3.2.1 DCOPF

As stated, this thesis puts emphasis on the DC based approach. The main benefit and reasoning behind it is to formulate transmission line flows as linear functions of the net power injected at the buses in the system. With this as a foundation, it is possible to achieve a convex optimisation problem.

The net injection vector in standard DCOPF needs a small adjustment to some classical definitions where it is said that the net injection is equal to the generation minus the load associated with the considered bus. In this case, the load is considered to be constant in the analysis. This leads to the introduction of the load curtailment vector, $\mathbf{C_p}$ in the expression for the net injection. It is used in such a way that if there is need to reduce load to maintain balance of active power, it is done by shedding, or curtailing, loads. The net injection vector, $\mathbf{P}$, is shown in Equation (3.13) [31].

$$\mathbf{P} = \mathbf{P_g} + \mathbf{C_p} - \mathbf{P_{load}} \tag{3.13}$$

The necessary building blocks to formulate the DCOPF problem have been formulated, by making use of Section 2.9.1. Following is a description of the constraints of the optimisation problem.

- Equality constraint: The power generation of the system must be larger or equal to the load requirement.

- Inequality constraint: The power flowing between buses are constrained to the current rating of the bus.
- Bound: The power generation at a bus cannot exceed the power generation capacity of the bus.
- Bound: The load curtailment at a bus cannot exceed the load demand at the bus.
- Bound: Non-negative constraints: The power generation and load curtailment at a bus cannot be negative.

When the OPF solver receives a system state, its goal is to find a feasible operating state subject to the aforementioned constraints. If a constraint is violated, the solver takes actions to restore the system to a feasible state. First, it attempts to reschedule generation. If that is not enough, load curtailments are considered. The order of actions is determined by an objective function that assigns costs to rescheduling generation and load curtailments. By setting higher costs for load curtailments, the solver prioritizes generation rescheduling. Different costs for load curtailments at each bus allow for a prioritised list, starting with the bus where curtailment costs are lowest [53]. This approach can be represented by a row vector of $2n$ elements, where n is the number of buses in the system. This vector is shown in Equation (3.14). The first n elements represent the cost associated with rescheduling generation, and the subsequent n elements represent the cost of load curtailments. In this analysis, the cost for rescheduling generation are uniformly set to zero, while the costs for load curtailments are determined based on the specifications provided in the input data, Table 3.3. Each cost element corresponds to a decision variable, which is optimised to minimise the overall cost. These decision variables are organised in a column vector, where the first n elements represents the generation, P_{gi}, at the buses, and the following n elements represent the load curtailments, C_i, at the buses [31]. The decision variables are illustrated in Equation (3.15).

$$\mathbf{W} = \begin{bmatrix} w_1 & w_2 & \dots & w_n & w_{n+1} & ... & w_{2n} \end{bmatrix} \tag{3.14}$$

$$\mathbf{X} = \begin{bmatrix} P_{g1} & P_{g2} & \dots & P_{gn} & C_1 & C_2 & \dots & C_n \end{bmatrix}^T \tag{3.15}$$

As the system is now represented in terms of vectors and matrices, the next step is to formulate the OPF problem. In accordance with [31], the optimisation problem is presented from the objective function (3.16) through the constraints (3.17)-(3.20).

$$\text{minimize} \quad f = \sum_{i=1}^{n} C_i \tag{3.16}$$

$$\text{s.t} \quad \sum_{i=1}^{n} P_{gi} + \sum_{i=1}^{n} C_i = \sum_{i=1}^{n} P_{load,i}, \qquad \forall i \in \mathcal{N} \tag{3.17}$$

$$|\mathbf{A} \cdot \mathbf{P}| \leq \mathbf{T_{lim}}, \qquad \forall l \in \mathcal{L} \tag{3.18}$$

$$0 \leq P_{gi} \leq P_{cap,i} \qquad \forall i \in \mathcal{N} \tag{3.19}$$

$$0 \leq C_i \leq P_{load,i} \qquad \forall i \in \mathcal{N} \tag{3.20}$$

In the formulation the set $\mathcal{N}$ represents the buses, and the set $\mathcal{L}$ represents the lines of the system. Constraint (3.17) depicts the power balance of the system; the sum of active power generation and load curtailments for each bus is equal to the total load of the system. Constraint (3.18) presents the limitation of the active power that can flow on the lines in the system. The absolute value in this constraint is present as the active power flow can flow in in two direction, either from bus $i \rightarrow j$ or bus $j \rightarrow i$, which may results in negative values when multiplying values from $\mathbf{A}$ and $\mathbf{P}$. Constraint (3.19) is limiting the active power generation associated with a bus. The last Constraint (3.20) limits the load to be curtailed to the load demand at the associated bus [31].

The optimisation problem described needs some modifications, in order to formulate it to Pyomo in a fitting manner. It is a necessity to formulate the problem in terms of the decision variables. The problem is formulated in Python, using the Pyomo framework, and Gurobi as the solver of choice. The reasoning for selection of framework and solver will be discussed in Chapter 4. Using the presented notations in this section, the concrete formulation in Pyomo is as the following.

- **Objective function**: The objective function is expressed in terms of the decision variables through Equation (3.21).

$$f = \mathbf{W_{genCost}} \cdot \mathbf{X_{P_g}} + \mathbf{W_{curtCost}} \cdot \mathbf{X_C} \tag{3.21}$$

  It could also be formulated by combining the cost vectors and decision variables into

one vector each, as shown in Equation (3.14) and Equation (3.15). This was just the Author's preference in management of the decision variables during implementation.

- **Equality constraint**: The Constraint (3.17) which states the power balance of the system is reformulated to Equation (3.22).

$$\mathbf{K} \cdot \mathbf{X_{P_g}} + \mathbf{K} \cdot \mathbf{X_C} = \sum_{i=1}^{n} P_{load,i} \tag{3.22}$$

  $\mathbf{K}$ is a row vector of n elements, with values equal to one. This way, an expression in terms of the decision variables is obtained. Again, it could be formulated by combining the decision variables to one vector, and increasing the size of $\mathbf{K}$ to be $2n$ elements with values of one [31].

- **Inequality constraint:** For the Constraint (3.18), which limits the power flow through transmission lines, the absolute value sign must be removed. This can be done by converting the constraint into two inequality constraints. Also, the load demand is constant, so the multiplication of $\mathbf{A}$ and $\mathbf{P_{load}}$ can be moved to the constant side of the inequality. The new inequalities are shown in as Constraint (3.23) and Constraint (3.24).

$$\mathbf{A} \cdot \mathbf{X_{P_g}} + \mathbf{A} \cdot \mathbf{X_C} \leq \mathbf{T_{lim}} + \mathbf{A} \cdot \mathbf{P_{load}} \tag{3.23}$$

$$-\mathbf{A} \cdot \mathbf{X_{P_g}} - \mathbf{A} \cdot \mathbf{X_C} \leq \mathbf{T_{lim}} - \mathbf{A} \cdot \mathbf{P_{load}} \tag{3.24}$$

  Again the decision variables could be combined into one vector. The formulation would then be as seen in Equation (3.25) and Equation (3.26), which is the approach used in [31].

$$\begin{bmatrix} \mathbf{A} & \mathbf{A} \end{bmatrix} \cdot \mathbf{X} \leq \mathbf{T_{lim}} + \mathbf{A} \cdot \mathbf{P_{load}} \tag{3.25}$$

$$-\begin{bmatrix} \mathbf{A} & \mathbf{A} \end{bmatrix} \cdot \mathbf{X} \leq \mathbf{T_{lim}} - \mathbf{A} \cdot \mathbf{P_{load}} \tag{3.26}$$

To summarize, the model formulation for DCOPF that is implemented in Python with

Pyomo, is shown in Equation (3.27).

$$\left.\begin{aligned}
&\text{minimize} && f = \mathbf{W_{genCost}} \cdot \mathbf{X_{P_g}} + \mathbf{W_{curtCost}} \cdot \mathbf{X_C} && \\
&\text{s.t} && \mathbf{K} \cdot \mathbf{X_{P_g}} + \mathbf{K} \cdot \mathbf{X_C} = \textstyle\sum_{i=1}^{n} P_{load,i} && \forall i \in \mathcal{N} \\
& && \mathbf{A} \cdot \mathbf{X_{P_g}} + \mathbf{A} \cdot \mathbf{X_C} \leq \mathbf{T_{lim}} + \mathbf{A} \cdot \mathbf{P_{load}} && \forall l \in \mathcal{L} \\
& && -\mathbf{A} \cdot \mathbf{X_{P_g}} - \mathbf{A} \cdot \mathbf{X_C} \leq \mathbf{T_{lim}} - \mathbf{A} \cdot \mathbf{P_{load}} && \forall l \in \mathcal{L} \\
& && 0 \leq P_{gi} \leq P_{cap,i} && \forall i \in \mathcal{N} \\
& && 0 \leq C_i \leq P_{load,i} && \forall i \in \mathcal{N}
\end{aligned}\right\} \tag{3.27}$$

3.2.2 DC-PSCOPF

As mentioned, one of the main contributions of this thesis is the implementation of DC-PSCOPF in the OPF analysis of the algorithmic approach in calculating reliability indices. This section explains how the method is implemented in Python, using the framework of Pyomo, and theory presented in Section 2.10.

The DCOPF formulation defined in Section 3.2.1, is extended to consider the outage of a component in the system. The constraints added to the optimisation problem, allow the DCOPF problem to manage post-contingency line flows. The approach is as follows.

The model in [50] is extended to account for load curtailments, including this as a decision variable in the mathematical formulation. The following mathematical formulation is applied to describe the post contingency formulations, denoted as DC-PSCOPF.

$$\text{minimize} \quad f = \sum_{i=1}^{n} C_i \tag{3.28}$$

$$\text{s.t} \quad \sum_{i=1}^{n} P_{gi} + \sum_{i=1}^{n} C_i = \sum_{i=1}^{n} P_{load,i} \qquad \forall i \in \mathcal{N} \tag{3.29}$$

$$|\mathbf{A} \cdot \mathbf{P}| \leq \mathbf{T_{lim}} \qquad \forall l \in \mathcal{L} \tag{3.30}$$

$$-\mathbf{T_{lim}} + \mathbf{G} \cdot \mathbf{P_{load}} \leq \mathbf{AP} \leq \mathbf{T_{lim}} + \mathbf{G} \cdot \mathbf{P_{load}} \qquad \forall \alpha \in \mathcal{A} \tag{3.31}$$

$$0 \leq P_{gi} \leq P_{cap,i} \qquad \forall i \in \mathcal{N} \tag{3.32}$$

$$0 \leq C_i \leq P_{load,i} \qquad \forall i \in \mathcal{N} \tag{3.33}$$

where $\mathbf{G} = \mathbf{A} + \mathbf{LODF} \cdot \mathbf{A}$. The set $\mathcal{A}$ is the set of active lines in the system. For

contingency cases where one line is on outage, this set has the size $\mathcal{A} = \mathcal{L} - 1$. If two lines on outage, $\mathcal{A} = \mathcal{L} - 2$, and so on. There is only one difference from the formulation of the DCOPF seen in (3.16)-(3.20), which is the inclusion of Constraint (3.31). This constraint considers the effect of post-contingency line flows in the system, resulting from a line outage, using the LODFs.

This formulation presents a highly effective approach to solving SCOPF problems by simultaneously handling pre- and post-contingency constraints. It achieves this by exclusively using linear distribution factors, the PTDFs and LODFs. Notably, these factors remain fixed throughout the analysis, enhancing computational efficiency.

Again, some modifications must be made in the formulation of the optimisation problem in Python with Pyomo. Following is a description of the model implemented, following the same reasoning as for the DCOPF model. As a result, the model below is obtained.

$$\text{minimize} \quad f = \mathbf{W_{genCost}} \cdot \mathbf{X_{P_g}} + \mathbf{W_{curtCost}} \cdot \mathbf{X_C} \tag{3.34}$$

$$\text{s.t.} \quad \mathbf{K} \cdot \mathbf{X_{P_g}} + \mathbf{K} \cdot \mathbf{X_C} = \sum_{i=1}^{n} P_{\text{load},i} \qquad \forall i \in \mathcal{N} \tag{3.35}$$

$$\mathbf{A} \cdot \mathbf{X_{P_g}} + \mathbf{A} \cdot \mathbf{X_C} \leq \mathbf{T}_{\text{lim}} + \mathbf{A} \cdot \mathbf{P}_{\text{load}} \qquad \forall l \in \mathcal{L} \tag{3.36}$$

$$-\mathbf{A} \cdot \mathbf{X_{P_g}} - \mathbf{A} \cdot \mathbf{X_C} \leq \mathbf{T}_{\text{lim}} - \mathbf{A} \cdot \mathbf{P}_{\text{load}} \qquad \forall l \in \mathcal{L} \tag{3.37}$$

$$\mathbf{A} \cdot \mathbf{X_{P_g}} + \mathbf{A} \cdot \mathbf{X_C} \leq \mathbf{T}_{\text{lim}} + [\mathbf{A} + \mathbf{LODF} \cdot \mathbf{A}] \cdot \mathbf{P}_{\text{load}} \qquad \forall \alpha \in \mathcal{A} \tag{3.38}$$

$$-\mathbf{A} \cdot \mathbf{X_{P_g}} - \mathbf{A} \cdot \mathbf{X_C} \leq \mathbf{T}_{\text{lim}} - [\mathbf{A} + \mathbf{LODF} \cdot \mathbf{A}] \cdot \mathbf{P}_{\text{load}} \qquad \forall \alpha \in \mathcal{A} \tag{3.39}$$

$$0 \leq P_{gi} \leq P_{\text{cap},i} \qquad \forall i \in \mathcal{N} \tag{3.40}$$

$$0 \leq C_i \leq P_{\text{load},i} \qquad \forall i \in \mathcal{N} \tag{3.41}$$

The only difference from the DCOPF formulation previously displayed, is the inclusion of Constraint (3.38) and Constraint (3.39). As for the DCOPF case with pre-contingencies, the post-contingency constraint is split in two. These two constraints handle the impact of the line(s) on outage on the remaining operating lines. Therefore, the set $\mathcal{A}$ varies with the amount of lines on outage. If the set of lines on outage are denoted as $\mathcal{O}$, the set of active lines may be denoted as $\mathcal{A} = \mathcal{L} - \mathcal{O}$. In this thesis, the set $\mathcal{O}$ has a maximum size of one. However, the implementation of LODFs consider multiple line outages, if necessary.

It is important to always be wary of the size of the matrices and vectors when formulating the optimisation problem. For instance, when calculating Constraint (3.38) and Constraint (3.39), it is of significance to remove an element from the sensitivity matrix $\mathbf{A}$ corresponding to the line that is on outage. The same applies for the parameter of line flow ratings, T_{lim}, that the line on outage is not included in the set $\mathcal{A}$ is removed from the correct index. An example of post-contingency line flow calculation using LODFs will be illustrated to help clarify how the LODFs work in this analysis, and how they may be applied for multiple line outages. This is illustrated in the following Section 3.3.

3.3 Post-contingency Line Flow Calculation Through LODFs: Examples

The following section presents two illustrative examples to clarify the utility of the LODFs in contingency analysis. First, an example is shown for a simple 4-bus system, inducing a single line outage. Subsequently, an example inducing multiple line outages is applied for the same system. The aim is to calculate the post-contingency line flows.

3.3.1 4-bus Example: Single Line Outage

Given the 4-bus system in Figure 3.3. P_2, P_3 and P_4 in figure represent the net injections on each bus. The network and bus parameters are given in Table 3.8 and Table 3.9, respectively.

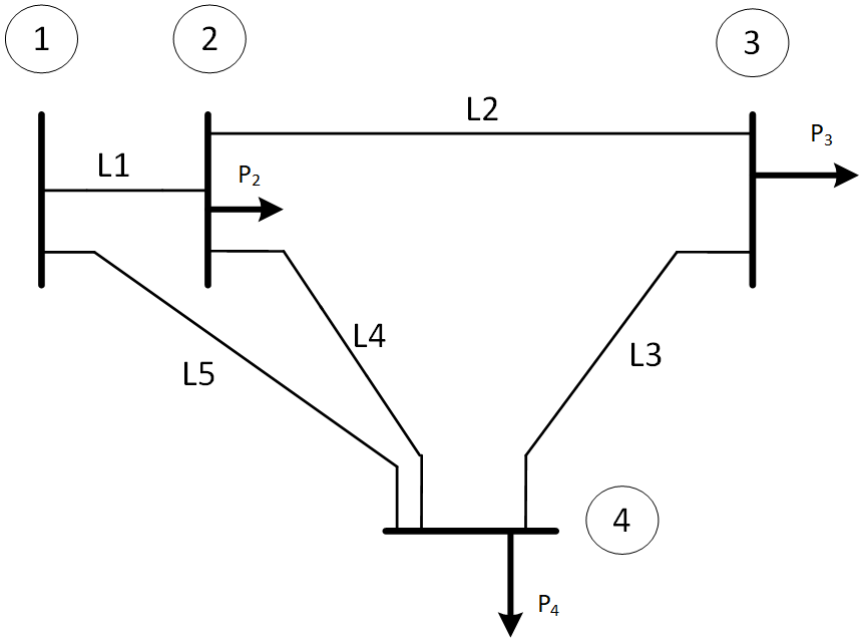

Figure 3.3: *4-bus system with no contingencies.*

Table 3.8: *Line data for 4-bus system, data given in p.u. Line losses are neglected* $R_{ij} = 0$.

Line [Frombus - Tobus]	Reactance [X]
L1: [1 - 2]	0.25
L2: [2 - 3]	0.1
L3: [3 - 4]	0.25
L4: [2 - 4]	0.25
L5: [1 - 4]	0.25

Table 3.9: *Bus data for 4-bus system*

Bus number	Loads
1 (slack)	-
2	-0.6
3	-1.25
4	-0.4

Say, an outage occurs for the line L3. The task at hand is to find the resulting post-contingency power flows in the network, through the LODFs. In order to achieve this, the theory presented in Section 2.9.2 is followed, and presented in a step-wise manner. The new topology is illustrated in Figure 3.4.

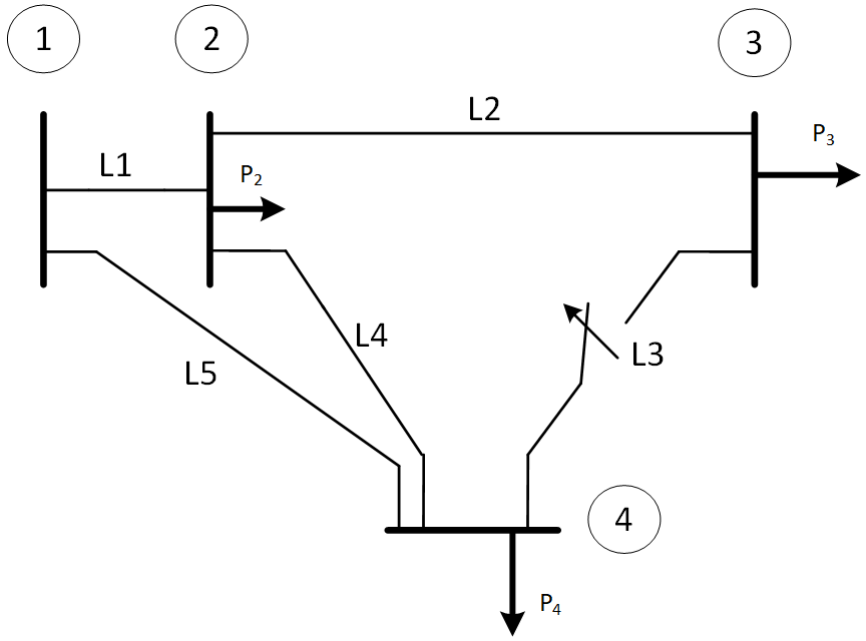

Figure 3.4: *4-bus system with contingency case: Outage of L3 connecting bus 3 and bus 4.*

The set $\mathcal{A}$ contains the lines not on outage (i.e. L1, L2, L4 and L5), and the set $\mathcal{O}$ contains the line on outage (i.e. L3). The first step is to calculate $\mathbf{PTDF}^{\mathbf{0}}_{\mathcal{A},\mathcal{O}}$ and $\mathbf{PTDF}^{\mathbf{0}}_{\mathcal{O},\mathcal{O}}$ from Equation (2.66). In order to do this, the matrices $\mathbf{\Phi}$, $\mathbf{\Psi}$, $\mathbf{X}_{\mathcal{A}}$ and $\mathbf{X}_{\mathcal{O}}$ must be calculated.

Given the system data, the matrices $\mathbf{\Phi}$, $\mathbf{\Psi}$, $\mathbf{X}_{\mathcal{A}}$ and $\mathbf{X}_{\mathcal{O}}$ can be determined as shown in (3.42) and (3.43).

$$\mathbf{\Phi^T} = \begin{bmatrix} 1 & -1 & 0 & 0 \\ 0 & 1 & -1 & 0 \\ 0 & 1 & 0 & -1 \\ 1 & 0 & 0 & -1 \end{bmatrix}, \qquad \mathbf{\Psi^T} = \begin{bmatrix} 0 & 0 & 1 & -1 \end{bmatrix}, \tag{3.42}$$

$$\mathbf{X}_{\mathcal{A}} = \begin{bmatrix} 0.25 & 0 & 0 & 0 \\ 0 & 0.1 & 0 & 0 \\ 0 & 0 & 0.25 & 0 \\ 0 & 0 & 0 & 0.25 \end{bmatrix}, \qquad \mathbf{X}_{\mathcal{O}} = \begin{bmatrix} 0.25 \end{bmatrix}. \tag{3.43}$$

The susceptance matrix for the base case conditions, $\mathbf{B^0}$, is calculated through Equa-

tion (2.51).

$$\mathbf{B} = \begin{bmatrix} 8 & -4 & 0 & -4 \\ -4 & 18 & -10 & -4 \\ 0 & -10 & 14 & -4 \\ -4 & -4 & -4 & 12 \end{bmatrix} \tag{3.44}$$

However, some adaptations have to be made. The determinant of $\mathbf{B^0}$ is zero, meaning the matrix is singular and thus cannot be inverted. To avoid problems with singular matrices, the principle of the slack bus is used. Utilising that our slack bus is bus number 1, $\mathbf{B_{sub}}$ is established by removing the rows and columns corresponding to bus 1.

$$\mathbf{B_{sub}} = \begin{bmatrix} 18 & -10 & -4 \\ -10 & 14 & -4 \\ -4 & -4 & 12 \end{bmatrix} \tag{3.45}$$

Then the $\mathbf{Z}$ matrix is constructed according to Equation (2.54). Note that it is the $\mathbf{Z}$ matrix that is used in Equation (2.62), in place of the $\mathbf{B^0}$. $\mathbf{PTDF^0_{\mathcal{A},\mathcal{O}}}$ and $\mathbf{PTDF^0_{\mathcal{O},\mathcal{O}}}$ are calculated,

$$\begin{aligned} \mathbf{PTDF^0_{\mathcal{A},\mathcal{O}}} &= \begin{bmatrix} 0.25 & 0 & 0 & 0 \\ 0 & 0.1 & 0 & 0 \\ 0 & 0 & 0.25 & 0 \\ 0 & 0 & 0 & 0.25 \end{bmatrix}^{-1} \begin{bmatrix} 1 & -1 & 0 & 0 \\ 0 & 1 & -1 & 0 \\ 0 & 1 & 0 & -1 \\ 1 & 0 & 0 & -1 \end{bmatrix} \begin{bmatrix} 0 & 0 & 0 & 0 \\ 0 & 0.1532 & 0.1371 & 0.097 \\ 0 & 0.1371 & 0.2016 & 0.1129 \\ 0 & 0.097 & 0.1129 & 0.1532 \end{bmatrix} \begin{bmatrix} 0 \\ 0 \\ 1 \\ -1 \end{bmatrix} \\ &= \begin{bmatrix} -0.1613 & -0.4839 & 0.3226 & 0.1613 \end{bmatrix}^T \end{aligned}$$

and,

$$\begin{aligned} \mathbf{PTDF^0_{\mathcal{O},\mathcal{O}}} &= \begin{bmatrix} 0.25 \end{bmatrix}^{-1} \begin{bmatrix} 0 & 0 & 1 & -1 \end{bmatrix} \begin{bmatrix} 0 & 0 & 0 & 0 \\ 0 & 0.1532 & 0.1371 & 0.097 \\ 0 & 0.1371 & 0.2016 & 0.1129 \\ 0 & 0.097 & 0.1129 & 0.1532 \end{bmatrix} \begin{bmatrix} 0 & 0 & 1 & -1 \end{bmatrix}^T \\ &= \begin{bmatrix} 0.5161 \end{bmatrix} \end{aligned}$$

Finally, using Equation (2.66), the LODFs are obtained.

$$\begin{aligned}\mathbf{LODF^c_{\mathcal{A},\mathcal{O}}} &= \begin{bmatrix}-0.1613 & -0.4839 & 0.3226 & 0.1613\end{bmatrix}^T \left(\begin{bmatrix}1\end{bmatrix} - \begin{bmatrix}0.5161\end{bmatrix}\right)^{-1} \\ &= \begin{bmatrix}-0.3333 & -1 & 0.6666 & 0.3333\end{bmatrix}^T\end{aligned}$$

With the LODFs defined, the new line flows of the system may be calculated through Equation (2.61).

$\mathbf{PL^0_{\mathcal{A}}}$ are the base case line flows of the active lines in the post-contingency state, and $\mathbf{PL^0_{\mathcal{O}}}$ is the base case line flow for the line(s) on outage. Next, the base case line flows are found. Here illustrated achievable in two different ways.

- Option 1: Using PTDFs. The PTDFs and the sensitivity matrix can be used to find the line flows of the system. This can be done by solving the system of equations (3.46).

$$\mathbf{P_{ij}} = \mathbf{A_{ij\times i}}\mathbf{P_i} \tag{3.46}$$

- Option 2: Through angle differences. The line flows can also be found as done in Equation (2.52). Note that the slack bus is not included in the set of equations, as δ_1 is fixed at 0.

  Solving Equation (2.52) for $\boldsymbol{\delta_i}$, opens the door to calculate the line flows through Equation (3.47).

$$P_{ij} = \frac{\delta_i - \delta_j}{X_{ij}} \tag{3.47}$$

In this case, the solution is found using option 1. The power transfer distribution factors are then established for each line.

$$\begin{aligned}
P_{12} &= \frac{z_{11}-z_{21}}{X_{12}}\cdot P_1 + \frac{z_{12}-z_{22}}{X_{12}}\cdot P_2 + \frac{z_{13}-z_{23}}{X_{12}}\cdot P_3 + \frac{z_{14}-z_{24}}{X_{12}}\cdot P_4 \\
P_{23} &= \frac{z_{21}-z_{31}}{X_{23}}\cdot P_1 + \frac{z_{22}-z_{32}}{X_{23}}\cdot P_2 + \frac{z_{23}-z_{33}}{X_{23}}\cdot P_3 + \frac{z_{24}-z_{34}}{X_{23}}\cdot P_4 \\
P_{34} &= \frac{z_{31}-z_{41}}{X_{34}}\cdot P_1 + \frac{z_{32}-z_{42}}{X_{34}}\cdot P_2 + \frac{z_{33}-z_{43}}{X_{34}}\cdot P_3 + \frac{z_{34}-z_{44}}{X_{34}}\cdot P_4 \\
P_{24} &= \frac{z_{21}-z_{41}}{X_{24}}\cdot P_1 + \frac{z_{22}-z_{42}}{X_{24}}\cdot P_2 + \frac{z_{23}-z_{43}}{X_{24}}\cdot P_3 + \frac{z_{24}-z_{44}}{X_{24}}\cdot P_4 \\
P_{14} &= \frac{z_{11}-z_{41}}{X_{14}}\cdot P_1 + \frac{z_{12}-z_{42}}{X_{14}}\cdot P_2 + \frac{z_{13}-z_{43}}{X_{14}}\cdot P_3 + \frac{z_{14}-z_{44}}{X_{14}}\cdot P_4
\end{aligned}$$

Illustrated in a more compact form of the sensitivity matrix **A**. The matrix **A** has the size of $l \times n$, where l represents the number of lines of the system, and n represents number of buses.

$$\mathbf{A} = \begin{bmatrix} 0 & -0.6129 & -0.5484 & -0.3871 \\ 0 & 0.1613 & -0.6452 & -0.1613 \\ 0 & 0.1613 & 0.3548 & -0.1613 \\ 0 & 0.2258 & 0.0968 & -0.2258 \\ 0 & -0.3871 & -0.4516 & -0.6129 \end{bmatrix}$$

The net injections are defined as $\begin{bmatrix} P_2 & P_3 & P_4 \end{bmatrix}^T = \begin{bmatrix} -0.7 & -0.5 & -0.9 \end{bmatrix}^T$. Bus 1 is excluded from this expression as it is the slack bus.

Through Equation (3.46), the following line flows are obtained

$$\begin{bmatrix} P_{12} & P_{23} & P_{34} & P_{24} & P_{14} \end{bmatrix}^T = \begin{bmatrix} 1.052 & 0.355 & -0.145 & -0.003 & 1.048 \end{bmatrix}^T$$

Using the network topology, the injections can be verified.

$$\begin{bmatrix} P_2 \\ P_3 \\ P_4 \\ P_1 \end{bmatrix} = \begin{bmatrix} P_{23} + P_{21} + P_{24} \\ P_{32} + P_{34} \\ P_{43} + P_{41} + P_{42} \\ P_2 + P_3 + P_4 \end{bmatrix} \approx \begin{bmatrix} -0.7 \\ -0.5 \\ -0.9 \\ 2.1 \end{bmatrix}$$

Note that some deviation in the values is present. This is due to decimal errors.

The flows and their direction are illustrated in Figure 3.5.

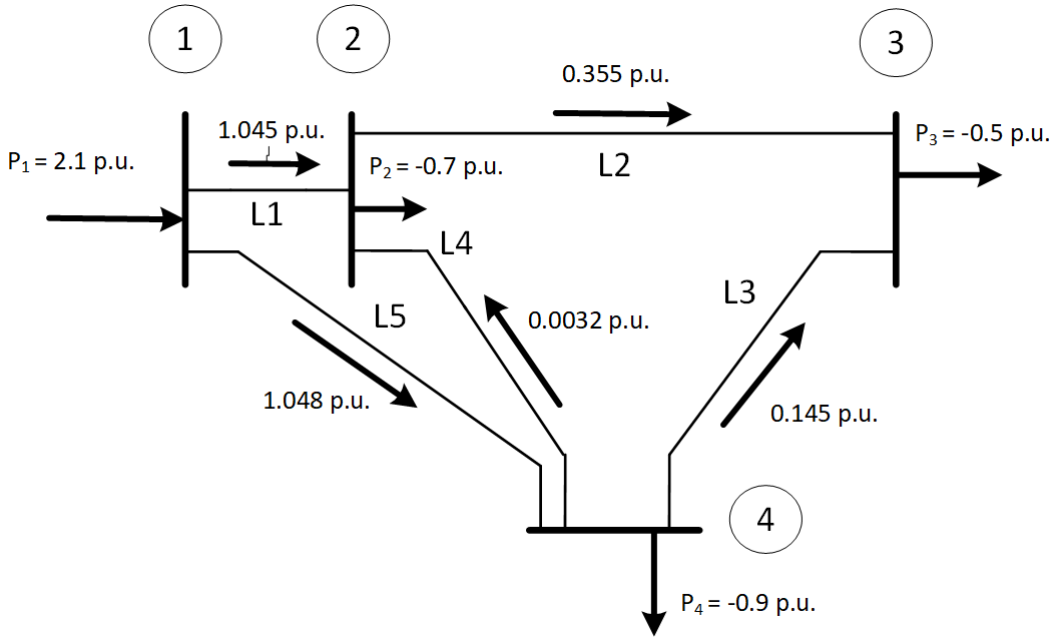

Figure 3.5: *4-bus system base case line flows.*

With knowledge of the base case line flows, the LODFs and the index of the line on outage, the line flows of the post-contingency case may be found using Equation (2.61).

$$\begin{bmatrix} Pc_{L1:1-2} \\ Pc_{L2:2-3} \\ Pc_{L4:2-4} \\ Pc_{L5:1-4} \end{bmatrix} = \begin{bmatrix} 1.093 \\ 0.5 \\ -0.0999 \\ 0.999 \end{bmatrix}$$

Figure 3.6 illustrates the post-contingency line flows.

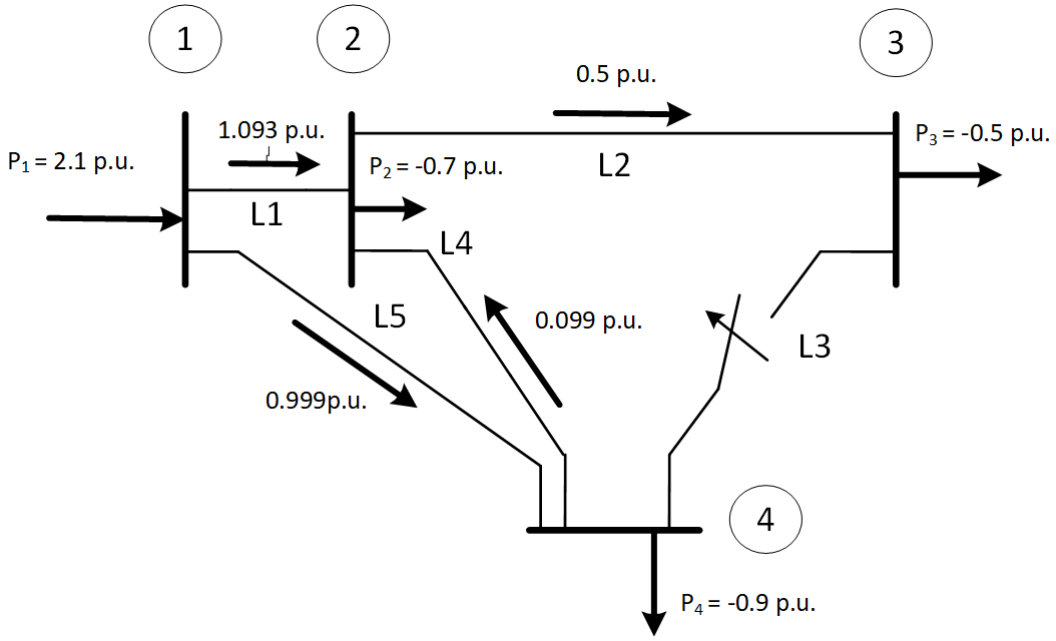

Figure 3.6: *4-bus system post-contingency line flows.*

Some deviations are present due to some shortcomings in the selection of decimals in calculations. Neglecting this, the system illustrates feasible power flows between nodes.

As mentioned, the procedure works with multiple lines on outage, making it a useful tool for contingency analysis.

3.3.2 4-bus Example: Multiple Line Outages

Next, an example is shown illustrating that the LODFs described in the previous example also work for multiple lines on outage. Consider again the system in Figure 3.3. This time, L1 and L4 are on outage. It is desired to determine the post-contingency line flows for the remaining lines. It is necessary to calculate the LODFs, similarly to the previous example. The base case power flows are naturally the same as for the previous case, and therefore not calculated.

The set $\mathcal{A}$ contains the lines not on outage (i.e. L2, L3 and L5), while the set $\mathcal{O}$ contains the lines on outage (i.e. L1 and L4). Note that the set $\mathcal{A}$ does not necessarily have to contain all the lines of the system that are not on outage. It could also solely be the lines that is of interest, which can be useful for larger networks. In this case, all lines are of interest.

Given the knowledge of which lines are on outage, including the network parameters, the matrices $\mathbf{\Phi}$, $\mathbf{\Psi}$, $\mathbf{X}_{\mathcal{A}}$ and $\mathbf{X}_{\mathcal{O}}$ can be determined.

$$\mathbf{\Phi^T} = \begin{bmatrix} 0 & 1 & -1 & 0 \\ 0 & 0 & 1 & -1 \\ 1 & 0 & 0 & -1 \end{bmatrix}, \qquad \mathbf{\Psi^T} = \begin{bmatrix} 1 & -1 & 0 & 0 \\ 0 & 1 & 0 & -1 \end{bmatrix}, \tag{3.48}$$

$$\mathbf{X}_{\mathcal{A}} = \begin{bmatrix} 0.1 & 0 & 0 \\ 0 & 0.25 & 0 \\ 0 & 0 & 0.25 \end{bmatrix}, \qquad \mathbf{X}_{\mathcal{O}} = \begin{bmatrix} 0.25 & 0 \\ 0 & 0.25 \end{bmatrix}. \tag{3.49}$$

The susceptance matrix $\mathbf{B^0}$ and coherent matrix $\mathbf{Z}$ are defined as in the previous example.

$$\mathbf{PTDF}^{\mathbf{0}}_{\mathcal{A},\mathcal{O}} = \begin{bmatrix} 0.1 & 0 & 0 \\ 0 & 0.25 & 0 \\ 0 & 0 & 0.25 \end{bmatrix}^{-1} \begin{bmatrix} 0 & 1 & -1 & 0 \\ 0 & 0 & 1 & -1 \\ 1 & 0 & 0 & -1 \end{bmatrix} \begin{bmatrix} 0 & 0 & 0 & 0 \\ 0 & 0.1532 & 0.1371 & 0.097 \\ 0 & 0.1371 & 0.2016 & 0.1129 \\ 0 & 0.097 & 0.1129 & 0.1532 \end{bmatrix} \begin{bmatrix} 1 & -1 & 0 & 0 \\ 0 & 1 & 0 & -1 \end{bmatrix}^T$$

$$= \begin{bmatrix} -0.161 & -0.1604 & 0.388 \\ 0.32 & 0.3216 & 0.2248 \end{bmatrix}^T$$

and,

$$\mathbf{PTDF}^{\mathbf{0}}_{\mathcal{O},\mathcal{O}} = \begin{bmatrix} 0.25 & 0 \\ 0 & 0.25 \end{bmatrix}^{-1} \begin{bmatrix} 1 & -1 & 0 & 0 \\ 0 & 1 & 0 & -1 \end{bmatrix} \begin{bmatrix} 0 & 0 & 0 & 0 \\ 0 & 0.1532 & 0.1371 & 0.097 \\ 0 & 0.1371 & 0.2016 & 0.1129 \\ 0 & 0.097 & 0.1129 & 0.1532 \end{bmatrix} \begin{bmatrix} 1 & -1 & 0 & 0 \\ 0 & 1 & 0 & -1 \end{bmatrix}^{T}$$

$$= \begin{bmatrix} 0.6128 & -0.2248 \\ -0.2248 & 0.4496 \end{bmatrix}$$

Which results in the LODFs,

$$\mathbf{LODF}^{\mathbf{c}}_{\mathcal{A},\mathcal{O}} = \begin{bmatrix} -0.161 & -0.1604 & 0.388 \\ 0.32 & 0.3216 & 0.2248 \end{bmatrix}^{T} \left(\begin{bmatrix} 1 & 0 \\ 0 & 1 \end{bmatrix} - \begin{bmatrix} 0.6128 & -0.2248 \\ -0.2248 & 0.4496 \end{bmatrix} \right)^{-1}$$

$$= \begin{bmatrix} -0.9875 & -0.9877 & 1.0027 \\ 0.9847 & 0.9877 & -0.00111 \end{bmatrix}^{T} \tag{3.50}$$

Which again results in the following post-contingency line flows, using Equation (2.61),

$$\begin{bmatrix} Pc_{L2:2-3} \\ Pc_{L3:3-4} \\ Pc_{L5:1-4} \end{bmatrix} = \begin{bmatrix} -0.687 \\ -1.187 \\ 2.1028 \end{bmatrix} \tag{3.51}$$

The line flows for this specific contingency scenario, with L1 and L4 on outage, are illustrated in Figure 3.7.

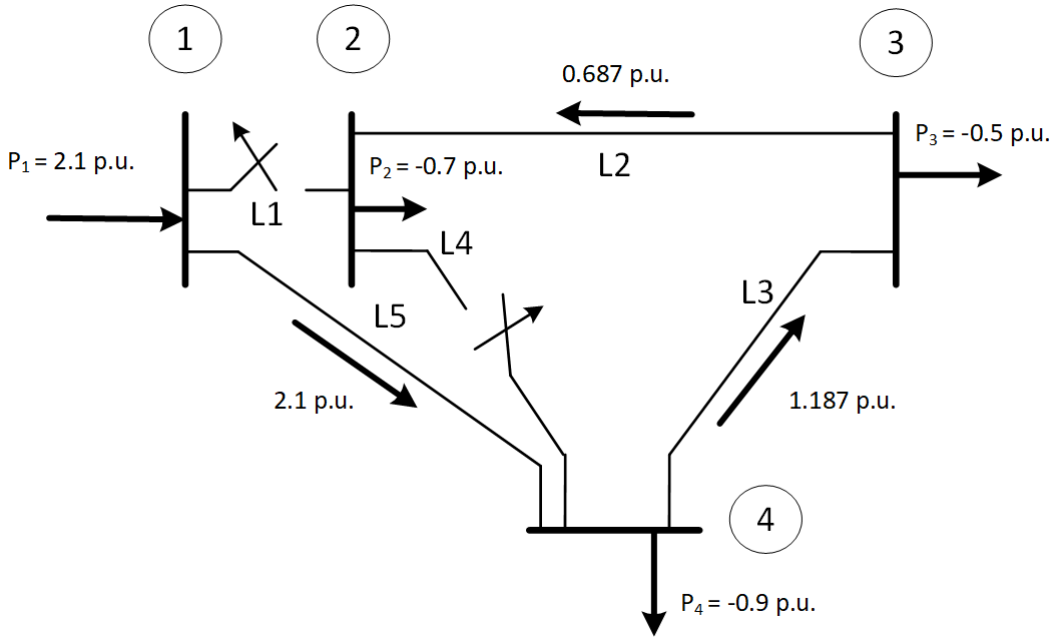

Figure 3.7: *4-bus system post-contingency line flows for outage of L1 and L4.*

Again, some deviation is present due to precision errors with decimals. Neglecting the small deviation, the power flows of the network seem feasible. All injected power at the slack bus follows the only path it can take towards bus 4, delivering 0.9 p.u. The remaining power transfers to bus 3, delivering to the load of 0.5 p.u. The remaining of load follows the last path, delivering to the load of 0.7 p.u.

4 Code Development and Programming

A significant portion of the efforts expended in this thesis involved the creation, and extension of a Python-based PSR tool. The objective was to devise a computational tool that can perform the HLII assessment, with OPF and SCOPF used in the contingency solver. The developed code is designed in a generalised manner, facilitating the implementation of most systems for the HLII assessment, regardless of the number of generators, buses, and transmission lines. It is essential that the system parameters follow the same input format as the test systems employed in this thesis.

The standard HLII assessment is implemented with a DCOPF formulation, using the MCS State Sampling method. The approach is based on the methodological approach of [22] and [31]. In-house software codes for composite system adequacy from the Department of Electric Energy (formerly, Department of Electric Power Engineering) were made available to this thesis work as a springboard and comparison for the code development conducted. Especially the work of [22] has been used as a foundation to build upon. The developed HLII DC-PSCOPF code is an extension of the standard HLII adequacy assessment. The approach of the standard HLII assessment is explained in Chapter 3.2.1, and the approach of DC-PSCOPF as the contingency solver is explained in Chapter 3.2.2.

Unlike the work conducted in [22], this thesis uses a different approach in the optimisation part of the algorithm. The approach in [22] took use of *Scipy* to handle the OPF formulations, this thesis takes use of *Pyomo* instead. *Pyomo* is an optimisation modeling language, while *Scipy* is a scientific library with numerical and scientific computing capabilities. Pyomo provides a higher level of abstraction and advanced features for optimization problems, while *Scipy* is a general-purpose library. As a result, the code treating optimisation is based on the adaptation of the methodology in [31], rather than a direct adaptation of the in-house Python code itself from [22].

4.1 Modelling in Python with Pyomo

This section aims to discuss and reason the choices made within the code development of this thesis. As mentioned, this thesis aimed to formulate the optimisation problem through the Pyomo framework in Python, using Gurobi as a solver.

4.1.1 Choice of Modelling Framework

To solve the OPF problem, it was decided to use the framework of Pyomo [54][55], as an alternative to the approach of the SciPy [56] method *optimize.minimize* used in [22] and the *fmincon* in MATLAB used in [31]. Pyomo is a Python-based open-source optimisation modeling language with a diverse set of optimisation capabilities for formulating and solving optimisation models. The formulated optimisation problems may be solved with commercial and open-source solvers.

The author of the thesis also finds the syntax of Pyomo understandable and intuitive to work with. Another advantage of selecting Pyomo as an optimisation tool framework is its inclusion in the educational curriculum of the study programmes at NTNU. At least for the author of the thesis, Pyomo has been featured in courses building up to the Master's thesis. Pyomo's use in courses allows for future students to apply their knowledge through the programming framework to further develop software codes handling complex optimisation problems within power system reliability. The formulation of the problems is similar to what is taught, when you learn your first optimisation problems written by hand. The mathematical modelling follows the central mathematical concepts of variables, parameters, constraints and objectives. In other words, a Pyomo model consists of modeling components that define the aspects of the mathematical model. These modelling components are shown below, related to their respective definitions in Pyomo through Python classes:

- `Set()` - This is set data which is used to define a model instance, initialized by the Python class.
- `Param()` - Parameter data which is used to define a model instance.

- `Var()` - Decision variables in a model.
- `Objective()` - Expressions to be minimised or maximised in a model.
- `Constraint()` - Constraint expressions which impose restrictions on decision variables in a model.

Pyomo is widely utilised, and documentation is easily accessible. For a more thorough introduction to Pyomo and its documentation, the reader is referred to [54][55].

With Pyomo, optimisation models may be expressed in a way which closely resembles the mathematical notation. In the eyes of the author of the thesis, this feature allows for the focus to be on the formulation of the optimisation problem, rather than getting mired in syntax. The syntax is intuitive, making it easier to communicate and understand the mathematical model structure. Since this thesis work aims to be a building block for the future, developing readable code was of importance.

4.1.2 Choice of solver

Pyomo in itself does not solve the optimisation problem that is mathematically formulated. Instead, Pyomo provides an interface that communicates with solvers, and users need to install a solver separately from Pyomo. The interface enables Pyomo to pass the formulated optimisation model to the solver of choice, retrieve a solution, and provide the result to the user.

Different solvers exist that handle different optimisation problems, some that are commercial and some that are open-source. Through an academic license, which is available as a student at NTNU, it is possible to gain access to Gurobi, which is the solver utilised in this thesis.

4.1.2.1 Gurobi

Gurobi [57] was the solver of choice for solving the mathematical models formulated in Pyomo. Gurobi is a commercial optimisation solver, which can be accessed through an

academic license. Gurobi is a flexible tool that can solve linear programming, mixed integer programming, quadratic programming, and other types of mathematical optimisation problems.

4.1.3 Modelling Approach

Before presenting the modeling hierarchy, and the connection between different Python files used in the approach, it is important to highlight the emphasis that is placed by the author of the thesis on promoting transparency in the overall structure. The approach follows a structured design, utilising multiple Python files to ensure clarity and re-usable code. The code is implemented in an object-oriented manner, for flexibility to apply to any type of system, as long as input data is of the correct format.

The total framework is not solely developed by the author of the thesis. The contributions of previous work, particularly from [22] and [31], have significantly influenced the model. By building upon their valuable work and insights, the approach aims to enhance and expand upon the existing solutions while including unique contributions. The approach developed in this thesis stands on the shoulders of the pioneering work of [22], which developed a framework for PSR adequacy assessment in Python. Figure 4.1 illustrates the complete hierarchy of Python files used in this thesis.

All credit and recognition for the scripts used in this work go to their original creators, and it is specified whether the scripts are developed in this thesis or not below. The development and availability of these scripts are attributed to the Department of Electric Energy and supervisor Vijay Venu Vadlamudi. The author of the thesis expresses gratitude and acknowledges their contributions in enabling the utilisation of these scripts for the purposes of this Master's thesis. Disclaimers are presented in the Python files themselves, as well.

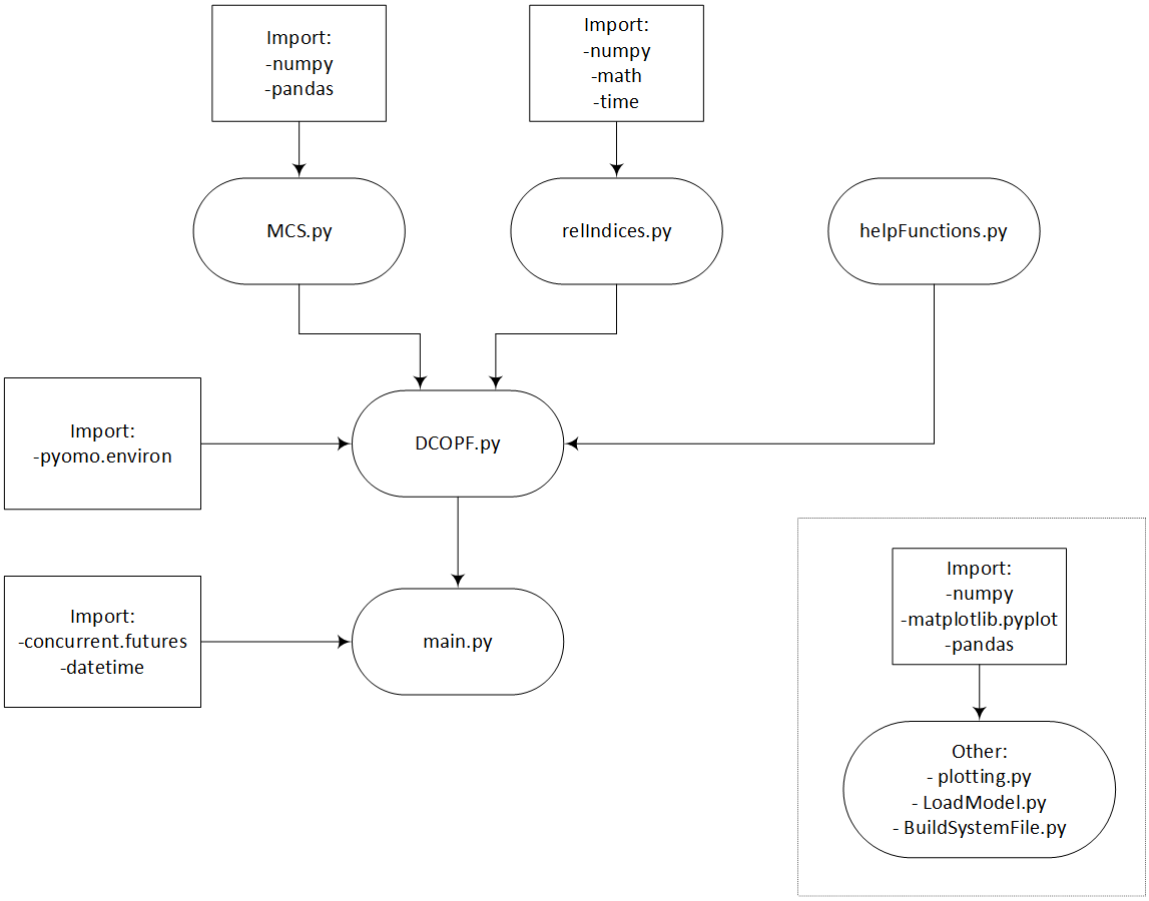

Figure 4.1: *Python files hierarchy for modeling approach in calculating reliability indices.*

Following is a brief description of each of the Python files, including the files' origin - i.e., if they are newly developed in this thesis, or belong to the previously developed PSR software from [22], or external libraries. It must be kept in mind that this is a brief description, to provide an overview. For a more thorough description, the scripts themselves provide detailed comments.

- `MCS.py`: This script contains classes and methods for conducting the MCS State Sampling method. The script utilises a filtering technique which is further described later in this chapter, in Section 4.3. This script is developed by [22]. There is some deviation from the original script from [22], but there are only minimal changes from the original.

- `relIndices.py`: This script calculates reliability indices. This includes the indices presented in theory, LOLE, LOLP and EENS. Additionally, it calculates the CoVs.

Both the indices and CoVs are presented for each individual bus and the entire system. This script is developed by [22].

- `helpFunctions.py`: This script includes helpful functions for the OPF formulations. This includes methods for calculating PTDFs and LODFs. This script was developed during the thesis work.

- `DCOPF.py`: This script contains the majority of implementation. A part of the script is from the work of [22]. In general, this considers the algorithmic approach before the contingency solver is involved. In other words, the part used from [22] provides the input for the contingency solver and OPF analysis. Further, the script contains a method for DCOPF and DC-PSCOPF, which both are implemented with the Pyomo framework. This integrated OPF part in Pyomo was developed during the thesis work.

- `main.py`: This is the main script to run the adequacy assessment. Here, the number of simulation years may be determined, as well as the choice to solve states in parallell or iteratively.

- `plotting.py`: This script illustrates the convergence of MCS through an example of coin tossing, and thus not related with the rest of hierarchy. This was developed during the thesis work.

- `LoadModel.py`: This script implements the load model. The script was developed by [22]. Some changes were made to the script to illustrate plots, which are seen in Figure 2.4.

- `BuildSystemFile.py`: This script was the original file to convert data read from Excel sheets describing RBTS and IEEE RTS into classes of lines, generators and buses. This approach showed some struggles in implementation, thus not utilised.

- The remaining files not mentioned, are packages which are not developed by the author nor the previous work of [22]. These packages contain modules that present functionality fitting for the implementation.

4.1.4 Challenges with Implementation

Due to limited time remaining and a tight deadline, the workload associated with implementing the CSCOPF with Benders decomposition, fully integrated with the adequacy assessment, proved to be overwhelming. Given the time constraints, a critical decision had to be made regarding the approach to pursue, in order to achieve results.

In light of this dilemma, the author of the thesis made the choice to go for a simpler approach: the DC-PSCOPF which handles pre- and post-contingency constraints simultaneously. By opting for a more straightforward approach, the aim was to streamline the implementation process and accelerate the generation of results within the available time-frame.

Despite being less complex than the CSCOPF with Benders decomposition, the DC-PSCOPF still holds some potential to offer insights in the application of SCOPF in adequacy assessment.

When implementing new methods at a later stage of the thesis work, certain drawbacks were still encountered despite opting for a simpler approach with the DC-PSCOPF rather than the CSCOPF. These drawbacks included long simulation times and some missing features in the implementation that required handling through throwing exceptions. In the following paragraphs, these issues and their implication will be discussed.

In the original proposed approach of CSCOPF, it was focused on only solving the subproblems where violations would be present, which could yield a shorter analysis. The LODFs would be used to calculate new line flows to identify overloaded lines. The subproblems would be solved only for the scenarios with overloaded lines, as generation rescheduling or load curtailments would be a necessary action in these cases, and yielding $w > 0$ in accordance with Equation (2.49). This is deducted from, recalling from Equation (2.49), that $w = 0$ does not result in any Benders Cut appended to the master problem. For scenarios with generator outages an optimisation problem cannot be ignored, as curtailments in the system are of essence: if a large generator is on outage, it is not certain the load balance is satisfied without curtailing load to keep the system balanced.

In the developed DC-PSCOPF it was planned to check all possible contingencies, sim-

ulating outages of each component for the system at hand. However, this was found to demand excessive computational effort within the limited time scope. This fact will be pointed out in the results presented in Chapter 5. To cope with the extensive simulation times, it was deemed necessary to only check a few select components and the consequence of their outage, to acquire reliability indices from an adequacy assessment. The selection of contingencies to check was based on the curiosity of the author of the thesis, as well as contingencies that would likely result in load curtailments.

In order to reduce the computational effort and also provide insightful analysis, it could be a solution to utilise the CSCOPF methodology described. The analysis would concentrate on generators and overloaded lines for each contingency case. This selective examination would reduce the number of problems analysed compared to the exhaustive N-1 analysis. At the same time it would give a better representation of which problems to solve, as it is not preemptively selected without the knowledge of overloaded lines.

The reason the argued better method is not utilised in this thesis, is because it is dependent on the solution of a base case problem. The reason why this is a problem, is because for each sampled state, a solution of a new base case is necessary. This contradicts with the utility of the formulated model, where pre- and post-contingency constraints are solved simultaneously, removing the need for base case (master problem) and subproblems. It could be done with a pre-analysis of the system, by first solving the base case system with no contingencies. Thus, the line flows of the system could be calculated. However, it would be needed a mapping of each sampled state and its base case solution. Thereafter, the post-contingency line flows could be found through the LODFs, and return a list of which line outages result in line overloads, for each specific sampled state. This selection of line outages would then be the scenarios checked as subproblems. This is, however, not done in this thesis work. However, many of the tools necessary to perform such an analysis are available through the work of this thesis and [22], which could be an interesting comparison of the selection of contingencies to assess. For example, selecting line outages from the said procedure, and comparing to selecting line outages with the lines most likely to be on outage, e.g., largest FOR value.

As mentioned, even though being a less complex approach, the implemented approach has some drawbacks, which has its root at the formulation and use of the LODFs in this

thesis. A challenge is handling cases where the outage of a line results in an isolated system, as it is required $-\mathbf{X}_{\mathcal{O}} + \mathbf{\Psi}^T [\mathbf{B}]^{0^{-1}} \mathbf{\Psi}$ is non-singular [49]. To provide some clarity on what this means, a simple example is illustrated.

Say, Figure 4.2 is the result of a sampled state for a given time increment. For the given case, L9 and L8 are on outage. This results in the isolation of bus 6, which is handled through the bus isolation algorithm depicted in 3.1.7.1 (work of [31] and implemented in Python by [22]).

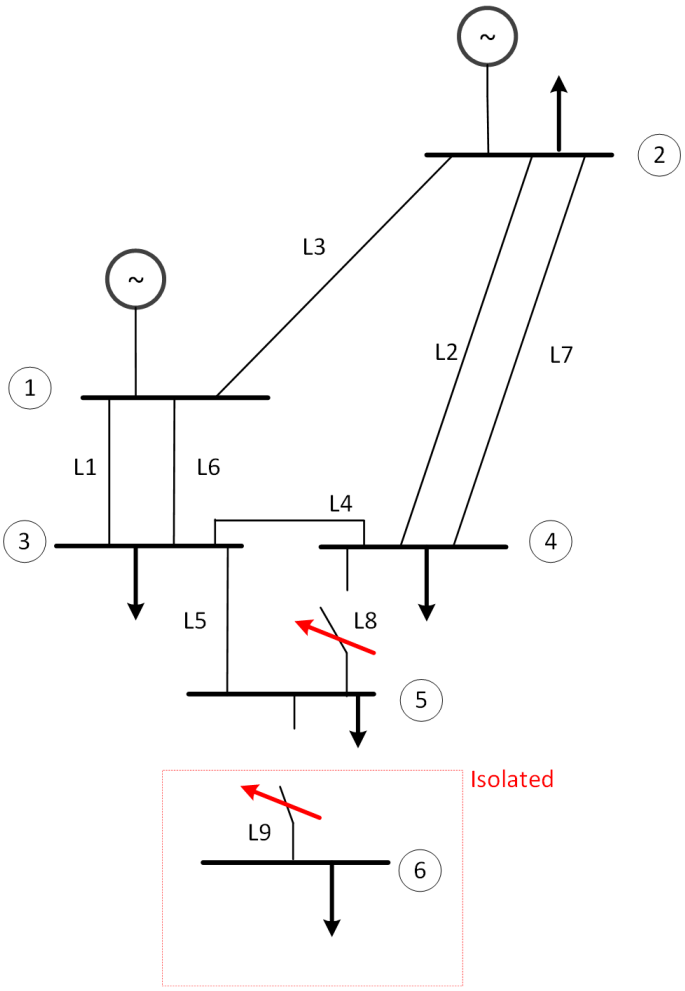

Figure 4.2: *Example of sampled system state for RBTS.*

When performing the DC-PSCOPF for the given system, it can lead to isolation of bus 5, with the outage of L5. This leads to the commented problem, of singularity and matrix inversion. In this thesis, the problem is handled by calculating the pseudo-inverse using the (`numpy.linalg.pinv()`) method from the numPy package in Python.

The problem is commented in references [49][52][58]. For the future, a solution method may be to adopt the approach of [52], which can detect potential isolated buses (only one line connected), and remove them from the analysis.

However, the use of the pseudo-inverse can represent a case of problem-shifting. By performing the DC-PSCOPF analysis, for the case where L5 in Figure 4.2 is on outage, bus 5 will be isolated. This is something that needs to be considered in the analysis as well, reconfiguring the system again, even though there are no issues by calculation of singular matrices.

To summarize, the developed method is far from perfected, but may still provide insight in the desired direction of SCOPF integration in PSR adequacy assessment.

4.2 Multi Processing

Given that the PSR MCS assessment involves analysing a vast number of system states, it is of interest to enhance the computational efficiency of the code. One approach to achieve this goal is by incorporating multi-processing functionality that allows for the analysis of multiple states in parallel, taking advantage of the multiple cores in modern CPUs.

The concurrent.futures.ProcessPoolExecutor [59] method in Python can be utilised to implement this functionality, creating a pool of workers based on the available CPU cores and distributing contingency states to each worker as they complete the assigned state. The investigated states are not completed in chronological order due to the varying time required to solve each contingency state. To map the indices back to the original order, each contingency state is attached with its original positional index, allowing for sorting in chronological order after all contingency states have been resolved [22]. Overall, parallel computing significantly reduces the computational time required to complete the PSR MCS assessment, particularly when analyzing a vast number of system states.

4.3 Contingency State Filtering

The computational time required for HLII adequacy assessment is quite significant. The most computationally intensive task in the HLII adequacy assessment is the contingency solver. To mitigate this, one approach is to reduce the computational time by minimising the number of states examined. This can be achieved by pre-screening the sampled states and excluding trivial states based on specific criteria. An example of a trivial state is a system state where no components are in an outage condition. Investigating such a state using the contingency solver would not result in any load curtailment and would therefore have no impact on the system reliability indices [22].

In the software codes of [22] which were built upon in this thesis, three filtering criteria are introduced as an alternative to reduce the amount of states being solved by the contingency analysis tool. A thorough description of the criteria can be seen in [31]. A duplicate state filtering method that recognizes the states that occur more than once, is also included in the approach of [22]. This is to even further increase the efficiency of simulations, building upon the base filtering criteria in [31]. The filtering criteria used and presented in [22] and [31], are here briefly presented on their functionality in this thesis. The filtering criteria are presented in Section 4.3.1 and 4.3.2.

4.3.1 Sampled State Filtering Criteria - Power System Components

The filtering criteria used in the sampling of states is presented in this section. First filtering procedures regarding components of the network are handled.

- **Load level criterion:** This criterion is established in order to identify contingency states where the total generation falls below the total hourly load demand multiplied with a constant value k. Equation (4.1) illustrates this criterion, where n represents the total number of buses in the system. The value of the constant k is influenced by the system's topology and the distribution pattern of generators [22].

$$\sum_{i=1}^{n} P_{gi} < k \sum_{i=1}^{n} P_{load,i} \tag{4.1}$$

- **Generators on outage criterion:** This criterion is based on the count of generators on outage. If the number of generators currently on outage is lower than a specified limit, the state is disregarded. According to [22], the combination of these two criteria has been found to be an efficient approach without significantly impacting the reliability assessment. It should be noted that these two criteria, filter out all the sampled states where no contingencies occur [22].

- **Lines on outage criterion:** This criterion involves checking all states in which one or more transmission lines are on outage. The criterion was found to have minimal impact on the overall number of contingency states. This is due to the transmission lines being more reliable than the generators in the test systems RBTS and IEEE RTS [22].

4.3.2 Duplicate Contingency State Filtering

Following the approach of [22], using a simultaneous sampling method, all states are sampled prior to examination by the OPF analysis tool. This unconventional approach enables the screening and filtration of all sampled states before they are subjected to the OPF analysis, or contingency solver tool. As a result, it becomes feasible to identify, quantify, and eliminate duplicate contingency states. As a consequence, this approach reduces the total number of contingency states that require further analysis [22].

The state filtering technique developed by [22], identifies contingency states that are identical, meaning they have the same load level and components on outage. As a consequence, these states contribute with the same values to the reliability indices when assessed by the contingency solver. An essential aspect of the filtering procedure, is to accurately associate the solution with the corresponding simulation years in which they occur. [22] introduces a year of state index, which stores the simulation years associated with each specific contingency state. For a more in-depth explanation, the reader is referred to [22] where an example is provided as well.

5 Case Studies

In this chapter, the testing and verification of the standard HLII software and the HLII SCOPF software that were developed are presented. Initially the test systems are described, outlining the system-specific parameters used in the contingency state filtering stage (Section 4.3.2) and the contingency solver. Furthermore, the load model and computer employed for the simulations are discussed.

The first case study aims to test the developed standard HLII software by applying it to RBTS and IEEE RTS. The second case study aims to test the HLII DC-PSCOPF software, for the same systems. Both case studies are subdivided into several cases.

5.1 Test systems

In this thesis, two distinct test systems are examined for the purpose of either enhancing theoretical comprehension or verifying the feasibility of the methods under investigation. The following section outlines each system in detail, with the intention of providing a comprehensive understanding of the parameters used and the rationale behind their selection.

5.1.1 Roy Billinton Test System (RBTS)

RBTS is a relatively simple power system comprising six buses and was originally created for educational purposes [23]. The system is characterized by a power factor of 0.2 at all buses and a yearly peak load of 185 MW. It comprises of 11 generators with a total generation capacity of 240 MW, where individual generator capacity ranges from 5 to 40 MW. The system includes 6 buses and 9 transmission lines interconnecting them. Comprehensive system data including generator data, bus specifications, network parameters, and outage data can be found in Appendix B. A graphical representation of the system topology is provided in Figure 5.1.

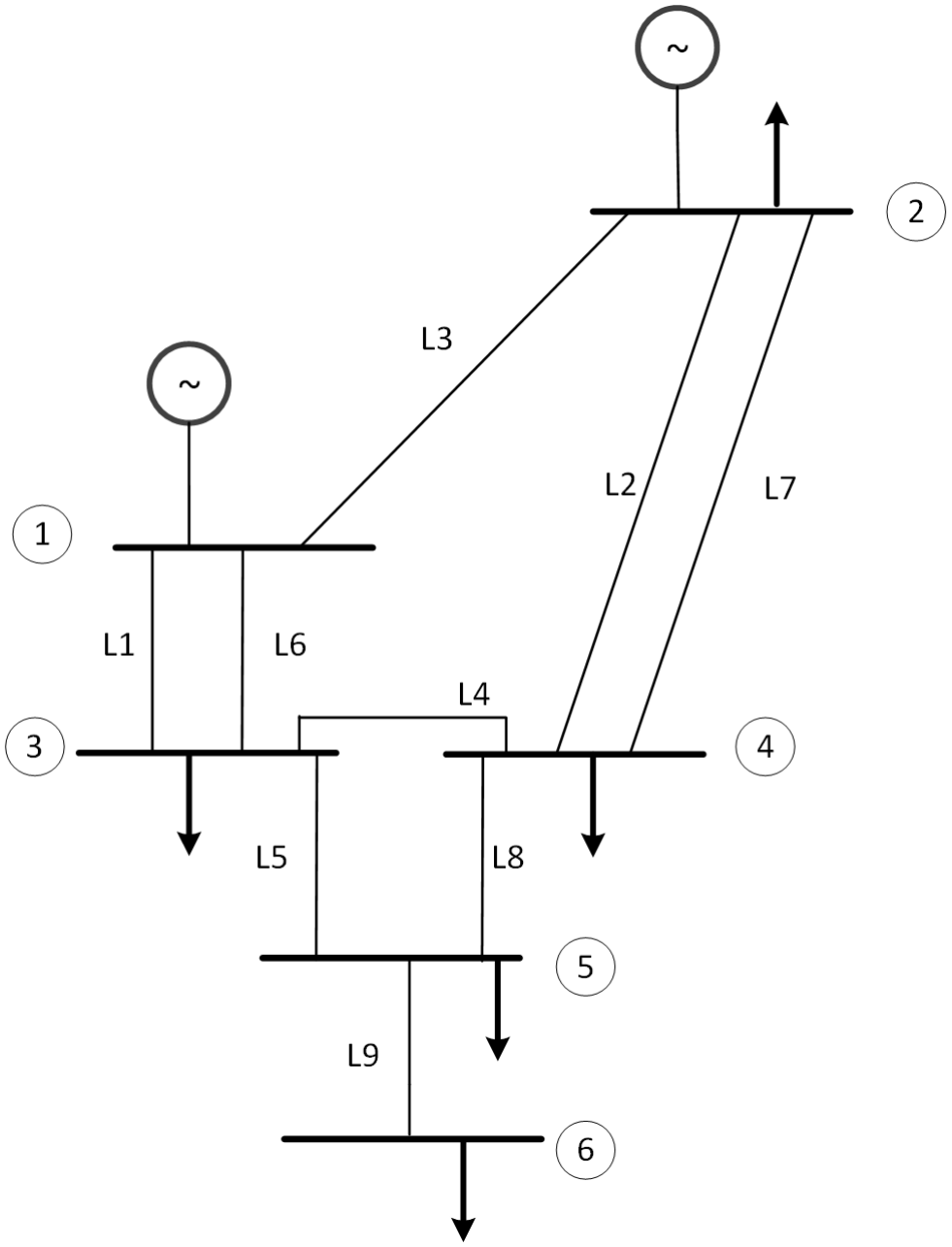

Figure 5.1: *Single line diagram of the RBTS. Adapted from [23] with MS Visio.*

5.1.1.1 System Specific Parameters

Table 5.1 presents the parameters for the contingency state filtering criteria described in Section 4.3.1 and 4.3.2. The parameters are identical to that of [22] and [31], due to the comparison done in Case 1 of the standard HLII assessment, seen in Section 5.4.1.

Table 5.1: *Filtering criteria from [22] and [31] applied to the RBTS for standard HLII assessment.*

Test System	Generation Capacity to Load	Max lines on outage	Max generators on outage	Duplicate filter
RBTS	1.04 x total load	1	2	Yes

5.1.2 IEEE Reliability Test System (IEEE RTS)

The IEEE RTS, also developed for educational purposes, exhibits a greater level of intricacy in contrast to the RBTS [60]. With a YPL of 2850 MW and a power factor of 0.2 at all its buses, the system encompasses 32 generating units ranging from 12 to 400 MW, resulting in a total generation capacity of 3405 MW. Additionally, the system contains voltage regulating units that incorporate a synchronous condenser, a reactor, and auto-transformers. It also comprises 38 lines that interconnect the buses. The system data, encompassing generator data, bus specifications, network parameters, and outage data, can be found in Appendix C. The system's grid topology is depicted in Figure 5.2.

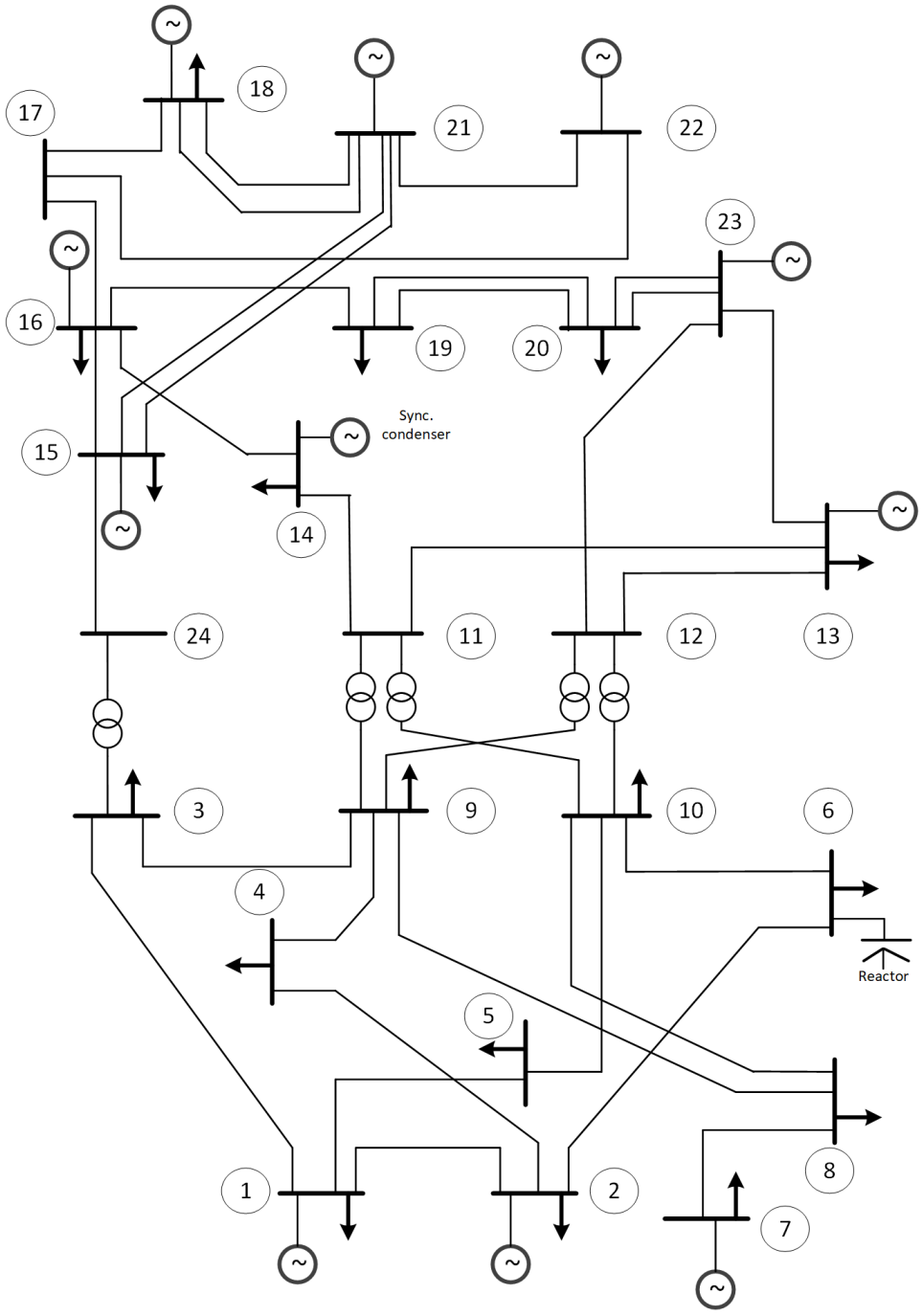

Figure 5.2: *Single line diagram of the IEEE RTS. Adapted from [60] with MS Visio.*

5.1.2.1 System Specific Parameters

The parameters for the IEEE RTS state filtering are presented in Table 5.2. The parameters are identical to [22], as the same code is applied.

Table 5.2: *Filtering criteria from [22] and [31] applied to the IEEE RTS for standard HLII assessment.*

Test System	Generation Capacity to Load	Max lines on outage	Max generators on outage	Duplicate filter
IEEE RTS	1.1 x total load	1	5	Yes

5.2 Load Model

The case studies employ an hourly load model, which is further elaborated in Section 2.2. The load data, derived from [60], are available in Appendix A. The HPL at any given time, t, can be calculated by applying Equation (5.1). The load model incorporates seasonal, weekly, daily and hourly fluctuations [60]. It is important to note that adopting this approach to estimate the load for hourly increments produces a total of 8736 hours in a year ($52 \cdot 7 \cdot 24$). The variables $L_{weekly,t}$ is represented as a percentage of YPL, $L_{daily,t}$ as a percentage of $L_{weekly,t}$, and $L_{hourly,t}$ as a percentage of $L_{daily,t}$.

$$HPL_t = YPL \cdot L_{weekly,t} \cdot L_{daily,t} \cdot L_{hourly,t} \tag{5.1}$$

5.3 NTNU Server Farm

The computational time performance is closely tied to the specific hardware that is used. In order to reduce the computational time, the Python code is executed using the remote desktop for IEL through the NTNU software farm. The computer that is used has 2 processors, Intel Xeon CPU E5-2690 v4 2.60GHz, and has a total of 28 cores. Make note that this number varies with the number of users connected to the computer. It does however make a large difference, as the cores of the authors laptop is 4 cores.

5.4 HLII Case Studies

To ensure the accuracy of the implementation of the DC-PSCOPF contingency solver, it is crucial to conduct a testing of the Python-based standard HLII assessment code. This step is critical to avoid any potential errors that may arise during the implementation process. Given that this thesis follows the methodological framework proposed by [22] and [31], it is necessary to compare the results. Even though [22] is already a Python-based approach, this thesis has modelled the optimisation with Pyomo, which is a different approach than in the work conducted in [22]. Also, the OPF formulation in this thesis is the DCOPF, while [22] utilised the ACOPF. Thus, it is deemed necessary to compare this approach with the standard HLII assessment as well. As the models are different, some deviation is expected. However, it is expected to observe a similar trend in the curtailment of loads at specific buses in the test systems RBTS and IEEE RTS.

All simulations have been done following the MCS State Sampling method explained in Section 3.1.2. The simulation period was tested for a period of 500 years. Dealing with high computational time was a problem in the testing of code. It is however a necessity as to achieve a satisfactory level of convergence for the MCS.

The standard HLII case studies will be presented in the following order:

- Case 1: Standard HLII assessment using the RBTS. The results from the simulations are presented, as well as a comparison with the benchmark results in [22].
- Case 2: Standard HLII assessment using the IEEE RTS. The results from the simulations are presented, as well as a comparison with the benchmark results in [22].
- Case 3: HLII assessment using the DC-PSCOPF software implemented on RBTS. Results are presented, and compared.
- Case 4: HLII assessment using the DC-PSCOPF software implemented on IEEE RTS. Results are presented, and compared.

After all the individual cases are presented, some discussion on the results will follow.

This includes a comparison of the most important features from each case, such as the simulation times and total system indices.

In the tables presented for CoVs, *nan* stands for not a number. This means that there were no cases of the given parameter.

5.4.1 Case 1: RBTS

The standard HLII assessment using State Sampling method on the RBTS is executed for 500 simulation years. The state sampling had a computational time of 11.437 seconds. The solving of states took 46.06 minutes, while the calculation of reliability indices took 0.306 seconds. The reliability indices for the simulation are found in Table 5.3 The CoVs are found in Table 5.4.

The highest curtailment is at Bus 6. This is an expected result, as it does not follow the N-1 criterion; meaning, bus isolation occurs more often for this bus. Due to the low curtailment cost in the optimisation problem definition, there is high curtailment at bus 3. As was to be expected, buses with no loads have no occurrence of any loss of load.

Table 5.3: *HLII State Sampling of the RBTS reliability indices, with 500 simulation years.*

Bus	LOLE [hours/year]	LOL SD [hours/year]	LOLP	EENS [MWh/year]	ENS SD [MWh/year]
2	0.000000	0.000000	0.000000	0.000000	0.000000
3	1.180000	1.080555	0.000135	9.567378	12.797377
4	0.000000	0.000000	0.000000	0.000000	0.000000
5	0.008000	0.089084	0.000001	0.106719	1.212348
6	9.894000	3.110428	0.001133	121.955647	39.618642
Total system	**11.074000**	**3.328742**	**0.001268**	**131.629744**	**41.960704**

Table 5.4: *Coefficient of Variation for RBTS 500 year simulation*

Bus #	LOLE	EENS
1	nan	nan
2	nan	nan
3	0.0410	0.0598
4	nan	nan
5	0.4980	0.5080
6	0.0141	0.0145
Tot	**0.0134**	**0.0143**

The results are compared to those of the RBTS HLII state sampling of [22]. Table 5.5 shows the comparison of indices from [22]; note that the ACOPF and a different optimisation tool was utilised for the calculation of indices. It can be seen that the reliability indices follow a similar trend. An observation of interest is that an overall increase can be seen in values of the indices in [22]. This is coherent with the ACOPF being a tighter constrained problem, resulting in an increased value of the optimisation problem, and thus more curtailed load.

Table 5.5: *Comparison of reliability indices from [22], simulation period of 500 years.*

Bus	LOLE [hours/year]	LOLE[22] [hours/year]	LOLP	LOLP[22]	EENS [MWh/year]	EENS[22] [MWh/year]
1	0.000000	0.000000	0.000000	0.000000	0.000000	0.000000
2	0.000000	0.000000	0.000000	0.000000	0.000000	0.000000
3	1.180000	1.948	0.000135	0.000223	9.567378	17.5218
4	0.000000	0.002	0.000000	0.000000	0.000000	0.0001
5	0.008000	0.012	0.000001	0.000001	0.106719	0.0860
6	9.894000	10.822	0.001133	0.001239	121.955647	124.9821
Total system	**11.074000**	**12.552**	**0.001268**	**0.001437**	**131.629744**	**142.5891**

5.4.2 IEEE RTS

The MCS State Sampling method was executed for 500 simulation years. The sampling of states was calculated in 79.7 seconds. The solving of states had a computational time of 113.67 minutes, while the indices were calculated in 0.588 seconds. The computational time for the same system in [22] had a simulation time of 55 minutes, in assessing the ACOPF. The execution of the DCOPF formulation in Pyomo is about twice the size. The system CoV (EENS) is 1.63%, while a CoV in [22] of 1.47% was achieved. In other words, the same level of convergence is reached. The large curtailment at bus 7 is due to the N-1 criterion not being fulfilled, and at bus 6 is due to the low curtailment cost.

The reliability indices from the code are presented in Table 5.6. It is observed that the largest EENS values are at bus 7, bus 9, bus 14 and bus 19. This trends similarly to the EENS indices of [22]. There is much curtailment at bus 7 due to the N-1 criterion not being satisfied, as there is only one transmission line connecting the bus to the rest of the system, which can be seen in Figure 5.2. The curtailment at bus 9 is correlated to its low curtailment cost.

Table 5.6: *HLII State Sampling of the RTS reliability indices, with 500 simulation years*

Bus	LOLE [hours/year]	LOL SD [hours/year]	LOLP	EENS [MWh/year]	ENS SD [MWh/year]
1	0.000000	0.000000	0.000000	0.000000	0.000000
2	0.000000	0.000000	0.000000	0.000000	0.000000
3	0.000000	0.000000	0.000000	0.000000	0.000000
4	0.002000	0.044677	0.000000	0.093174	2.081348
5	0.002000	0.044677	0.000000	0.075056	1.676628
6	0.010000	0.099499	0.000001	0.846942	8.707685
7	2.960000	1.648757	0.000339	227.680624	130.626990
8	0.002000	0.044677	0.000000	0.202413	4.521572
9	9.424000	2.892788	0.001079	862.232041	314.446521
10	0.124000	0.347310	0.000014	7.511028	28.462876
11	0.000000	0.000000	0.000000	0.000000	0.000000
12	0.000000	0.000000	0.000000	0.000000	0.000000
13	0.000000	0.000000	0.000000	0.000000	0.000000
14	2.896000	1.647175	0.000332	257.673730	179.438266
15	0.000000	0.000000	0.000000	0.000000	0.000000
16	0.000000	0.000000	0.000000	0.000000	0.000000
17	0.000000	0.000000	0.000000	0.000000	0.000000
18	0.008000	0.089084	0.000001	0.463576	5.575295
19	0.636000	0.755979	0.000073	51.147785	75.508030
20	0.000000	0.000000	0.000000	0.000000	0.000000
21	0.000000	0.000000	0.000000	0.000000	0.000000
22	0.000000	0.000000	0.000000	0.000000	0.000000
23	0.000000	0.000000	0.000000	0.000000	0.000000
24	0.000000	0.000000	0.000000	0.000000	0.000000
Total system	12.392000	3.297019	0.001418	1407.926369	512.620993

Table 5.7 shows the CoVs for the 500 year simulation period for the IEEE RTS.

Table 5.7: *Coefficient of Variation for the IEEE RTS DCOPF formulation*

Bus #	LOLE	EENS
1	nan	nan
2	nan	nan
3	nan	nan
4	0.9990	0.9990
5	0.9990	0.9990
6	0.4450	0.4598
7	0.0249	0.0257
8	0.9990	0.9990
9	0.0137	0.0163
10	0.1253	0.1695
11	nan	nan
12	nan	nan
13	nan	nan
14	0.0254	0.0311
15	nan	nan
16	nan	nan
17	nan	nan
18	0.4980	0.5379
19	0.0532	0.0660
20	nan	nan
21	nan	nan
22	nan	nan
23	nan	nan
24	nan	nan
Tot	0.0119	0.0163

Table 5.8 shows the comparison of indices from [22]. It is observed that the system indices

follow a similar trend. Even though the procedure in [22] uses ACOPF, and this thesis uses DCOPF, the results from [22] are used as a reference point. Given this difference, the result is as expected. The DCOPF is a relaxed version of the ACOPF, so it is expected a lower objective value in the optimisation problem, which is to minimise load curtailment. Overall, it can be seen lower values for the indices in the DCOPF formulation.

Table 5.8: *HLII State Sampling of the RTS reliability indices, with 500 simulation years*

Bus	LOLE	LOLE[22]	LOLP	LOLP[22]	EENS	EENS[22]
1	0.000000	0.5600	0.000000	0.000064	0	0.5282
2	0.000000	0.4440	0.000000	0.000051	0	0.2649
3	0.000000	0.4220	0.000000	0.000048	0	0.7519
4	0.002000	0.3840	0.000000	0.000044	0.093174	0.2418
5	0.002000	0.4040	0.000000	0.000046	0.075056	0.1533
6	0.010000	3.3040	0.000001	0.000378	0.846942	41.6690
7	2.960000	3.3560	0.000339	0.000384	227.680624	225.2893
8	0.002000	0.3980	0.000000	0.000046	0.202413	0.6885
9	9.424000	12.2920	0.001079	0.001407	862.232041	1071.3724
10	0.124000	0.5400	0.000014	0.000062	7.511028	9.9534
11	0.000000	0.0000	0.000000	0	0	0
12	0.000000	0.0000	0.000000	0	0	0
13	0.000000	0.4040	0.000000	0.000046	0	0.0025
14	2.896000	4.0580	0.000332	0.000465	257.673730	314.3406
15	0.000000	0.4300	0.000000	0.000049	0	0.0092
16	0.000000	0.3860	0.000000	0.000044	0	0.0057
17	0.000000	0.0000	0.000000	0	0	0
18	0.008000	0.4660	0.000001	0.000053	0.463576	1.1076
19	0.636000	1.2580	0.000073	0.000144	51.147785	64.5627
20	0.000000	0.4040	0.000000	0.000046	0	0.0452
21	0.000000	0.0000	0.000000	0	0	0
22	0.000000	0.0000	0.000000	0	0	0
23	0.000000	0.0000	0.000000	0	0	0
24	0.000000	0.0000	0.000000	0	0	0
Total system	12.392000	18.0540	0.001418	0.002067	1407.926369	1730.9864

5.5 DC-PSCOPF HLII Case Studies

The DC-PSCOPF HLII adequacy assessment was executed for 500 simulation years. The states were sampled with MCS State Sampling method, and duplicated states were filtered out using the criteria described in Section 4.3. As the optimisation problem for DC-PSCOPF has to consider several more optimisation problems than the DCOPF, it is expected quite much longer runtime for the code.

A test was done for 1 year, where all components were assessed, performing a N-1 analysis. This resulted in a simulation time of 7 minutes for the RBTS. The same was tested for IEEE RTS, which resulted in a simulation time of around 13 minutes. Scaling this up to 500 years resulted in too high computation time (58 hours for RBTS, 108 hours for IEEE RTS).

These are heavy computations to perform, so it was rather tested for some select components, and how their outage would affect the reliability indices for a simulation period of 500 years.

It is important again to achieve the full simulation run of 500 years, in order to achieve convergence for the MCS State Sampling method.

5.5.1 RBTS - Largest generator outage and FOR line

For this scenario, it was tested the DC-PSCOPF for the outage of the largest generator, and the line with the largest FOR value. This makes this scenario not a complete N-1 study. The sampling of states was done in 14.792 seconds. The solving of states was done in 80.415 minutes, while the indices were calculated in 0.543 seconds. The CoV was found to be 1.4%. Table 5.9 illustrates the reliability indices calculated.

Table 5.9: *HLII State Sampling of the RBTS reliability indices, with 500 simulation years.*

Bus	LOLE [hours/year]	LOL SD [hours/year]	LOLP	EENS [MWh/year]	ENS SD [MWh/year]
2	0.000000	0.000000	0.000000	0.000000	0.000000
3	5.652000	2.360275	0.000647	135.079762	69.321787
4	0.000000	0.000000	0.000000	0.000000	0.000000
5	0.012000	0.108885	0.000001	0.140799	1.300975
6	9.824000	3.165600	0.001125	120.045144	39.514351
Total system	**15.460000**	**3.963887**	**0.001770**	**255.265705**	**79.659806**

Table 5.10 shows the CoVs for the 500 year simulation period for the RBTS DC-PSCOPF simulation.

Table 5.10: *Coefficient of Variation for the RBTS reliability indices, 500 year simulation DC-PSCOPF*

Bus	LOLE	EENS
1	nan	nan
2	nan	nan
3	0.0187	0.0230
4	nan	nan
5	0.4058	0.4132
6	0.0144	0.0147
Tot	0.0115	0.0140

5.5.2 IEEE RTS - Largest generator outage and FOR line

For this scenario, it was tested the DC-PSCOPF for the outage of the largest generator, and the line with the largest FOR value. This makes this scenario not a complete N-1 study.

The MCS State Sampling was executed for 500 years. The sampling of states was done in 66.63 seconds. The solving of states took 188.879 minutes, and the indices calculation took 2.052 seconds. The system CoV was found to be 0.68%.

The results overall prove similar trends to that of the DCOPF conducted in the previous section. The main difference is an overall increase in the value of the indices. This makes sense, as it is a more constrained optimisation problem, which leads to an increase in the objective function (more load curtailed). Table 5.11 illustrates the indices calculated.

Table 5.11: *HLII State Sampling of the RTS reliability indices, with 500 simulation years for DC-PSCOPF.*

Bus	LOLE [hours/year]	LOL SD [hours/year]	LOLP	EENS [MWh/year]	ENS SD [MWh/year]
1	0.000000	0.000000	0.000000	0.000000	0.000000
2	0.000000	0.000000	0.000000	0.000000	0.000000
3	0.002000	0.044677	0.000000	0.218412	4.878958
4	0.002000	0.044677	0.000000	0.071572	1.598804
5	0.002000	0.044677	0.000000	0.082236	1.837011
6	0.002000	0.044677	0.000000	0.183120	4.090598
7	2.754000	1.679727	0.000315	214.071762	132.882183
8	0.002000	0.044677	0.000000	0.139094	3.107125
9	52.344000	7.295044	0.005992	7527.096179	1072.879536
10	3.328000	1.814502	0.000381	273.520050	177.139886
11	0.000000	0.000000	0.000000	0.000000	0.000000
12	0.000000	0.000000	0.000000	0.000000	0.000000
13	0.000000	0.000000	0.000000	0.000000	0.000000
14	45.082000	6.827538	0.005160	4737.578030	821.888888
15	0.000000	0.000000	0.000000	0.000000	0.000000
16	0.000000	0.000000	0.000000	0.000000	0.000000
17	0.000000	0.000000	0.000000	0.000000	0.000000
18	0.536000	0.710425	0.000061	39.864205	75.462017
19	14.276000	3.806287	0.001634	1238.451285	384.739585
20	0.004000	0.063119	0.000000	0.375051	6.140540
21	0.000000	0.000000	0.000000	0.000000	0.000000
22	0.000000	0.000000	0.000000	0.000000	0.000000
23	0.000000	0.000000	0.000000	0.000000	0.000000
24	0.000000	0.000000	0.000000	0.000000	0.000000
Total system	55.078000	7.483844	0.006305	14031.650997	2126.779525

Table 5.12 shows the CoVs for the 500 year simulation period for the IEEE RTS.

Table 5.12: *Coefficient of Variation for the IEEE RTS DCOPF formulation*

Bus	LOLE	EENS
1	nan	nan
2	nan	nan
3	0.9990	0.9990
4	0.9990	0.9990
5	0.9990	0.9990
6	0.9990	0.9990
7	0.0273	0.0278
8	0.9990	0.9990
9	0.0062	0.0064
10	0.0244	0.0290
11	nan	nan
12	nan	nan
13	nan	nan
14	0.0068	0.0078
15	nan	nan
16	nan	nan
17	nan	nan
18	0.0593	0.0847
19	0.0119	0.0139
20	0.7057	0.7322
21	nan	nan
22	nan	nan
23	nan	nan
24	nan	nan
Tot	0.0061	0.0068

5.5.3 RBTS - 2 largest generators, and 3 largest FOR lines

In this scenario, the DC-PSCOPF was tested for the outage of the two largest generators, and 3 lines with the largest FOR values. This results in a total of 5 optimisation problems that are checked for the given contingency state. For comparison, this would only be one optimisation problem for the DCOPF. Naturally, this leads to larger computational time - but a closer version to the N-1 analysis. For this specific case, the sampling of states was 15.182 seconds, the solving of states was 239.143 minutes, and indices were calculated in 0.527 seconds. The system CoV was found to be 1.34%.

The results provide a similar trend to that shown in Section 5.5.1. The main difference is an overall increase in values of the reliability indices. The results can be seen in Table 5.13.

Table 5.13: *HLII State Sampling of the RBTS reliability indices, with 500 simulation years. Outage of 2 generators and 3 lines*

Bus	LOLE [hours/year]	LOL SD [hours/year]	LOLP	EENS [MWh/year]	ENS SD [MWh/year]
1	0.000000	0.000000	0.000000	0.000000	0.000000
2	0.000000	0.000000	0.000000	0.000000	0.000000
3	6.438000	2.475915	0.000737	136.946972	67.481222
4	0.000000	0.000000	0.000000	0.000000	0.000000
5	0.010000	0.099499	0.000001	0.114809	1.162594
6	9.980000	3.131709	0.001142	122.954998	39.205534
Total system	**16.404000**	**4.012578**	**0.001878**	**260.016780**	**78.165858**

Table 5.14 shows the CoVs for the 500 year simulation period for this scenario.

Table 5.14: *Coefficient of Variation for the RBTS reliability indices, 500 year simulation DC-PSCOPF*

Bus	LOLE	EENS
1	nan	nan
2	nan	nan
3	0.0172	0.0220
4	nan	nan
5	0.4450	0.4529
6	0.0140	0.0143
Tot	0.0109	0.0134

5.5.4 IEEE RTS - 2 largest generators, and 3 largest FOR lines

In this scenario, the DC-PSCOPF was tested for the outage of the 2 largest generators and the two largest FOR values for the IEEE RTS. The sampling of states was done in 72.024 seconds. The solving of states was done in 566.28 minutes, while the indices calculation was done in 1.968 seconds. The system CoV was found to be 0.63%, which was a satisfactory level of convergence.

The results are presented in Table 5.15.

Table 5.15: *HLII State Sampling of the RTS reliability indices, with 500 simulation years for DC-PSCOPF, 2 generators and 3 lines.*

Bus	LOLE [hours/year]	LOL SD [hours/year]	LOLP	EENS [MWh/year]	ENS SD [MWh/year]
1	0.000000	0.000000	0.000000	0.000000	0.000000
2	0.000000	0.000000	0.000000	0.000000	0.000000
3	0.000000	0.000000	0.000000	0.000000	0.000000
4	0.002000	0.044677	0.000000	0.112807	2.519928
5	0.000000	0.000000	0.000000	0.000000	0.000000
6	0.002000	0.044677	0.000000	0.198554	4.435364
7	3.180000	1.765106	0.000364	245.133395	139.669458
8	0.006000	0.077227	0.000001	0.596842	8.044533
9	51.962000	6.980871	0.005948	7485.191257	996.810623
10	3.312000	1.834845	0.000379	263.243959	170.321296
11	0.000000	0.000000	0.000000	0.000000	0.000000
12	0.000000	0.000000	0.000000	0.000000	0.000000
13	0.000000	0.000000	0.000000	0.000000	0.000000
14	44.784000	6.255345	0.005126	4687.939930	747.654370
15	0.000000	0.000000	0.000000	0.000000	0.000000
16	0.000000	0.000000	0.000000	0.000000	0.000000
17	0.000000	0.000000	0.000000	0.000000	0.000000
18	0.474000	0.673293	0.000054	39.227005	73.778084
19	14.062000	3.629622	0.001610	1226.690792	381.138893
20	0.008000	0.089084	0.000001	0.188175	3.162414
21	0.000000	0.000000	0.000000	0.000000	0.000000
22	0.000000	0.000000	0.000000	0.000000	0.000000
23	0.000000	0.000000	0.000000	0.000000	0.000000
24	0.000000	0.000000	0.000000	0.000000	0.000000
Total system	55.114000	7.101057	0.006309	13948.522716	1959.961165

Table 5.16 shows the CoVs for the 500 year simulation period for the IEEE RTS.

Table 5.16: *Coefficient of Variation for the IEEE RTS DCOPF formulation*

Bus	LOLE	EENS
1	nan	nan
2	nan	nan
3	0.9990	0.9990
4	0.9990	0.9990
5	0.9990	0.9990
6	0.9990	0.9990
7	0.0248	0.0255
8	0.5756	0.6028
9	0.0060	0.0060
10	0.0248	0.0289
11	nan	nan
12	nan	nan
13	nan	nan
14	0.0062	0.0071
15	nan	nan
16	nan	nan
17	nan	nan
18	0.0635	0.0841
19	0.0115	0.0139
20	0.4980	0.7516
21	nan	nan
22	nan	nan
23	nan	nan
24	nan	nan
Tot	0.0058	0.0063

5.6 Summary and Discussion of Results

Table 5.17 illustrates the simulation times for the cases presented. For DC-PSCOPF case 1 refers to Section 5.5.1 and 5.5.2, and DC-PSCOPF case 2 refers to Section 5.5.3 and 5.5.4.

Table 5.17: *Simulation times for 500 year MCS.*

	DCOPF	DC-PSCOPF, case 1	DC-PSCOPF, case 2
RBTS	00:46:15	01:20:37	03:59:24
IEEE RTS	01:55:05	03:10:01	09:27:31

6 Conclusions and Further Work

In the concluding chapter of this Master's thesis, the key findings and insights gained from the research journey of the author of the thesis are presented. This chapter serves as a reflection on the process of working on the thesis, on the main findings of the thesis, and also an exploration for future work.

The journey of working on this thesis has been both challenging and rewarding. It involved reviewing literature, identifying suitable problem statements, model development, and analysis. Ambitious problem statements were initially devised, and had to be toned down in scale and scope subsequently, keeping in mind the constraints on time and feasibility of execution.

Writing the thesis has been a significant learning experience - all from improving communication with supervisors, communicating complex ideas in a simple yet effective manner, and developing a deeper pedagogical understanding of the topics of optimal power flow and power system reliability.

The contributions of this thesis have hopefully succeeded in providing valuable insights into the application of optimal power flow in the assessment of power system reliability. While the work conducted has laid a foundation on the use of security constrained optimal power flow in power system reliability, numerous opportunities remain unexplored. Some of these ambitious targets that were not met could be seen in Figure D.1.

In the following subsections, the main conclusions of this thesis work are presented, and then some proposals for further work on continuing the work carried out in this thesis are presented.

6.1 Conclusions

The purpose of this thesis was to further develop the in-house PSR adequacy assessment software tools at the Department of Electric Energy (NTNU), to incorporate the DC-PSCOPF in the HLII adequacy assessment. In the thesis, the MCS State Sampling

method [25] and Python software codes developed by [22], have been used as a foundation and stepping-stone for further development. The thesis adapted the DCOPF approach of [31] to the optimisation framework of Pyomo [54][55] in Python, in order to conduct HLII adequacy assessment. The DCOPF formulation was extended to the DC-PSCOPF. As a result, two in-house Python scripts were developed. One for the DCOPF HLII assessment, and one for the DC-PSCOPF HLII assessment.

By building on the work of [22], this thesis aimed to expand the foundation for continued work using Python in PSR studies, by integrating the use of the Pyomo framework. The aim has been to expand the foundation with respect to the OPF assessment within PSR adequacy assessment. Of emphasis in this thesis has been the presentation of the proposed methodology in a transparent manner. In order to achieve this, the algorithmic approach was presented in a detailed manner, allowing for replication of results and opportunity to extend the work.

The adaptation of the DC-based methodological approach of [31] was found to be successful when applied to the RBTS and the IEEE RTS. This was concluded through the observed similar trends of the main reliability indices and CoVs of [22], which adapted the AC-based methodological approach of [31]. The deviation in the indices is explained by the different OPF formulations. The thesis of [22] used an AC-based approach, while this thesis conducted a DC-based approach; even though these theses use different formulations, the results show correlation. The indices of [22] showed overall greater values than the indices found in this thesis. This correlates well as the DCOPF is a linearized version of the ACOPF.

It will be necessary to conduct a verification of the implemented DC-PSCOPF in order to ensure its accuracy and reliability as a tool to be used in the PSR adequacy assessment. The methodology utilised yielded interesting results, with the overall indices indicating higher values compared to those obtained from the DCOPF. This is expected, as the DC-PSCOPF imposes tighter constraints, resulting in a more constrained solution than the DCOPF.

6.2 Further Work

Throughout the journey of this thesis work, several aspects and ideas that were initially considered were not implemented or did not yield desired outcomes. However, these discoveries have opened up a myriad of possibilities for the natural continuation and exploration of the thesis work. The unexplored avenues discovered during the thesis work, which will allow for potential advancements in the field of PSR are discussed here. Figure D.1 illustrates some possible avenues which could be explored.

The first potential avenue involves developing diverse approaches for the MCS, such as the State Duration approach and the State Transition approach, explained in Section 2.5.3 and Section 2.5.4, respectively. These are sequential MCS methods, which make it possible to derive frequency based indices [25].

It is both possible and, perhaps, essential to verify the developed DC-PSCOPF method. The developed method has not been compared with any other methods, as no comparable results have been found in the literature. This process may involve testing, and validation against known benchmark results of similar developed methods.

Another interesting avenue is to implement the CSCOPF as described in Section 2.8.1, for example using Benders Decomposition. As argued, this approach holds the potential to provide more accurate results compared to the PSCOPF implemented in this thesis. It could also reduce the computational efforts; only analyzing the contingencies that result in violation of constraints, instead of having to preemptively select contingencies for analysis.

It is proposed to expand the model to an ACOPF formulation, which considers more variables in the power system, such as voltage angles and line losses. Moreover, the ACOPF can be extended to the AC-PSCOPF framework, incorporating security constraints as done in this thesis for the DC-PSCOPF. This progression will enhance the precision in the optimisation model. For even further progress, even an AC-based CSCOPF method could be implemented.

To mitigate the issue of long simulation times in the Python script, optimising the model is crucial. This can for example be done through reformulations of the model, or using

other approaches in the coding structure.

References

[1] Cain, Mary B and O'neill, Richard P and Castillo, Anya and others, "History of optimal power flow and formulations," Federal Energy Regulatory Commission, vol. 1, pp. 1–36, 2012.

[2] Statnett, "Års- og bærekraftsrapport 2022," 2022. [Online]. Available: https://www.statnett.no/globalassets/om-statnett/investorrelasjoner/arsrapporter/ars--og-barekraftsrpaport-2022.pdf

[3] J. Choi, T. D. Mount, and R. J. Thomas, "Transmission expansion planning using contingency criteria," IEEE Transactions on Power Systems, vol. 22, no. 4, pp. 2249–2261, 2007.

[4] R. P. O'Neill, E. A. Krall, K. W. Hedman, and S. S. Oren, "A model and approach for optimal power systems planning and investment," Math. Program, 2011.

[5] A. Seifu, S. Salon, and G. List, "Optimization of transmission line planning including security constraints," IEEE Transactions on Power Systems, vol. 4, no. 4, pp. 1507–1513, 1989.

[6] D. K. Molzahn, J. T. Holzer, B. C. Lesieutre, and C. L. DeMarco, "Implementation of a large-scale optimal power flow solver based on semidefinite programming," IEEE Transactions on Power Systems, vol. 28, no. 4, pp. 3987–3998, 2013.

[7] J. Nocedal, A. Wächter, and R. A. Waltz, "Adaptive barrier update strategies for nonlinear interior methods," SIAM Journal on Optimization, vol. 19, no. 4, pp. 1674–1693, 2009.

[8] D. Phan and J. Kalagnanam, "Distributed methods for solving the security-constrained optimal power flow problem," in 2012 IEEE PES Innovative Smart Grid Technologies (ISGT). IEEE, 2012, pp. 1–7.

[9] R. Jamalzadeh, F. Zhang, and M. Hong, "An economic dispatch algorithm incorporating voltage management for active distribution systems using generalized benders decomposition," in 2016 IEEE Power and Energy Society General Meeting (PESGM). IEEE, 2016, pp. 1–5.

[10] G. Oliveira, A. Costa, and S. Binato, "Large scale transmission network planning using optimization and heuristic techniques," IEEE Transactions on Power systems, vol. 10, no. 4, pp. 1828–1834, 1995.

[11] A. Wächter and L. T. Biegler, "On the implementation of an interior-point filter line-search algorithm for large-scale nonlinear programming," Mathematical programming, vol. 106, pp. 25–57, 2006.

[12] R. J. Vanderbei, "Loqo:an interior point code for quadratic programming," Optimization Methods and Software, vol. 11, no. 1-4, pp. 451–484, 1999. [Online]. Available: https://doi.org/10.1080/10556789908805759

[13] F. Zhang, "Solving Large Security-Constrained Optimal Power Flow for Power Grid Planning and Operations," Case Western Reserve University, 2020.

[14] M. Rausand and A. Hoyland, System reliability theory: models, statistical methods, and applications. John Wiley & Sons, 2003, vol. 396.

[15] R. Billinton and R. N. Allan, "Power-system Reliability in Perspective," Electronics and Power, vol. 30, no. 3, pp. 231–236, Mar 1984.

[16] R. Billinton and E. Khan, "A security based approach to composite power system reliability evaluation," IEEE Transactions on Power Systems, vol. 7, no. 1, pp. 65–72, 1992.

[17] X. Luo, C. Singh, and A. Patton, "Loss-of-load state identification using self-organizing map," in 1999 IEEE Power Engineering Society Summer Meeting. Conference Proceedings (Cat. No.99CH36364), vol. 2, 1999, pp. 670–675 vol.2.

[18] C. Singh, X. Luo, and H. Kim, "Power system adequacy and security calculations using monte carlo simulation incorporating intelligent system methodology," in 2006 International Conference on Probabilistic Methods Applied to Power Systems, 2006, pp. 1–9.

[19] T. Vrana and E. Johansson, "Overview of analytical power system reliability assessment techniques," 05 2011.

[20] M. Bhuiyan and R. Allan, "Modelling multistate problems in sequential simulation of power system reliability studies," IEE Proceedings-Generation, Transmission and Distribution, vol. 142, no. 4, pp. 343–349, 1995.

[21] A. Sankarakrishnan and R. Billinton, "Sequential monte carlo simulation for composite power system reliability analysis with time varying loads," IEEE Transactions on power Systems, vol. 10, no. 3, pp. 1540–1545, 1995.

[22] I. G. Birkeland and K. Bjørgve, "Reactive power considerations in reliability assessment of power systems," NTNU, Trondheim, 2021, Master thesis.

[23] R. Billinton, R. Allan, I. Sjarief, L. Goel, and K. S. So, "A Reliability Test System for Educational Purposes - Basic Data," IEEE Transactions on Power Systems, vol. 6, no. 2, pp. 813–820, May 1991.

[24] R. Billinton and R. N. Allan, Reliability Evaluation of Power Systems, 2nd ed. Plenum Press, 1994.

[25] R. Billinton and W. Li, Reliability Assessment of Electric Power Systems Using Monte Carlo Methods, 1st ed. Plenum Press, 1994.

[26] R. Billinton and S. Kumar, "Indices for Use in Composite Generation and Transmission System Adequacy Evaluation," International Journal of Electrical Power & Energy Systems, vol. 12, no. 3, pp. 147–155, Jul 1990.

[27] R. Allan, "Power System Reliability Assessment - A Conceptual and Historical Review," Reliability Engineering & System Safety, vol. 46, no. 1, pp. 3–13, 1994.

[28] Power Systems Engineering Committee, "Reliability Indices for Use in Bulk Power Supply Adequacy Evaluation," IEEE Transactions on Power Apparatus and Systems, vol. PAS-97, no. 4, pp. 1097–1103, Jul 1978.

[29] Re-powering Markets, ser. Electricity Market Series. OECD, 3 2016. [Online]. Available: https://www.oecd-ilibrary.org/energy/re-powering-markets_9789264209596-en

[30] W. Li and J. Zhou, "Probabilistic Reliability Assessment of Power System Operations," Electric Power Components and Systems, vol. 36, no. 10, pp. 1102–1114, Sep 2008.

[31] O. S. Laengen, "Application of Monte Carlo Simulation to Power System Adequacy Assessment," NTNU, Trondheim, 2018, Master thesis.

[32] S. Frank and S. Rebennack, "An introduction to optimal power flow: Theory, formulation, and examples," Taylor & Francis, vol. 48, no. 12, pp. 1172–1197, 12 2016. [Online]. Available: https://www.tandfonline.com/doi/abs/10.1080/0740817X.2016.1189626

[33] C. Globe, "Nominal pi model of a medium transmission line," Online. [Online]. Available: https://circuitglobe.com/nominal-pi-model-of-a-medium-transmission-line.html

[34] M. Farivar and S. H. Low, "Branch flow model: Relaxations and convexification-part i," IEEE Transactions on Power Systems, vol. 28, no. 3, pp. 2554–2564, 2013.

[35] P. Murty, "Power Flow Studies," in Power Systems Analysis, 2nd ed. Boston, USA: Butterworth-Heinemann, 2017, ch. 10, pp. 205–276.

[36] D. Mehta, D. K. Molzahn, and K. Turitsyn, "Recent advances in computational methods for the power flow equations," in 2016 American Control Conference (ACC), 2016, pp. 1753–1765.

[37] B. Stott, J. Jardim, and O. Alsac, "DC Power Flow Revisited," IEEE Transactions on Power Systems, vol. 24, no. 3, pp. 1290–1300, 8 2009. [Online]. Available: http://ieeexplore.ieee.org/document/4956966/

[38] F. Capitanescu, "Critical review of recent advances and further developments needed in ac optimal power flow," Electric Power Systems Research, vol. 136, pp. 57–68, 2016.

[39] D. Phan and J. Kalagnanam, "Some efficient optimization methods for solving the security-constrained optimal power flow problem," IEEE Transactions on Power Systems, vol. 29, no. 2, pp. 863–872, 2013.

[40] S. H. Low, "Convex relaxation of optimal power flow—part ii: Exactness," IEEE Transactions on Control of Network Systems, vol. 1, no. 2, pp. 177–189, 2014.

[41] L. L. Lai, J. Ma, R. Yokoyama, and M. Zhao, "Improved genetic algorithms for optimal power flow under both normal and contingent operation states," International Journal of Electrical Power & Energy Systems, vol. 19, no. 5, pp. 287–292, 1997.

[42] V. J. Gutierrez-Martinez, C. A. Cañizares, C. R. Fuerte-Esquivel, A. Pizano-Martinez, and X. Gu, "Neural-network security-boundary constrained optimal power flow," IEEE Transactions on Power Systems, vol. 26, no. 1, pp. 63–72, 2010.

[43] M. L. Ellingsen, "Security-constrained optimal power flow in meshed distribution grids," NTNU, Trondheim, 2020, Master thesis.

[44] S. Chatzivasileiadis, "Optimization in Modern Power Systems DTU Course 31765 Lecture Notes," 2018. [Online]. Available: https://arxiv.org/abs/1811.00943

[45] F. Capitanescu, J. M. Ramos, P. Panciatici, D. Kirschen, A. M. Marcolini, L. Platbrood, and L. Wehenkel, "State-of-the-art, challenges, and future trends in security constrained optimal power flow," Electric power systems research, vol. 81, no. 8, pp. 1731–1741, 2011.

[46] A. Monticelli, M. V. F. Pereira, and S. Granville, "Security-constrained optimal power flow with post-contingency corrective rescheduling," IEEE Transactions on Power Systems, vol. 2, no. 1, pp. 175–180, 1987.

[47] Z. Yang, H. Zhong, Q. Xia, and C. Kang, "Fundamental review of the opf problem: Challenges, solutions, and state-of-the-art algorithms," Journal of Energy Engineering, vol. 144, no. 1, p. 04017075, 2018.

[48] A. M. Geoffrion, "Generalized benders decomposition," Journal of optimization theory and applications, vol. 10, pp. 237–260, 1972.

[49] J. Guo, Y. Fu, Z. Li, and M. Shahidehpour, "Direct calculation of line outage distribution factors," IEEE Transactions on Power Systems, vol. 24, no. 3, pp. 1633–1634, 2009.

[50] V. H. Hinojosa and F. Gonzalez-Longatt, "Preventive security-constrained dcopf formulation using power transmission distribution factors and line outage distribution factors," Energies, vol. 11, no. 6, 2018. [Online]. Available: https://www.mdpi.com/1996-1073/11/6/1497

[51] R. Billinton and D. Huang, "Basic Concepts in Generating Capacity Adequacy Evaluation," in International Conference on Probabilistic Methods Appplied to Power Systems, 2006, pp. 1–6.

[52] T. Guler and G. Gross, "Detection of island formation and identification of causal factors under multiple line outages," IEEE Transactions on Power Systems, vol. 22, no. 2, pp. 505–513, 2007.

[53] W. Wangdee and R. Billinton, "Impact of load shedding philosophies on bulk electric system reliability analysis using sequential monte carlo simulation," Electric Power Components and Systems, vol. 34, no. 3, pp. 355–368, 2006. [Online]. Available: https://doi.org/10.1080/15325000500241266

[54] M. L. Bynum, G. A. Hackebeil, W. E. Hart, C. D. Laird, B. L. Nicholson, J. D. Siirola, J.-P. Watson, and D. L. Woodruff, Pyomo–optimization modeling in python, 3rd ed. Springer Science & Business Media, 2021, vol. 67.

[55] W. E. Hart, J.-P. Watson, and D. L. Woodruff, "Pyomo: modeling and solving mathematical programs in python," Mathematical Programming Computation, vol. 3, no. 3, pp. 219–260, 2011.

[56] P. Virtanen, R. Gommers, T. E. Oliphant, M. Haberland, T. Reddy, D. Cournapeau, E. Burovski, P. Peterson, W. Weckesser, J. Bright, S. J. van der Walt, M. Brett, J. Wilson, K. J. Millman, N. Mayorov, A. R. J. Nelson, E. Jones, R. Kern, E. Larson, C. J. Carey, İ. Polat, Y. Feng, E. W. Moore, J. VanderPlas, D. Laxalde, J. Perktold, R. Cimrman, I. Henriksen, E. A. Quintero, C. R. Harris, A. M. Archibald, A. H. Ribeiro, F. Pedregosa, P. van Mulbregt, and SciPy 1.0 Contributors, "SciPy 1.0: Fundamental Algorithms for Scientific Computing in Python," Nature Methods, vol. 17, pp. 261–272, 2020.

[57] Gurobi Optimization, LLC, "Gurobi Optimizer Reference Manual," 2023. [Online]. Available: https://www.gurobi.com

[58] T. Guler, G. Gross, and M. Liu, "Generalized line outage distribution factors," IEEE Transactions on Power Systems, vol. 22, no. 2, pp. 879–881, 2007.

[59] miscellaneous. (2021) concurrent.futures — Launching parallel tasks. Python Software Foundation. [Online]. Available: https://docs.python.org/3/library/concurrent.futures.html

[60] Reliability Test System Task Force, "IEEE Reliability Test System," IEEE Transactions on Power Apparatus and Systems, vol. PAS-98, no. 6, pp. 2047 – 2054, Nov 1979.

[61] R. Billinton and W. Wangdee, "Impact of Load Shedding Philosophies on Bulk Electric System Reliability Analysis Using Sequential Monte Carlo Simulation," Electric Power Components and Systems, vol. 34, no. 3, pp. 355–368, 2006.

Appendices

A Load Data

Table A.1: *Weekly peak load in percent of annual peak [60].*

Week	Peak load [%]	Week	Peak load [%]
1	86.2	27	75.5
2	90.0	28	81.6
3	87.8	29	80.1
4	83.4	30	88.0
5	88.0	31	72.2
6	84.1	32	77.6
7	83.2	33	80.0
8	80.6	34	72.9
9	74.0	35	72.6
10	73.7	36	70.5
11	71.5	37	78.0
12	72.7	38	69.5
13	70.4	39	72.4
14	75.0	40	72.4
15	72.1	41	74.3
16	80.0	42	74.4
17	75.4	43	80.0
18	83.7	44	88.1
19	87.0	45	88.5
20	88.0	46	90.9
21	85.6	47	94.0
22	81.1	48	89.0
23	90.0	49	94.2
24	88.7	50	97.0
25	89.6	51	100.0
26	86.1	52	95.2

Table A.2: *Daily peak load in percent of weekly peak [60].*

Day	Peak load [%]
Monday	93
Tuesday	100
Wednesday	98
Thursday	96
Friday	94
Saturday	77
Sunday	75

Table A.3: *Hourly peak load in percent of daily peak [60].*

	Winter weeks 1-8 & 44-52		Summer weeks 18-30		Spring/Fall Weeks 9-17 & 31-43	
Hour	Weekday	Weekend	Weekday	Weekend	Weekday	Weekend
00-01	67	78	64	74	63	75
01-02	63	72	60	70	62	73
02-03	60	68	58	66	60	69
03-04	59	66	56	65	58	66
04-05	59	64	56	64	59	65
05-06	60	65	58	62	65	65
06-07	74	66	64	62	72	68
07-08	86	70	76	66	85	74
08-09	95	80	87	81	95	83
09-10	96	88	95	86	99	89
10-11	96	90	99	91	100	92
11-12	95	91	100	93	99	94
12-13	95	90	99	93	93	91
13-14	95	88	100	92	92	90
14-15	93	87	100	91	90	90
15-16	94	87	97	91	88	86
16-17	99	91	96	92	90	85
17-18	100	100	96	94	92	88
18-19	100	99	93	95	96	92
19-20	96	97	92	95	98	100
20-21	91	94	92	100	96	97
21-22	83	92	93	93	90	95
22-23	73	87	87	88	80	90
23-00	63	81	72	80	70	85

B RBTS Data

Table B.1: *The generator data for the RBTS [23].*

Capacity [MW]	Bus	Q_{min} [MVar]	Q_{max} [MVar]	FOR
10	1	0	7	0.020
20	1	-7	12	0.025
40	1	-15	17	0.030
40	1	-15	17	0.030
5	2	0	5	0.010
5	2	0	5	0.010
20	2	-7	12	0.015
20	2	-7	12	0.015
20	2	-7	12	0.015
20	2	-7	12	0.015
40	2	-15	17	0.020

Table B.2: *Bus specifications for the RBTS [23] including IEAR [61].*

Bus	Share of load	V_{min} [pu]	V_{max} [pu]	IEAR [$/kWh]	Priority
1	0	0.97	1.05	0	–
2	0.1081	0.97	1.05	9.6325	1
3	0.4595	0.97	1.05	4.3769	5
3	0.2162	0.97	1.05	8.0267	3
4	0.1081	0.97	1.05	8.6323	2
4	0.1081	0.97	1.05	5.5132	0

Table B.3: *Network parameters and outage data for the RBTS [23].*

Line	From	To	R [pu]	X [pu]	B/2 [pu]	Current rating [pu]	FOR
1	1	3	0.0342	0.18	0.0106	0.85	0.00171
2	2	4	0.1140	0.60	0.0352	0.71	0.00568
3	1	2	0.0912	0.48	0.0282	0.71	0.00455
4	3	4	0.0228	0.12	0.0071	0.71	0.00114
5	3	5	0.0228	0.12	0.0071	0.71	0.00114
6	1	3	0.0342	0.18	0.0106	0.85	0.00171
7	2	4	0.1140	0.60	0.0352	0.71	0.00568
8	4	5	0.0228	0.12	0.0071	0.71	0.00114
9	5	6	0.0228	0.12	0.0071	0.71	0.00114

C IEEE RTS Data

Table C.1: *Generator data for the IEEE RTS [60].*

Capacity [MW]	Bus	Q_{min} [MVar]	Q_{max} [MVar]	FOR
12	15	0	7	0.02
12	15	0	7	0.02
12	15	0	7	0.02
12	15	0	7	0.02
12	15	0	7	0.02
20	1	0	10	0.1
20	1	0	10	0.1
20	2	0	10	0.1
20	2	0	10	0.1
50	22	-10	16	0.01
50	22	-10	16	0.01
50	22	-10	16	0.01
50	22	-10	16	0.01
50	22	-10	16	0.01
50	22	-10	16	0.01
76	1	-25	30	0.02
76	1	-25	30	0.02
76	2	-25	30	0.02
76	2	-25	30	0.02
100	7	0	60	0.04
100	7	0	60	0.04
100	7	0	60	0.04
155	15	-50	80	0.04
155	16	-50	80	0.04
155	23	-50	80	0.04
155	23	-50	80	0.04
197	13	0	80	0.05
197	13	0	80	0.05
197	13	0	80	0.05
350	23	-25	150	0.08
400	18	-50	200	0.12
400	21	-50	200	0.12
0	14	-50	200	0
0	6	-100	0	0

Table C.2: *Bus specifications for the IEEE RTS [60] including IEAR [61].*

Bus	Share of load	V_{min} [pu]	V_{max} [pu]	IEAR [$/kWh]	Priority
1	0.038	0.97	1.05	8.9815	3
2	0.034	0.97	1.05	7.3606	5
3	0.063	0.97	1.05	5.8990	11
4	0.026	0.97	1.05	9.5992	1
5	0.025	0.97	1.05	9.2323	2
6	0.048	0.97	1.05	6.5238	9
7	0.044	0.97	1.05	7.0291	8
8	0.060	0.97	1.05	7.7742	4
9	0.061	0.97	1.05	3.6623	17
10	0.068	0.97	1.05	5.1940	14
11	0	0.97	1.05	0	–
12	0	0.97	1.05	0	–
13	0.093	0.97	1.05	7.2813	6
14	0.068	0.97	1.05	4.3717	16
15	0.111	0.97	1.05	5.9744	10
16	0.035	0.97	1.05	7.2305	7
17	0	0.97	1.05	0	–
18	0.117	0.97	1.05	5.6149	13
19	0.064	0.97	1.05	4.5430	15
20	0.045	0.97	1.05	5.6836	12
21	0	0.97	1.05	0	–
22	0	0.97	1.05	0	–
23	0	0.97	1.05	0	–
24	0	0.97	1.05	0	–

Table C.3: *Network parameters and outage data for the IEEE RTS [60].*

Line	From	To	R [pu]	X [pu]	B/2 [pu]	Current rating [pu]	FOR
1	1	2	0.0026	0.0139	0.23055	1.93	0.000438164
2	1	3	0.0546	0.2112	0.0286	2.08	0.000581853
3	1	5	0.0218	0.0845	0.01145	2.08	0.00037657
4	2	4	0.0328	0.1267	0.01715	2.08	0.000445007
5	2	6	0.0497	0.1920	0.0260	2.08	0.000547645
6	3	9	0.0308	0.1190	0.0161	2.08	0.000433602
7	3	24	0.0023	0.0839	0	5.1	0.001750356
8	4	9	0.0268	0.1037	0.01405	2.08	0.00041079
9	5	10	0.0228	0.0883	0.01195	2.08	0.000387977
10	6	10	0.0139	0.0605	1.2295	1.93	0.001316757
11	7	8	0.0159	0.0614	0.0083	2.08	0.000342349
12	8	9	0.0427	0.1651	0.02235	2.08	0.000502031
13	8	10	0.0427	0.1651	0.02235	2.08	0.000502031
14	9	11	0.0023	0.0839	0	5.1	0.001750356
15	9	12	0.0023	0.0839	0	5.1	0.001750356
16	10	11	0.0023	0.0839	0	5.1	0.001750356
17	10	12	0.0023	0.0839	0	5.1	0.001750356
18	11	13	0.0061	0.0476	0.04995	6	0.000502031
19	11	14	0.0054	0.0418	0.04395	6	0.000489486
20	12	13	0.0061	0.0476	0.04995	6	0.000502031
21	12	23	0.0124	0.0966	0.1015	6	0.000652542
22	13	23	0.0111	0.0865	0.0909	6	0.000614918
23	14	16	0.0050	0.0389	0.0409	6	0.000476941
24	14	16	0.0022	0.0173	0.0182	6	0.000414212
25	15	21	0.0063	0.0490	0.0515	6	0.000514575
26	15	21	0.0063	0.0490	0.0515	6	0.000514575
27	15	24	0.0067	0.0519	0.05455	6	0.000514575
28	16	17	0.0033	0.0259	0.02725	6	0.000439305
29	16	19	0.0030	0.0231	0.02425	6	0.000426758
30	17	18	0.0018	0.0144	0.01515	6	0.000401665
31	17	22	0.0135	0.1053	0.1106	6	0.000677623
32	18	21	0.0033	0.0259	0.02725	6	0.000439305
33	18	21	0.0033	0.0259	0.02725	6	0.000439305
34	19	20	0.0051	0.0396	0.04165	6	0.000476941
35	19	20	0.0051	0.0396	0.04165	6	0.000476941
36	20	23	0.0028	0.0216	0.02275	6	0.000426758
37	20	23	0.0028	0.0216	0.02275	6	0.000426758
38	21	22	0.0087	0.0678	0.0712	6	0.000564749

D Original Flowchart Approach

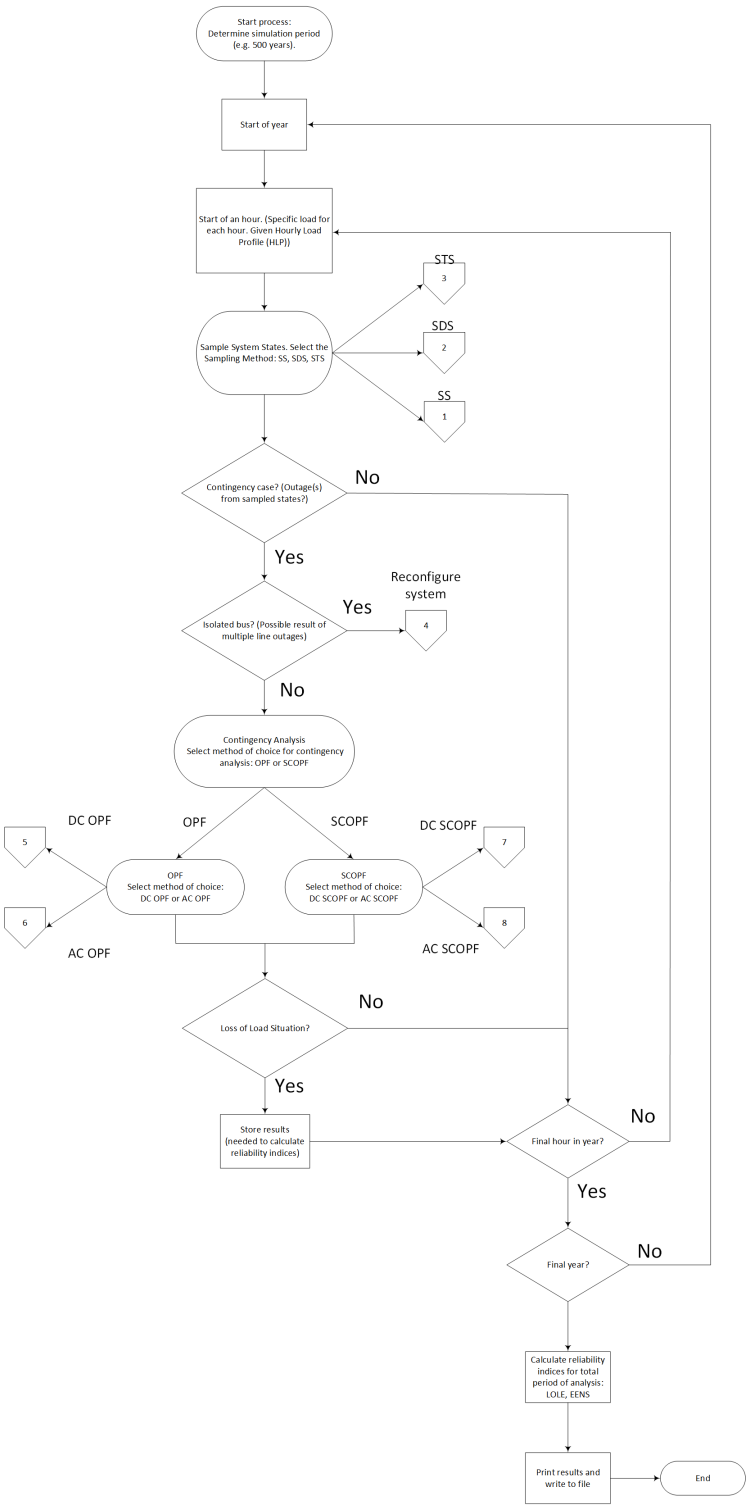

Figure D.1: *Complete algorithmic approach: Included selection of methods ACOPF, AC-SCOPF, DCOPF, DC-SCOPF and MCS methods. SS: State Sampling Approach, SDS: State Duration Samplingm, STS: State Transition Sampling.*

E Software Codes

(Restricted Public Access)

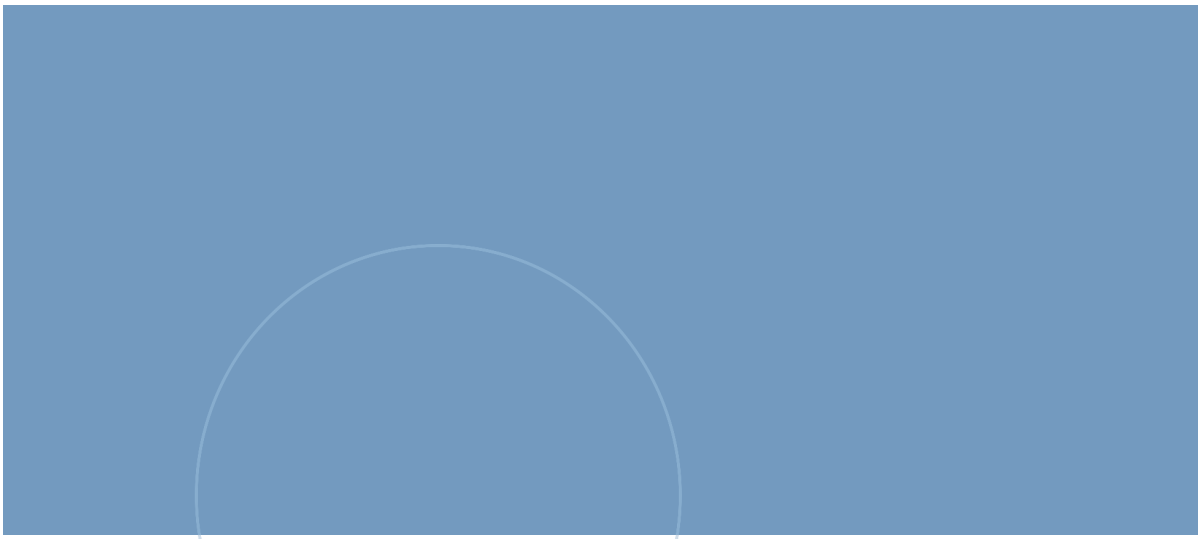

NTNU
Norwegian University of
Science and Technology